ISSN 1068-9761 (Print)
ISSN 2541-9935 (Online)

LIGHT & ENGINEERING

Volume 33, Number 4, 2025

Editorial of Journal
"Light & Engineering" (Svetotekhnika), Moscow

The purpose and content of «Light & Engineering» is to develop the science of light within the framework of ray, photometric concepts and the application of results for a comfortable light environment, as well as for visual and non-visual light technologies, including medicine. The light engineering science is a field of science and technology and its subject is the development of methods for generation and spatial redistribution of optical radiation, as well as its conversion to other forms of energy and use for various purposes.

The scope of journal includes articles in the following areas:

- Sources of light;
- Light field theory;
- Photometry, colorimetry and radiometry of optical radiation;
- Visual and non-visual effects of radiation on humans;
- Control and regulation devices for light sources;
- Light devices, their design and production technology;
- Light devices for the efficient distribution and transportation of the light energy: hollow light guides, optical fibers;
- Lighting and irradiation installations;
- Light signaling and light communication;
- Light remote sensing;
- Mathematical modelling of light devices and installations;
- Energy savings in light installation;
- Innovative light design solutions;
- Photobiology, including problems of using light in medicine;
- Disinfection of premises, drinking water and smell elimination by UV radiation technology;
- Light transfer in the ocean, space and other mediums;
- Light and engineering marketing;
- Legal providing and regulation of energy effective lighting;
- Light conversion to other forms of energy;
- Standardization in field of lighting;
- Light in art and architecture design;
- Education in field of light and engineering.

Journal “Light & Engineering” had been founded by Prof. Julian B. Aizenberg in 1993

LIGHT & ENGINEERING

СВЕТОТЕХНИКА

Editorial of Journal “Light & Engineering/Svetotekhnika”

Moscow, 2025

Publishing House: Editorial of Journal "Light & Engineering" (Svetotekhnika), Moscow

Editorial Office:

Russia, VNISI, Rooms 334 and 346
106 Prospekt Mira, Moscow 129626

Tel: +7.495.682.58.46
E-mail: lights-nr@inbox.ru
http://www.l-e-journal.com

General Director: Nataliya C. Sherri
Editorial Manager: Marina I. Titarenko
Issuing editor: Pavel A. Fedorishchev
Art and CAD Editor: Andrei M. Bogdanov
Content-manager: Eugene S. Sery
Editorial secretary: Elena A. Bulgakova

Scientific Editors:
Sergei G. Ashurkov
Alexander Yu. Basov
Tatiana V. Smirnova (Meshkova)
Raisa I. Stolyarevskaya

Light & Engineering is an international scientific Journal subscribed to by readers in many different countries. It is the English edition of the journal "Svetotekhnika" the oldest scientific publication in Russia, established in 1932.

Establishing the English edition "Light and Engineering" in 1993 allowed Russian illumination science to be presented the colleagues abroad. It attracted the attention of experts and a new generation of scientists from different countries to Russian domestic achievements in light and engineering science. It also introduced the results of international research and their industrial application on the Russian lighting market.

The scope of our publication is to present the most current results of fundamental research in the field of illumination science. This includes theoretical bases of light source development, physiological optics, lighting technology, photometry, colorimetry, radiometry and metrology, visual perception, health and hazard, energy efficiency, semiconductor sources of light and many others related directions. The journal also aims to cover the application illumination science in technology of light sources, lighting devices, lighting installations, control systems, standards, lighting art and design, and so on.

"Light & Engineering" is well known by its brand and design in the field of light and illumination. Each annual volume has six issues, with about 80–120 pages per issue. Each paper is reviewed by recognized world experts.

CONTENTS

VOLUME 33 NUMBER 4 2025

LIGHT & ENGINEERING

Light & Engineering
Vol. 33, No. 4, pp. 4–14, 2025

https://doi.org/10.33383/2025-019
Svetotekhnika # 3, 2025, pp. 4–10

ASSESSING LIGHTING PREFERENCES IN NOCTURNAL URBAN ENVIRONMENTS: A PHOTO STIMULI SURVEY ON SAFETY PERCEPTION AND VISUAL COMFORT

Lanlan Wei[1*], Grega Bizjak[1], Matija Svetina[2], and Matej B. Kobav[1]

[1]*Faculty of Electrical Engineering, University of Ljubljana, Ljubljana, Slovenia*
[2]*Faculty of Philosophy, University of Ljubljana, Ljubljana, Slovenia*
[*]*E-mail: lanlan.wei@fe.uni-lj.si*

ABSTRACT

Outdoor public lighting is essential for shaping nocturnal urban environments, as it significantly enhances visibility and fosters a sense of safety perception and visual comfort in public spaces, thus, influencing their usage. While extensive research has been conducted on lighting parameters such as luminance, illuminance, uniformity, and glare, there remains a lack of focus on user preferences for actual outdoor lighting settings. This study aims to address this gap by investigating photo stimuli based on public lighting preferences in a real outdoor environment in Ljubljana, Slovenia. In this research, 116 participants evaluated their levels of comfort, confidence, and spatial awareness based on nine virtual images from two distinct locations featuring various lighting settings, these included continuous and less-continuous lighting environments, low-mounted (4.5 m) lighting poles vs. high-mounted (12 m) lighting poles, three distinct CCTs, and both overhead and peripheral lighting environments. Participants rated each lighting scene on a 5-point scale, facilitating an assessment of their preferences. The analysis revealed a significant preference for continuous, high-mounted (12 m) lighting poles with a natural white CCT in the square area, and for overhead lighting in the road area. The most substantial difference in user experience was observed between continuous and less-continuous lighting environment, while variations in pole height, CCT, and lighting position demonstrated comparatively minor impacts. Notably, the influence of CCT on participants' perceptions of safety, comfort, and spatial awareness was the least significant among the factors examined.

These findings provide valuable insights into the design of urban lighting aimed at enhancing safety and comfort, thereby informing future urban planning and lighting design practices.

Keywords: public outdoor lighting, user preferences, urban environment, comfort, urban planning

1. INTRODUCTION

Public outdoor lighting, integrated with the urban context, shapes night time environments by influencing visual task performance, safety perception, and overall comfort [1]. For young people, who frequently engage in night time activities, well-designed lighting can enhance their sense of safety while fostering inviting and sociable spaces. The prospect-refuge theory [2–3] posits that physical attributes, such as prospect (visibility), concealment, and entrapment, directly influence perceptions of danger or fear of crime [4–7], which in turn impact user preferences and well-being. Illumination plays a critical role in modulating these attributes by improving visual clarity (e.g., obstacle recognition [8–9]), enabling social judgments (e.g., emotion and gaze direction detection [10]), and enhancing pedestrian safety feeling and reassurance [11–17].

Research underscores that specific lighting parameters – such as illuminance, uniformity, luminaires height, and CCT – significantly shape perceptions of urban environment. For instance, uniform, bright, and overhead lighting is often preferred in public spaces for its ability to illuminate broader surroundings rather than isolated pathways [7, 18–19]. Higher illuminance levels are linked to improved pedestrian reassurance, visual adaptation, and detail recognition, whereas inadequate lighting amplifies feelings of vulnerability. However, Fotios et al. [16, 20–21] empirically demonstrated a nonlinear relationship between lighting parameters and the perception of safety through their study. The research substantiates two critical findings:

1. In spatial lighting design, optimizing light distribution (particularly through minimizing low-illuminance areas) proves more effective in enhancing individuals' safety perception than merely increasing absolute illuminance levels;

2. A threshold effect exists between illuminance levels and safety enhancement outcomes – beyond a critical value (approximately (5–7) lx), further illuminance revealing no sustained linear correlation with perceived safety improvements.

Another critical parameter is CCT, which affects emotional responses and spatial recognition. Warmer light (e.g., 2700 K) is associated with comfort and intimacy, while cooler light (e.g., 4000 K) promotes alertness and energy [22–24]. However, while extensive research has been conducted on lighting parameters such as illuminance, spectrum, luminaire position, uniformity, and glare [8–11], there remains a lack of focus on user preferences for outdoor lighting settings.

For young populations, the interplay between lighting design and spatial context is pivotal for balancing safety and visual comfort. Overhead lighting reduces dark corners and potential hiding spots, enhancing security through clear visibility. In contrast, peripheral lighting emphasizes vertical surfaces and architectural features, fostering sociability by creating spatial depth [25–27]. Luminaire's height further shapes spatial perception: taller lighting poles evoke openness, while shorter ones promote intimacy [28–29].

This study aims to address this gap by investigating photo stimuli based on public lighting preferences in real outdoor environments in Ljubljana, Slovenia. Using 1:1 scale simulated photos of a familiar urban site – including a public square and a pedestrian road – this study simulated various lighting scenarios. Through photo-stimulus evaluations and questionnaire surveys, the study explores the following questions:

- How do continuity, pole height, and variations in white lighting in open squares influence perceived safety and visual comfort?
- What impact does overhead lighting have on the perception of road spaces?
- What lighting settings align most closely with young people's preferences?

By analysing these responses, the study aims to advance evidence-based guidelines for nocturnal urban environments design that prioritizes safety, visual comfort, and liveability for younger demographics.

2. METHODOLOGY

2.1. Participants

A total of 116 participants from the Faculty of Electrical Engineering took part in this study. The participants consisted of 14 females (12 %) and 102 males (88 %), all of whom were undergraduate students aged between 22 and 25 years. All participants had normal or corrected-to-normal vision and reported being familiar with the location and its surroundings. The study took place in the Electrical Engineering Faculty from April to May 2021. Due to COVID-19 safety protocols, participants were required to maintain 1.5 m. The darkroom used for the experiment could accommodate 12 participants at a time. As a result, participants were grouped into cohorts of 8 to 10 people, and each group underwent the same experimental procedure.

Regarding participants' night time walking habits, most reported that they typically walk outdoors between sunset and 10:00 pm (N=92, 78 %). A smaller group reported walking between midnight and sunrise (N=6,5 %), while the remaining participants did not engage in night time walking. When asked about the primary purpose of their outdoor walks, the majority indicated 'Relaxation, entertainment, and fitness' (N=105,9 %), while fewer participants cited 'Walking for business or professional reasons' (N=11,7 %).

Participation in the study was entirely voluntary, and no financial compensation was provided to participants. The research procedure was reviewed and approved by the Ethics Committee at the University

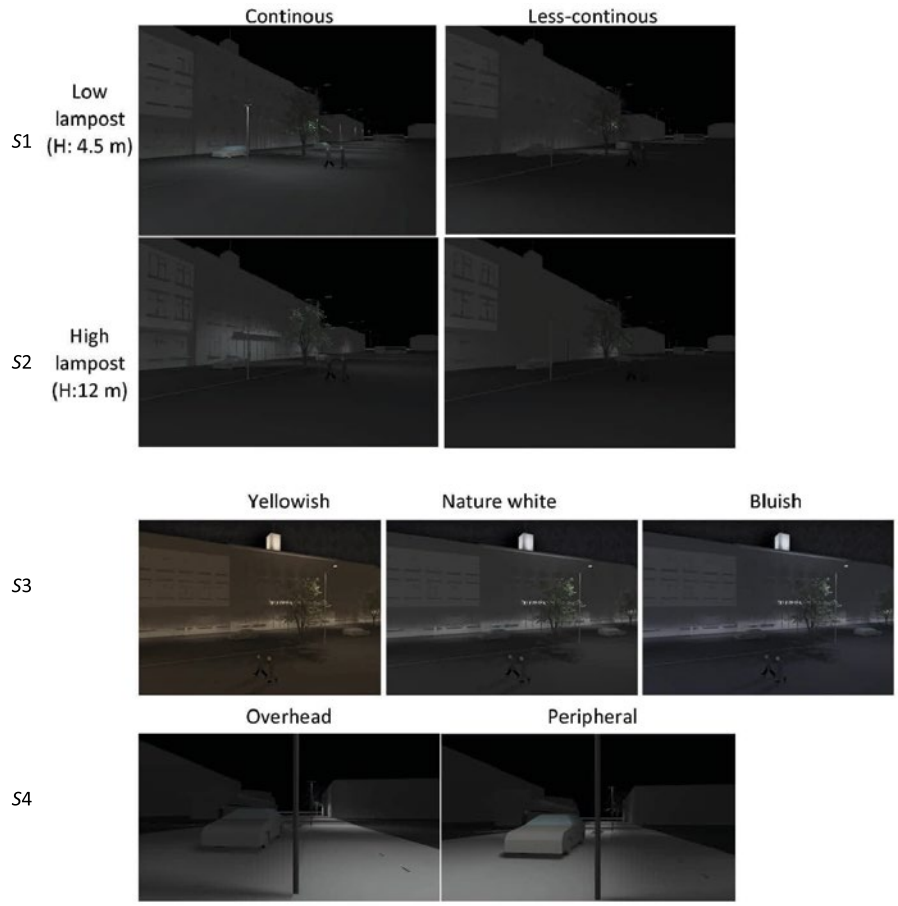

Fig. 1. Visual photo stimuli and scene descriptions

of Ljubljana, and all participants provided informed consent before their involvement.

2.2. Photo Stimuli

The study utilized four groups of simulated lighting scenes of the Ljubljana Central Railway Station to assess participants' preferences and perceptions. These stimuli were based on lighting models from previous studies [19], encompassing variations in uniformity, lighting position, and environmental context. The renderings depicted real lighting settings from the experimental selection square, including high and low-pole lighting configurations, as well as three CCT settings. To enhance the realism of the study, we captured photographs of the actual scene at night, measured its dimensions, and used the real photometric data to create a 3D model in DIALux software to simulate five groups of lighting conditions. The study utilized visual stimuli from two locations, selected for their representative characteristics and relevance to nocturnal pedestrian experience.

Location *A* is main square in front of the railway station.

A prototypical Central European town square, (121×26) m^2, surrounded by residential and commercial areas, 1 km from the city centre. Perceived as relatively safe, it featured three lighting variations:

– Scene 1 (*S*1): continuous vs. less-continuous illumination;

– Scene 2 (*S*2): low-mounted (4.5 m) lighting poles vs. high-mounted (12 m) lighting poles;

– Scene 3 (*S*3): three CCTs – warm (2200 K), neutral (4000 K), and cool (5700 K).

Location *B* is transitional roadway to the city centre.

A connecting space with a two-lane roadway (3.5 m per lane) and pedestrian paths (1.5 m each). The study compared:

– Scene 4 (*S*4): overhead lighting on pedestrian paths vs. peripheral lighting aimed on the vehicle path.

To isolate lighting effects, all non-lighting elements – tree placement, signage, and facade luminance – remained constant.

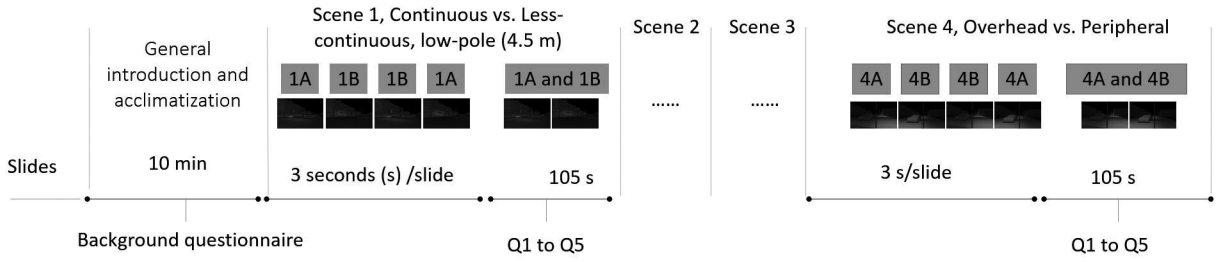

Fig. 2. Timeline of the experimental procedure for each lighting scene

Fig. 1. shows visual photo stimuli and scene descriptions.

2.3. Instruments and Procedures

To maintain consistent illumination and mitigate the influence of external lighting, the use of mobile phones was prohibited throughout the presentation phase. The standardised protocol was meticulously adhered to across all experimental groups. The experiment was conducted in a completely dark classroom at the Faculty of Electrical Engineering, University of Ljubljana. Images were projected onto a screen measuring (300×230) cm^2, (W×H), using a digital projector. The luminance of the images was carefully adjusted via computer and projector to ensure an average ground surface luminance of 1.0 cd/m², which was measured with a luminance meter during every experiment in the dark classroom.

Each image was displayed for 3 s, followed by a simultaneous presentation of two images for comparison. Participants viewed the images and answered questions after each set, with the next set of images presented only after all participants had completed their responses. To maintain participants' dark adaptation, the use of mobile phones was strictly prohibited during the session. The same procedure was repeated for each group of participants. Fig. 2 illustrates the experimental procedure.

The procedure began by displaying each image to participants for 3 s. To ensure robust perceptual engagement, the same set of comparative images was presented twice. During the questionnaire phase, pairs of images were shown simultaneously for an average duration of 105 s, allowing participants to compare and rate them. Participants were required to evaluate the images based on specific questions:

– Question 1 (Q1), visual comfort ("comfort" refers to visual comfort, which is explained to the participant orally): "How comfortable do you feel with picture *A*? How comfortable do you feel with picture *B*?";

– Question 2 (Q2), confident: "How confident do you feel with picture *A*? How confident do you feel with picture *B*?";

– Question 3 (Q3), orientation: "To what extent does lighting help you become oriented with picture *A*? To what extent does lighting help you become oriented with picture *B*?";

– Question 4 (Q4), distance estimation: "How much does the lighting help you estimate the distance to other pedestrians and objects with picture *A*? How much does the lighting help you estimate the distance to other pedestrians and objects with picture *B*?";

– Question 5 (Q5), safety perception: "How much does the lighting in picture *A* assist in identifying potential unsafety? How much does the lighting in picture *B* assist in identifying potential unsafety?".

The study employed a five-point scale, ranging from 1 (not at all) to 5 (very much), to assess two key dimensions of each lighting stimulus: emotional responses (questions 1 and 2) and orientational aspects (questions 3 and 4). Question 5 focused on evaluating "How much the lighting helps in estimating potential unsafety?". This question served as a crucial measure of public space quality, aligning with the principles of prospect-refuge theory. Unlike evaluations solely based on psychological feelings of fear or stress, the assessment of potential unsafety incorporated both psychological and spatial considerations, providing a comprehensive evaluation of the lighting's impact on public spaces [3, 6–7].

3. RESULTS

All survey questions were fully answered, allowing for a comprehensive analysis of the col-

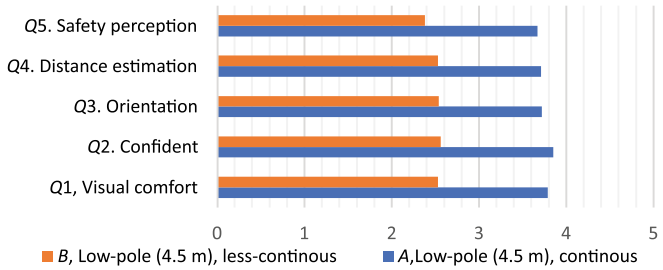

Fig. 3. The mean score distribution of ratings for continuous and less-continuous lighting environments with low-pole lighting (4.5 m)

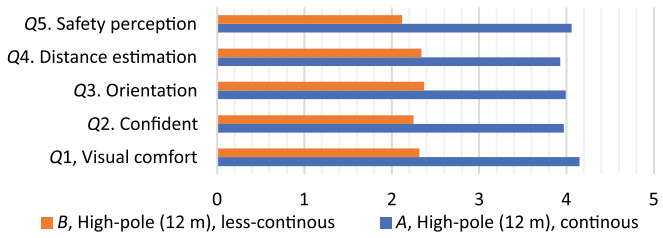

Fig. 4. The mean score distribution of continuous and less-continuous lighting environments with high-pole (12 m) lighting environment

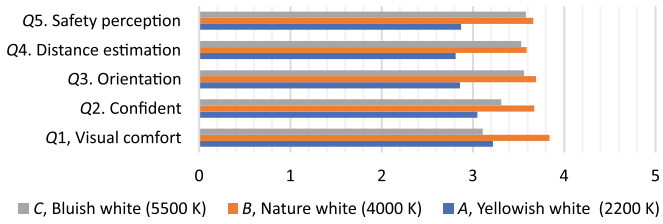

Fig. 5. The mean score distribution of yellowish-white, natural white, and bluish-white lighting environments

lected data. The inter-item reliability of responses to the five questions was assessed, revealing a strong correlation among them. The Cronbach's alpha test confirmed high internal consistency, with an acceptable reliability score (α=0.935). To analyse the results, we first calculated the mean values for all lighting conditions. A repeated measures analysis of variance (ANOVA) was then used to compare differences between continuous vs. less-continuous lighting and high-pole vs. low-pole lighting. Additionally, paired *t*-tests were conducted separately for each model to further examine these differences. Table 1 presents the findings across all lighting conditions (9 scenes × 5 questions), with results reported at a 95 % confidence level. The mean values ranged from 2.12 to 4.15, the high-pole (12 m) continuous lighting scene received the highest ratings across all five questions.

3.1. Continuous versus Less-Continuous

A repeated-measures ANOVA was conducted to compare participant preferences between continuous and less-continuous lighting configurations in a square urban environment. Results demonstrated a significant overall preference for continuous lighting across multiple perceptual dimensions ($F(1, 647) = 76.26$, $p < 0.001$, $d = –1.32$), with large effect sizes indicating practical significance. Participants consistently rated continuous lighting higher than less continuous lighting across all five questions in the low-pole configuration. Statistically significant differences were observed for: $Q1$ (visual comfort): $F(1, 127) = 14.83$, $p < 0.001$, Cohen's $d = –1.35$; $Q3$ (orientation): $F(1, 128) = 20.01$, $p < 0.001$, $d = –1.20$; $Q4$ (distance estimation): $F(1, 128) = 19.83$, $p < 0.001$, $d = –1.28$; $Q5$ (safety perception): $F(1, 128) = 12.68$, $p < 0.001$, $d = –1.32$. However, $Q2$ (confidence) showed no statistically significant difference after Bonferroni correction for multiple comparisons ($F(1, 128)= 8.09$, $p = 0.05$, $d = –1.44$; adjusted $\alpha = 0.01$). Fig. 3. shows the mean score distribution of ratings for continuous and less-continuous lighting environments with low-pole lighting (4.5 m).

In high-pole lighting settings, participants consistently demonstrated a strong preference for continuous illumination over less continuous alternatives across four critical perceptual dimensions. A repeated-measures ANOVA confirmed statisti-

Table 1. Mean Scores and Standard Deviations, for Nine Simulated Lighting Scenes across Five Questions

Lighting Scene			*Q*1		*Q*2		*Q*3		*Q*4		*Q*5	
			M	(*SD*)	*M*	(*SD*)	*M*	(*SD*)	*M*	(*SD*)	*M*	(*SD*)
Square area	1	*A*, low-pole (4.5 m), continuous	3.79	0.96	3.85	0.93	3.72	1.06	3.71	0.98	3.67	1.00
		B, low-pole (4.5 m), less-continuous	2.53	0.82	2.56	0.85	2.54	0.93	2.53	0.94	2.38	0.91
	2	*A*, high-pole (12 m), continuous	4.15	0.82	3.97	0.84	3.99	1.12	3.93	0.95	4.06	0.96
		B, high-pole (12 m), less-continuous	2.32	0.94	2.25	0.84	2.37	0.96	2.34	0.95	2.12	0.95
	3	*A* yellowish colour (2200 K)	3.22	1.32	3.05	1.16	2.86	1.11	2.81	1.09	2.87	1.11
		B, nature white (4000 K)	3.84	0.86	3.67	0.97	3.69	1.10	3.59	1.18	3.66	1.12
		C, bluish colour (5500 K)	3.11	1.13	3.31	1.15	3.56	1.17	3.53	1.19	3.58	1.17
Road area	4	*A*, overhead	3.88	1.01	3.84	0.96	3.77	1.07	3.72	1.05	3.76	1.10
		B, peripheral	2.56	0.95	2.63	0.93	2.74	0.98	2.86	0.91	2.82	0.97

cally significant advantages of continuous lighting in: *Q*1 (visual comfort): $F(1, 128) = 14.23$, $p < 0.001$, *Cohen's d* = –2.09; *Q*2 (confidence): $F(1, 128) = 11.30$, $p < 0.001$, $d = –2.07$; *Q*3 (orientation): $F(1, 128) = 15.31$, $p < 0.001$, $d = –1.63$; and *Q*4 (distance estimation): $F(1, 128) = 13.76$, $p < 0.001$, $d = –1.69$. Despite the large effect sizes (d = 1.63 – 2.09), *Q*5 (safety perception) did not maintain statistical significance after Bonferroni correction for multiple comparisons ($F(1, 128) = 8.05$, p = 0.05, $d = –2.03$). Fig. 4 with the mean distributions.

3.2. Yellowish, Natural, and Bluish White Lighting Environment

A paired-sample *t*-test analysis revealed a consistent preference for the natural white lighting scene over both the yellowish and bluish alternatives. Fig. 5 illustrates the distribution of mean scores across all five perceptual dimensions, highlighting the natural white scene as the highest-rated condition. In contrast, the yellowish scene received the lowest ratings across all metrics, while the bluish scene occupied an intermediate position, closely trailing natural white. Statistical analysis further confirmed a significant preference for natural white light over yellowish light in most cases, whereas differences between natural white and bluish light were less consistently significant. Fig. 5 provides a comprehensive breakdown of mean differences (*MD*), *F*-ratios, *p*-values, and Cohen's *d* for matched-pair comparisons across the three CCT conditions.

When considering all five perceptual dimensions together: natural vs. yellowish white: $F(1, 648) = 133.07$, $p < 0.001$, $d = –0.67$; yellowish vs. bluish: $F(1, 648) = 26.73$, $p < 0.001$, $d = –0.42$; natural vs. bluish white: $F(1, 648) = 337.92$, $p < 0.001$, $d = –0.23$. Effect sizes, as measured by Cohen's d, ranged from small to medium (d = –0.23 to –0.67), with the most pronounced effect observed in the comparison between natural white and yellowish white.

3.3. Overhead versus Peripheral

Previous studies [19] have investigated the overhead versus peripheral lighting modes in urban

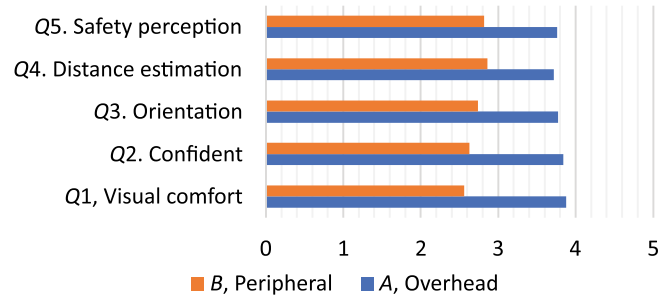

Fig. 6. The mean score distribution of overhead and peripheral lighting environments

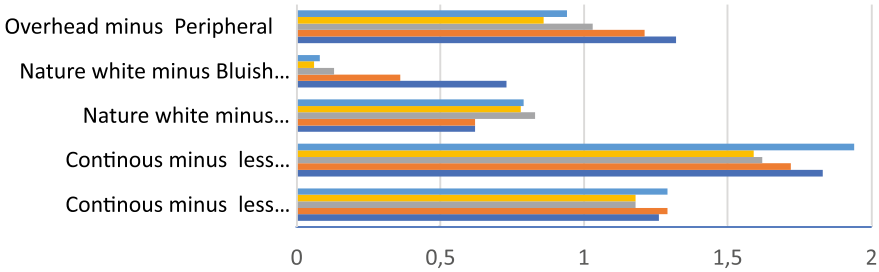

	Continous minus less continous under low-pole (4.5 m)	Continous minus less continous under high-pole (12 m)	Nature white minus Yellowish white	Nature white minus Bluish white	Overhead minus Peripheral
*Q*5. Safety perception	1.29	1.94	0.79	0.08	0.94
*Q*4. Distance estimation	1.18	1.59	0.78	0.06	0.86
*Q*3. Orientation	1.18	1.62	0.83	0.13	1.03
*Q*2. Confident	1.29	1.72	0.62	0.36	1.21
*Q*1. Visual comfort	1.26	1.83	0.62	0.73	1.32

Fig. 7. The mean score differences within each of the lighting scenes

squares. Our study builds on this prior research by examining these lighting settings in road environments, which are more representative of typical overhead and peripheral lighting scenes in Slovenia. This broader context allows for a deeper understanding of how these lighting modes impact pedestrians' perceptions of safety and comfort. The results indicate that overhead lighting consistently received higher ratings than peripheral lighting across all five evaluation questions, with mean differences ranging from 0.87 to 1.27. Fig. 6 illustrates the distribution of mean scores, clearly showing the overall preference for overhead lighting.

Question 1: the *F*-test revealed a significant difference between overhead and peripheral lighting settings ($F(1, 128) = 5.36$, $p = 0.022$, $d = –1.30$), indicating that overhead lighting was rated significantly higher. Questions 2, 3, 4, and 5: no statistically significant differences were observed.

When all five questions were considered together, the analysis revealed a statistically significant overall difference between the two lighting settings ($F(1, 648) = 11.01$, $p < 0.001$, $d = –0.32$). However, according to Cohen's *d*, the effect size was small, suggesting that the practical significance of this finding may be limited.

Fig. 6 provides a visual comparison of the mean scores, illustrating the preference for overhead lighting across all questions, even where differences were not statistically significant.

3.4. Perceptual Differences between Lighting Scenes

The results of this experiment revealed a clear preference for continuous lighting, high-pole configurations, natural white illumination, and overhead lighting over their respective alternatives: less-continuous lighting, low-pole configurations, yellowish and bluish illumination, and peripheral lighting. Fig. 7 highlights the most pronounced differences, with continuous versus less-continuous

lighting in high-pole settings exhibiting the largest mean difference (1.59 to 1.94). In contrast, the difference in low-pole settings was smaller (1.18 to 1.29), likely due to the greater extent of dark areas created by less-continuous lighting in high-pole configurations, which more significantly impacts perceptions of comfort, safety, and spatial cognition. Additionally, a substantial difference was observed between overhead and peripheral lighting (0.86 to 1.32), suggesting a strong preference for illumination concentrated in the immediate surroundings rather than positioned peripherally along the roadway. Comparisons between natural white and bluish lighting revealed minimal differences (0.06 to 0.73), particularly in spatial cognition assessments, where differences ranged from 0.06 ($Q4$) to 0.08 ($Q5$).

Overall, these findings offer valuable insights into lighting preferences in urban environments, emphasizing the significant influence of continuity, pole height, CCT, and light placement on perceptions of safety, visual comfort, and spatial awareness.

4. DISCUSSION

The influence of lighting on human perception has been widely studied, but there is still a lack of unified and reliable theories explaining the specific effects of lighting scenes on preference. In this study, we aimed to fill this gap by combining and building upon previous research to investigate the impact of lighting on human emotions and spatial cognition. Our findings supported our hypothesis that, in open public spaces, people generally prefer the lighting atmosphere created by continuous, high poles, whereas in street areas overhead lighting is more favourable than peripheral lighting. Our findings are compatible with prior studies, such as those by Nasar [19] and the prospect-refuge theory [30], which found that uniform illumination (in our case, we used continuous instead of uniform illumination) was a higher preference. Overhead lighting settings also received higher preference compared to peripheral lighting. However, this study did not investigate high or low illuminance levels, since people generally prefer brighter environments [13, 31–32]. Furthermore, although images with natural white CCT received the most preferences, this study did not consider the non-visual effects of lighting on the night time environment.

5. CONCLUSION

This study systematically evaluates nocturnal urban lighting preferences through a photo-stimuli survey of 116 participants in Ljubljana, focusing on safety perception and visual comfort. Analysis of nine simulated scenarios revealed a robust preference for continuous illumination, high-pole configurations (12 m), natural white spectra (4000 K), and overhead placement.

This study provides empirical insights into lighting preferences in nocturnal urban environments, emphasizing the interplay between safety perception and visual comfort. A strong preference for continuous illumination, high-pole configurations, natural white (4000 K), and overhead placement. Based on participants' answers these configurations significantly enhanced visual comfort, confidence, distance estimation, and safety perception, highlighting the critical role of predictability and spatial coherence in night-time urban design.

Key variability emerged between continuous and less-continuous illumination both under high and low lighting poles, the overhead vs. peripheral positioning exerting secondary influence. Minimal divergence across CCTs suggests spectral uniformity may hold lesser perceptual weight than spatial distribution in lighting design. While aligned with theories linking predictability to preference (e.g., Nasar's environmental appraisal [18], prospect-refuge principles), these findings derive from controlled photographic simulations; validation in real-world nocturnal settings remains critical.

The results underscore a pressing tension in urban retrofitting: while energy-efficient upgrades dominate policy agendas, neglecting user-centric factors – comfort, aesthetic integration, and contextual appropriateness – risks undermining public space quality. High-pole lighting, though effective in fostering perceived safety and spaciousness, demands judicious application to mitigate light pollution and energy excess. Furthermore, poor maintenance (e.g., flickering, vandalism) may erode perceptual benefits, emphasizing the need for holistic lifecycle management.

As a foundational investigation, this work advocates for expanded field studies incorporating diverse urban typologies (residential, commercial, arterial corridors) and environmental variables (temperature, weather, cleanliness). Future research must also disentangle the non-visual impacts of

spectral composition, such as circadian disruption, to advance lighting systems that harmonize human well-being, ecological sustainability, and aesthetic coherence.

6. LIMITATIONS OF EXISTING RESEARCH

Several limitations of this study should be considered when interpreting the results.

Firstly, the experiment was conducted within a relatively short timeframe. While participants were acquainted with the location of the images used in the experiment, temporal variations may have influenced observers' perceptions. Previous studies have demonstrated that immersion in an environment has a more significant impact on perception compared to viewing natural scenes or images.

Secondly, the sample predominantly comprised individuals under the age of 30, comprising 90 % of the participants. This demographic skew limits the generalizability of the results.

Future research endeavours should focus on exploring the interactions within complex scenes in real urban environments to gain a deeper understanding of the influence of lighting settings and parameters on people's perceptions. Moreover, efforts should be made to encompass a broader range of demographic groups, including varying age and gender categories, to ensure greater diversity within the study population.

ACKNOWLEDGMENTS

This research was partially funded by Slovenian Research Agency, grant number P2–0356.

REFERENCES

1. Boyce, P.R. The benefits of light at night // Building and Environment, 2019, # 151, pp. 356–367. https://doi.org/10.1016/j.buildenv.2019.01.020

2. Caborn, J.M. The experience of landscape // Landscape Planning, 1975, # 2, pp. 101–109. https://doi.org/10.1016/0304–3924(75)90022–2

3. Fisher, B.S., Nasar, J.L. Fear of crime in relation to three exterior site features // Environment and Behavior, 1992, Vol. 24, # 1, pp. 35–65. https://doi.org/10.1177/0013916592241002

4. Nasar, J.L., Fisher, B., Grannis, M. Proximate physical cues to fear of crime // Landscape and Urban Planning, 1993, Vol. 26, # (1–4), pp. 161–178. https://doi.org/10.1016/0169–2046(93)90014–5

5. Herzog, T.R., Kutzli, G.E. Preference and perceived danger in field/forest settings // Environment and Behavior, 2002, Vol. 34, # 6, pp. 819–835. https://doi.org/10.1177/001391602237250

6. Nasar, J.L., Jones, K.M. Landscapes of fear and stress // Environment and Behavior, 1997, Vol. 29, # 3, pp. 291–323. https://doi.org/10.1177/0013916597029 00301

7. Haans, A., de Kort, Y.A.W. Light distribution in dynamic street lighting: Two experimental studies on its effects on perceived safety, prospect, concealment, and escape // Journal of Environmental Psychology, 2012, Vol. 32, # 4, pp. 342–352. https://doi.org/10.1016/j.jenvp.2012.05.006

8. Uttley, J., Fotios, S., Cheal, C. Effect of illuminance and spectrum on peripheral obstacle detection by pedestrians // Lighting Research & Technology, 2017, Vol. 49, # 2, pp. 211–227. https://doi.org/10.1177/1477153515602954

9. Fotios, S., Mao, Y., Uttley, J., Cheal, C. Road lighting for pedestrians: Effects of luminaire position on the detection of raised and lowered trip hazards // Lighting Research & Technology, 2020, Vol. 52, # 1, pp. 79–93. https://doi.org/10.1177/1477153519827067

10. Fotios, S., Yang, B., Cheal, C. Effects of outdoor lighting on judgments of emotion and gaze direction // Lighting Research & Technology, 2015, Vol. 47, # 3, pp. 301–315. https://doi.org/10.1177/1477153513510311

11. Van Rijswijk, L., Haans, A. Illuminating for safety: Investigating the role of lighting appraisals on the perception of safety in the urban environment // Environment and Behavior, 2018, Vol. 50, # 8, pp. 889–912. https://doi.org/10.1177/0013916517718888

12. Wu, S., Kim, M. The relationship between the pedestrian lighting environment and perceived safety // Journal of Digital Landscape Architecture, 2016, # 1, pp. 57–66. https://doi.org/10.14627/537612007

13. Fotios, S., Monteiro, A.L., Uttley, J. Evaluation of pedestrian reassurance gained by higher illuminances in residential streets using the day – dark approach // Lighting Research & Technology, 2019, Vol. 51, # 4, pp. 557–575. https://doi.org/10.1177/1477153518775464

14. Dong, M., Fotios, S., Lin, Y. The influence of luminance, observation duration and procedure on the recognition of pedestrians' faces // Lighting Research & Technology, 2015, Vol. 47, # 6, pp. 693–704. https://doi.org/10.1177/1477153514539781

15. Boyce, P.R., Eklund, N.H., Hamilton, B.J., Bruno, L.D. Perceptions of safety at night under different lighting conditions // Lighting Research &

Technology, 2000, Vol. 32, # 2, pp. 79–9. https://doi.org/10.1177/096032710003200205

16. Fotios, S., Yang, B., Cheal, C. Effects of outdoor lighting on judgements of emotion and gaze direction // In Proceedings of CIE 2014 Lighting Quality and Energy Efficiency Conference, CIE, 2014, pp. 1–10.

17. Boomsma, C., Steg, L. Feeling safe in the dark: Examining the effect of entrapment, lighting levels, and gender on feelings of safety and lighting policy acceptability // Environment and Behavior, 2014, Vol. 46, # 2, pp. 193–212. https://doi.org/10.1177/0013916512453838

18. Nasar, J.L., Bokharaei, S. Impressions of lighting in public squares after dark // Environment and Behavior, 2017, Vol. 49, # 3, pp. 227–254. https://doi.org/10.1177/0013916515626546

19. Nasar, J.L., Bokharaei, S. Lighting modes and their effects on impressions of public squares // Journal of Environmental Psychology, 2017, Vol. 49, pp. 96–105. https://doi.org/10.1016/j.jenvp.2016.12.007

20. Fotios, S., Cheal, C. Erratum: Lighting for subsidiary streets: Investigation of lamps of different SPD. Part 2 – Brightness // Lighting Research & Technology, 2009, Vol. 41, # 4, pp. 381–383. https://doi.org/10.1177/1477153509347231

21. Fotios, S., Unwin, J., Farrall, S. Road lighting and pedestrian reassurance after dark: A review // Lighting Research & Technology, 2015, Vol. 47, # 4, pp. 449–469. https://doi.org/10.1177/1477153514524587

22. Holyoke, T.C., Heschong, L. Thermal delight in architecture // The Antioch Review, 1980, Vol. 38, # 2. https://doi.org/10.2307/4638315

23. Fotios, S. LRT Digest 1, maintaining brightness while saving energy in residential roads // Lighting Research & Technology, 2013, Vol. 45, # 1, pp. 7–21. https://doi.org/10.1177/1477153512464141

24. Wei, M., Houser, K. W., Orland, B., Lang, D., Ram, N., Sliwinski, M. Field study of office worker responses to fluorescent lighting of different CCT and lumen output // Journal of Environmental Psychology, 2014, # 39, pp. 62–76. https://doi.org/10.1016/j.jenvp.2014.04.009

25. Pan, W., Du, J. Impacts of urban morphological characteristics on nocturnal outdoor lighting environment in cities: An empirical investigation in Shenzhen // Building and Environment, 2021, # 192, 107587 p. https://doi.org/10.1016/j.buildenv.2021.107587

26. Gjerde, M. Visual evaluation of urban streetscapes: How do public preferences reconcile with those held by experts? // Urban Design International, 2011, Vol. 16, # 3. https://doi.org/10.1057/udi.2011.10

27. Boyce, P.R. Lighting for driving: Roads, vehicles, signs, and signals / CRC Press, 2008.

28. Moreno, I., Avendaño-Alejo, M., Saucedo-A, T., Bugarin, A. Modeling LED street lighting // Applied Optics, 2014, Vol. 53, # 20, pp. 4420–4429. https://doi.org/10.1364/ao.53.004420

29. Boyce, P.R. Human factors in lighting (3rd ed.) / CRC Press, 2014.

30. Nasar, J.L., Fisher, B. "Hot spots" of fear and crime: A multi-method investigation // Journal of Environmental Psychology, 1993, Vol. 13, # 3. https://doi.org/10.1016/S0272–4944(05)80173–2

31. Fotios, S., Cheal, C. Using obstacle detection to identify appropriate illuminances for lighting in residential roads // Lighting Research & Technology, 2013, Vol. 45, # 3, pp. 362–376. https://doi.org/10.1177/1477153512444112

32. Boomsma, C., Steg, L. Feeling safe in the dark: Examining the effect of entrapment, lighting levels, and gender on feelings of safety and lighting policy acceptability // Environment and Behavior, 2014, Vol. 46, # 2, 193–212. https://doi.org/10.1177/0013916512453838

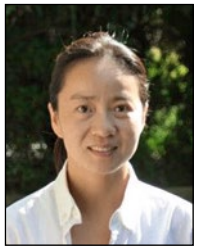

Lanlan Wei,
M. Arch. She is a Ph. D. Candidate at the University of Ljubljana, Faculty of Electrical Engineering. She has over 15 years of experience in lighting design, application, and urban planning. She worked with Signify China for more than a decade. Currently, she is an optical engineer and researcher specializing in road lighting applications in EU

Grega Bizjak,
Ph. D. He is a Full Professor and Head of Laboratory of Lighting and Photometry at Faculty of Electrical Engineering, University of Ljubljana. He is active in the field of lighting and photometry as well as in the field of electrical power engineering. His main research interests in lighting are photometry, energy efficient indoor and outdoor lighting, use of daylight and use of LEDs in lighting applications. Prof. Bizjak is President of Slovenian National Committee of CIE and representative of Slovenia in CIE Division 2

Matija Svetina,
Ph. D., Professor of Developmental Psychology at the University of Ljubljana, Department of Psychology. He is currently involved in several projects related to experimental, environmental, and urban psychology, including the assessment of cognitive and emotional load during environmental information processing, place attachment in the context of cultural heritage, and the assessment of psychological comfort in urban environments. He has been a research fellow and visiting professor at several academic institutions in Europe and North America

Matej Bernard Kobav,
Ph. D., Assistant Professor at the Laboratory of Lighting and Photometry at Faculty of Electrical Engineering, University of Ljubljana. The main part of his research field is in the field of lighting. He is mainly engaged in measurements, lighting simulations and exploitation of daylight in the indoor premises. He is also the general secretary of Lighting Engineering Society of Slovenia and Slovenian representative in CIE Division 3

Light & Engineering
Vol. 33, No. 4, pp. 15–26, 2025

https://doi.org/10.33383/2024-094
Svetotekhnika # 3, 2025, pp. 70–79

LIVING ROOM ATMOSPHERES: EXPLORING HOW LUMINANCE CONTRAST AND COLOUR INFLUENCE DOMESTIC SPACE

Ipek Yalcin and *Nilgun Olgunturk

Department of Interior Architecture and Environmental Design, Faculty of Art, Design and Architecture, Bilkent University, Ankara, Turkey
**E-mail: onilgun@bilkent.edu.tr*

ABSTRACT

Living rooms are shaped by functional, aesthetic, and socio-economic choices and formed by visual factors such as luminance contrast and colour schemes that create distinct atmospheres. Using a single living room image with digitally manipulated luminance contrast levels and colour schemes (warm, cool, and grey), 35 Turkish participants evaluated the emotional and cognitive effects of these variations. Results indicate that luminance contrast significantly shapes the perception of atmosphere, with higher contrast contributing to more vibrant and lively spaces, while low-contrast grey schemes led to more subdued, negative associations. Gender differences emerged in the perception of certain adjectives, such as 'depressing' and 'uncomfortable'. By examining how visual elements create distinct atmospheres in domestic spaces, this study offers insights relevant to interior design and domestic architecture, contributing to a deeper understanding of how material and sensory elements influence the experience of home environments.

Keywords: luminance contrast, colour schemes, perceived atmosphere, emotional response, living room interiors, interior design

1. INTRODUCTION

Recent studies on the atmosphere have focused on this aesthetic value of space as how it emerges in certain conditions and how it can be created in different contexts. Among the key elements contributing to an environment's atmosphere is light, yet limited research explores its role in quality, specifically within home environments. Given the centrality of the home in a person's daily life cycle, especially the living room, investigating how light influences the atmosphere in residential spaces is necessary.

The living room is unique within the topic of residential spaces, as it does not only serve as a functional space but also as a place where individuals express their identities into physical environments through design elements [1]. The living room becomes a reflection of a person's preferences for colour, light, shape, and other physical aspects [2]. This makes the physical components of living rooms, including daylight availability, surface areas, and material choices, particularly significant yet these have received relatively little attention [3]. Living rooms are central spaces within homes, serving as both functional and atmospheric environments that influence the daily experiences of their inhabitants. Light, as Bohme asserts, is a primary contributor to the atmosphere in any environment, but it cannot be understood in isolation from surrounding surfaces, which vary in colour and material [4]. Visual factors like colour and light are "spatial, holistic, dynamic, and contextual", as noted by Arnkil et al. [5]. Thus, these elements must be evaluated together, especially in residential spaces, where elements like warm and cool tones, as well as light and dark contrasts, play an essential role in shaping the atmosphere [6]. Focusing on the interplay between lighting and design elements, this study investigates how luminance contrast and co-

lour schemes impact the perceived atmosphere in living rooms.

Luminance contrast, or the variation in an object's brightness from its backdrop, is the fundamental for vision. Additionally, in the material and sensory dimensions of domestic life, different luminance contrasts can evoke different emotional responses in people, particularly in how people experience home spaces on a sensory and emotional level. By examining how luminance contrast and colour shape the atmosphere of home environments, this research aims to offer valuable insights into designing interiors that foster both emotional resonance and functional efficiency. The optimization of luminance contrast can enhance the overall experience of living spaces by balancing visual elements, like luminance contrast and colour, to influence the perception of domestic spaces.

2. LITERATURE REVIEW

Current study concentrates on whether or not there is a significant difference in perceived atmosphere descriptions depending on the luminous contrast levels and colour schemes in images. Therefore, the method of this study is based on two main concepts: perceived atmosphere and light as luminance contrast, a unified approach to study distribution of light in the built environments.

2.1. Perceived Atmosphere and Light

Defined as the effect, the atmosphere can be the interactions between subject and object and subject to subject [7]. In 2008, Vogels compiled a list of descriptive atmospheric statements to assess the experienced atmospheres by the observers in the built environments [8]. The following inquiries examined the effects of light uniformity and intensity on spatial impressions in real-life or controlled situations where the generated atmosphere questionnaire assessed different lighting conditions [9]. A posteriori to these approaches that explored perceived atmosphere and its relation to light in an environment, here, the luminance contrast measure is proposed to consider different light qualities in more complicated contexts, such as common conditions. Images are one practical way to study these complex and diverse conditions which frequently reflect real spaces and depict designed subjects [10]. When comparing the room's atmosphere and lighting, images statistically replicate the lighting impression of real-world settings or physically-based models [11]. It is possible to probe the perceived atmosphere and measure light in that environment by evaluating images as atmospheric sceneries. Hence previous studies denote no observed differences in the way the real and virtual environments were perceived for the lighting or room impressions based on subjective evaluations of appearance (brightness, CCT, distribution) and high-order perceptions (pleasantness, interest, spaciousness, excitement, and complexity) [12]. The simulations' reliability on the computer screen and video projector was also evaluated against a mock-up in which the contrast and brightness of the lighting were equivalent across different mediums [13].

While light is a fundamental atmosphere generator, colour is a key visual attribute to be considered in represented environments. According to a recent survey, black, grey, and white are seen as colours independent of one's degree of colour expertise [14]. One response to why white, grey, and black are colours is "because we see and distinguish them". A further reaction to these colours and their unique relationship to contrast is "Because contrast differences can be observed and they can be named and differentiated". These findings draw attention to the relation between contrast and light especially for achromatic images, however, the subject of living room atmosphere can't be explored without colour. Unlike prior studies focusing primarily on colour for aesthetic concerns, this research emphasizes luminance contrast as the dominant variable, while colour is treated as a secondary contextual element. This controlled setting makes it possible to investigate how emotional and cognitive perceptions of space are influenced by visual cues such as luminance contrast, which advances our knowledge of how we interpret home interiors. Therefore, luminance contrast was investigated to utilise it as a unified variable for studying light, material, and colour within the space.

2.2. Luminance Contrast

Contrast in an image or display context is the variation in brightness within the same field of vision [15]. Brightness, the perceptual correlation of light intensity, and spatial frequency, the rate at which stimuli vary in a specific region, are the primary components of any visual input associated

with contrast measurements. Scenes are interpreted in terms of spatial frequencies [16]. The spatial frequency, a property of any periodic structure that quantifies the frequency at which sinusoidal components of the structure repeat per unit of distance, may be used to indicate the light intensity in the stimulus [17]. Because all components mix into a single smooth representation, "observers are unaware of the individual spatial frequency components in most cases" [18]. Still, the image's appearance varies with different spatial frequencies, as does the information transmitted. Different methods might be used to quantify luminance contrast depending on these factors. Depending on how contrast is interpreted in various images, the photo metric measurement of contrast can lead to identical or entirely different findings.

The approach used to calculate contrast in the context of visual input may also be based on simple or complex features of the image. Natural images become more complicated as changes in spatial frequency, brightness, and distribution characteristics are amplified. To address this issue, an alternative method between the perceived and measured physical contrast for complex images was proposed as "spatial luminance contrast" [19]. To assess contrast, this process computes the brightness variation between adjacent pixels. The pixel brightness variation between adjacent pixels is determined using a pyramid method for various resolution levels of the same image. Each level generates a new pixel value representing a new pixel of the lower-resolution image by calculating the brightness contrast of eight surrounding pixels around the core pixel. Next, a higher level in the resolution pyramid's value is defined using these values again. The total contrast value of the same image is determined for every resolution level, from high to low. Hence, this method considers brightness, spatial frequency, and contrast for complex images.

Spatial Luminance Contrast was utilised over architectural images in 2016 by Rockcastle et al. [20]. They discovered that visual interest with subjective ratings may be predicted by this combination metric, RAMMG. Based on subjective assessments, the RAMMG5 measure was determined to be consistent with the fifth level of the resolution pyramid method. Thus, the monitor luminance of pixel contrast for the experimental images is calculated using this method in the current research.

In lighting quality assessment, research has increasingly focused on objective criteria to complement traditional subjective evaluations. Budak, Zheltov, and Meshkova conducted an extensive study at 21 Moscow Metro stations, developing a new criterion for lighting quality based on the spatial and angular distribution of luminance [21]. Their work demonstrated that luminance mapping, derived from RAW-format images adjusted with luminance meter readings, provided a strong correlation with expert assessments of lighting quality. This method enabled a more structured and empirical approach to evaluating how light interacts with architectural spaces. Similarly, their 2021 study introduced the concept of luminance spatial-angular distribution (LSAD), which aimed to improve upon the limitations of conventional metrics like the unified glare rating (UGR) [22]. By formulating an integral equation for LSAD, they highlighted the necessity of spatial brightness variations in assessing lighting quality, showing that a purely intensity-based evaluation lacks the nuance required for real-world applications.

While these studies rely on meticulously recorded luminance distributions and expert evaluations, the approach taken in this research provides an alternative yet complementary perspective. The algorithm proposed in this article employs pixel luminance values to calculate contrast, inherently capturing brightness variations across an image. Unlike LSAD, which emphasizes the angular distribution of luminance and its effect on perceived glare, this algorithm probes whether luminance contrast metrics can serve as an efficient proxy for lighting quality assessment. By focusing on contrast variations rather than absolute luminance levels, this method has the potential to assess how lighting affects the atmosphere of a scene – offering a computationally efficient way to bridge objective measurements with perceptual experience. In essence, while the referenced studies provide a high-precision framework for structured lighting analysis, this research explores a more adaptable and scalable approach that may prove valuable in dynamic or less-controlled environments where direct luminance measurements are impractical.

3. METHODS AND PROCEDURE

This study has two phases to investigate luminance contrast, colour attributes, and perceived at-

mosphere in the living room. The first phase is conducted to specify atmosphere adjectives concerning luminance contrast. Then, the image set was generated for a structured variance of luminance contrast values and three colour attributes as the second phase. Together, the experiment presented each image separately and collected atmosphere adjective ratings per image viewing.

3.1. First Phase: Atmosphere Adjectives

In a preliminary investigation, terms describing an atmosphere with light-related environments were regrouped. Vogels' three categories [8]; related to the emotion or mood evoked by the environment, related to the atmosphere of the environment, and terms that provide a more or less objective description of the environment, were formed by gathering adjectives from earlier studies about impressions of light, light, and atmosphere. Adjectives that did not fit into any category were removed, including those that described light sources, expressed views, evaluated the design style, and dealt with other senses (taste, hearing, touch, etc.). The environment-related adjectives were translated into Turkish. In addition to adjectives with the same or similar meanings, adjectives that lost their meaning after translation were also removed. Finally, the following statement was used to control the remaining adjectives' validity as atmospheric words: "This area/location is _____". A total of 54 Turkish atmosphere adjectives were finalized and rated in the preliminary atmosphere and light research. The results showed the prolonged impacts of light on a scene's overall atmosphere. The Principal Component Analysis results identified three components. The adjectives in the second component, referred to as luminance contrast, were proven to be linked with the contrast levels of the images, see Table 1. Contrarily, components one and three describe the perceived environment of light in terms of concepts other than luminance contrast. These adjectives will be rated in the online questionnaire to test a significant difference between perceived atmosphere adjectives concerning luminous contrast levels with the basic colour categories as warm, cool, and grey schemes.

Fig. 1. The original living room image

3.2. Second Phase: the Image Set

Image properties relating to its format were requisite of the RAMMG contrast measure. Several living room images were taken with a *Canon 60D DSLR* camera with an *EF-S 18–135mm f3.5–5.6 Lens*. The primary goal was to have surfaces in the living room that could be adjusted to different light levels and colour combinations. Content was also a crucial component of the living room. Any connotations for trends and culture and the aesthetics of photographic framing were limited by capturing generic scenes from the living room. The selected living room contained modern everyday items such as screens and designed items at a minimum. No human figures were included while preserving a variety of daylight, different functions, sizes, and geometry of space and materials. No additional criteria were used to maintain the conventional living room in the images regarding the room's atmosphere.

RGB channels of the selected living room image in Fig. 1 were converted to a single grey-scale layer to calculate the luminance contrast of the original image. Using Python programming software, version 3.10.4 (2022), the standard RGB to grey-scale conversion formula below was applied to the image. Thus, the value of each pixel was the weighted sum of the corresponding pixels' red, green, and blue pixels contribution:

$$L = 0.2126\ \mathrm{R} + 0.7152\ \mathrm{G} + 0.0722\ \mathrm{B}. \qquad (1)$$

The original image's RAMMG 5 luminance contrast measure provided a baseline before manipulating for other contrast levels. After manipulating the main surface brightness, such as the wall, ceiling, and floor areas, the original image's low, med, and high luminance contrast versions were obtained. The colour attributes of these photographs were then adjusted in cool, warm, and grey categories by

Table 1. Atmosphere Adjectives which Correlate with the Luminance Contrast of Images

Lively	Lifeless	Exciting	Depressing	Dynamic	Subdued
Bright	Dark	Roomy	Narrow	Transparent	Blurry
Intimate	Gloomy	Uncomfortable			

manipulating the textile colours of the sofa, pillows, curtains, and the reflected light colours on the hard surfaces in Fig. 2. Since this study primarily probes the luminance contrast of images, the colour alterations were adjusted to the target luminance contrast values set after the original image.

Due to the relative values subject to the display properties, luminance contrast results or histograms of calibrated images were not featured here. Instead, these results were grouped into low, med, and high contrast categories. This way, these luminance contrast categories could be referred to in future studies' varying displays and image sets. The image count and sample size were also bound to the rated atmosphere adjectives. While it's beneficial to keep the image variety, the duration of the experiment was another constraint. In conclusion, nine images, three for each contrast category, were specified for their colour attributes and RAMMG5 results.

3.3. Procedure

All the subjects have provided informed consent and the experiment ethical approval was obtained from Bilkent University Ethics Committee with No2022_02_22_01. Participants in this experiment had to be native Turkish speakers without any visual impairments. The online experiment contained a screen brightness calibration. The participants were asked to adjust their computer screens to view the wide range of grey colours through a brightness calibration graphic. Additionally, they were asked to complete the survey in a dark environment where the only light source would be the screen.

There were no time restrictions on the display duration of the images. Each participant was asked to rate fifteen atmosphere adjectives separately while viewing a single image. All nine images and the order of adjectives were randomized for the entire questionnaire. This way, three different levels of luminance contrast with warm, cool, and grey colour attributes were viewed for the same living room.

4. RESULTS

35 Turkish participants, 14 male and 21 female, completed the online experiment. Their average age was 30, and they were between 19 and 38. All participants had undergraduate (10), graduate (13) or Ph. D. (12) level educations and majored in varying fields such as interior architecture and environmental design, architecture, communication and design, management, dentistry, and law. With IBM SPSS Statistics software version 28 (2001), one-way ANOVA and post hoc tests were performed to determine the difference in rated atmosphere adjectives in relation to the luminance contrast and colour attribute of images, respectively.

Analysing the data using analysis of variance (ANOVA) or another test that implies normalcy may increase risk of a false positive result if the measurement variable is not normally distributed. However, simulation studies using a range of non-normal distributions have demonstrated, a moderate deviation from normality does not significantly affect the false positive rate of an ANOVA [23–25]. The data set appeared to be mostly normal after examining the frequency histogram, therefore this study continued with ANOVA tests to examine gender, colour, and luminance contrast differences among 15 atmosphere adjectives which have been rated in 5-point Likert scale between "strongly disagree" to "strongly agree".

Fig. 2. The warm, grey, and cool colour variations of med level luminance contrast category image

Table 2. Separate Post Hoc Test Results for Luminance Contrast and Colour Groups for Atmosphere Adjective Ratings

Multiple Comparisons (Tukey HSD) between Contrast Groups				**Multiple Comparisons (Tukey HSD) between Colour Groups**			
Atmosphere Adjectives (Dependent Variable)	(*I*) Luminance Contrast	(*J*) Luminance Contrast	Mean Difference (*I-J*)	Atmosphere Adjectives (Dependent Variable)	(*I*) Colour	(*J*) Colour	Mean Difference (*I-J*)
Lively	Low Contrast	Med	–182	Lively	Warm	Cool	1.192*
		High	–.566*			Grey	1.333*
	High Contrast	Med	384		Grey	Cool	–141
Bright	Low Contrast	Med	–.455*	Lifeless	Warm	Cool	–1.202*
		High	–.929*			Grey	–1.242*
	High Contrast	Med	.475*		Grey	Cool	40
Dark	Low Contrast	Med	.616*	Bright	Warm	Cool	.758*
		High	1.162*			Grey	.616*
	High Contrast	Med	–.545*		Grey	Cool	141
Gloomy	Low Contrast	Med	.545*	Dark	Warm	Cool	–.869*
		High	.909*			Grey	–.747*
	High Contrast	Med	–364		Grey	Cool	–121
Depressing	Low Contrast	Med	.444*	Intimate	Warm	Cool	.727*
		High	.687*			Grey	.919*
	High Contrast	Med	–242		Grey	Cool	–192
Roomy	Low Contrast	Med	–283	Gloomy	Warm	Cool	–.899*
		High	–.455*			Grey	–.707*
	High Contrast	Med	172		Grey	Cool	–192
Narrow	Low Contrast	Med	364	Exciting	Warm	Cool	.828*
		High	.424*			Grey	1.061*
	High Contrast	Med	–61		Grey	Cool	–232
Uncomfortable	Low Contrast	Med	374	Depressing	Warm	Cool	–.687*
		High	.505*			Grey	–.424*
	High Contrast	Med	–131		Grey	Cool	–263
Dynamic	Low Contrast	Med	–30	Uncomfortable	Warm	Cool	–.566*
		High	–.566*			Grey	–.586*
	High Contrast	Med	.535*		Grey	Cool	20

Multiple Comparisons (Tukey HSD) between Contrast Groups				**Multiple Comparisons (Tukey HSD) between Colour Groups**			
Atmosphere Adjectives (Dependent Variable)	(*I*) Luminance Contrast	(*J*) Luminance Contrast	Mean Difference (*I-J*)	Atmosphere Adjectives (Dependent Variable)	(*I*) Colour	(*J*) Colour	Mean Difference (*I-J*)
Subdued	Low Contrast	Med	162	Dynamic	Warm	Cool	.818*
		High	.495*			Grey	1.101*
	High Contrast	Med	–333		Grey	Cool	–283
Blurry	Low Contrast	Med	.414*	Subdued	Warm	Cool	–1.000*
		High	.515*			Grey	–1.192*
	High Contrast	Med	–101		Grey	Cool	192
*The mean difference is significant at the 0.016 level.				Blurry	Warm	Cool	–343
						Grey	–.455*
					Grey	Cool	111
				*The mean difference is significant at the adjusted 0.016 level.			

4.1. Analysis

The effect of colour and luminance contrast was analysed separately for all adjectives. No effect of colour category was observed for the atmosphere adjectives roomy, narrow, and transparent (p=0.181, 0.016, and 0.042 at p<0.016 significance level adjusted for one way ANOVA). Levene test for homogeneity of variance only showed bright adjective as not suitable for Tukey HSD Post Hoc test. Additionally, no effect of luminance contrast was observed for the atmosphere adjective lifeless, exciting, transparent, and intimate (p=0.021, 0.093, 0.030, and 0.438 at p<0.016 significance level adjusted for one way ANOVA). Post Hoc test, Tukey HSD results show which contrast groups or colour group ratings differed for the remaining adjectives, see Table 2.

A second analysis compared the means of the combination of colour and luminance contrast per atmosphere adjective. Describing positive and negatively associated adjectives is an alternative way to interpret their relation to contrast and colour variances. Positively associated atmosphere adjectives were agreed upon, rating means were above neutral, for high or low contrast in warm images, see Table 3. Except for the bright adjective, which was agreed for high contrast grey images, and roomy adjective, which was agreed for high contrast grey and warm images.

Negatively associated atmosphere adjectives were rated above neutral (3.00), in other words agreed on for cool and grey images of varying contrast levels. However, no image with warm colours was agreed for negative atmosphere adjectives. Low contrast grey images were perceived as dark and lifeless atmospheres for the living room image, see Table 4. Hence, the low contrast grey combination in the living room was the agreed rating result for all the negative adjectives.

Additionally, the atmosphere adjective responses for depressing, narrow, uncomfortable, and transparent were found statistically different between genders. Transparent and narrow adjectives are significant at the 0.01 level, depressing and uncomfortable adjectives are significant at the 0.05 level (2-tailed Spearman's correlation).

5. CONCLUSIONS

This study explores how homes are experienced and understood, providing insights into how design elements such as lighting and colour shape that experience. By focusing on luminance contrast and colour, the research highlights how physical and sensory factors – like light and material choices – affect the feel and functionality of domestic spaces. The use of a controlled, single living room image with pixel-based luminance contrast calculations

Table 3. Means of the Positive Atmosphere Ratings on 5-Point Liker-Scale from "Strongly Disagree" to "Strongly Agree"

Contrast and Colour Combination per Adjective		Mean	Contrast and Colour Combination per Adjective		Mean
Lively	Low contrast – Cool	1.85	Dynamic	Low contrast-Cool	1.94
	Med contrast – Grey	2.24		Med contrast-Grey	2.03
	High contrast – Warm[a]	3.88		High contrast-Warm[a]	3.70
	Med contrast – Warm	2.82		Med contrast-Warm	2.45
	High contrast – Grey	2.15		High contrast-Grey	2.24
	High contrast – Cool	2.36		High contrast – Cool	2.52
	Med contrast – Cool	2.18		Med contrast – Cool	2.36
	Low contrast – Grey	1.58		Low contrast – Grey	1.70
	Low contrast – Warm[a]	3.27		Low contrast – Warm[a]	3.12
Intimate	Low contrast – Cool	2.61	Bright	Low contrast – Cool	2.21
	Med contrast – Grey	2.52		Med contrast – Grey	2.88
	High contrast – Warm [a]	3.61		High contrast – Warm	3.88
	Med contrast – Warm	3.00		Med contrast – Warm	2.88
	High contrast – Grey	2.61		High contrast – Grey[a]	3.18
	High contrast – Cool	2.58		High contrast – Cool	2.67
	Med contrast – Cool	2.73		Med contrast – Cool	2.55
	Low contrast – Grey	2.21		Low contrast – Grey	1.79
	Low contrast – Warm[a]	3.48		Low contrast – Warm	2.94
Exciting	Low contrast – Cool	1.76	Roomy	Low contrast – Cool	2.73
	Med contrast – Grey	1.82		Med contrast – Grey	2.94
	High contrast – Warm[a]	3.12		High contrast – Warm [a]	3.24
	Med contrast – Warm	2.45		Med contrast – Warm	2.91
	High contrast – Grey	2.00		High contrast – Grey[a]	3.03
	High contrast – Cool	2.18		High contrast – Cool	2.88
	Med contrast – Cool	2.18		Med contrast – Cool	2.79
	Low contrast – Grey	1.61		Low contrast – Grey	2.27
	Low contrast – Warm[a]	3.03		Low contrast – Warm	2.79

[a]Rated adjective mean is above the neutral (3.00) and agreed in varying degrees

allowed us to isolate and examine the specific effects of luminance and colour. Findings indicate that luminance contrast is a dominant factor in how individuals cognitively process and emotionally respond to interior spaces, with lower contrasts, particularly in grey schemes, leading to negative perceptions such as lifelessness.

The exploratory nature of this study also uncovered interesting patterns in how participants rated atmosphere adjectives. Notably, gender differences emerged, with female participants diverging from male participants on terms such as 'depressing', 'narrow', 'uncomfortable', and 'transparent'. While male participants remained neutral on these descriptors, female participants disagreed, reflecting a more nuanced perception of the space based on luminance contrast and colour. This finding underscores the complexity of perceived atmosphere, which cannot always be captured through simple bipolar descriptions or linear correlations.

A prior study found that different brightness and perceived uniformity combinations may indicate the same atmosphere dimensions [9]. For example, perceived uniformity was found to change greatly without influencing the perceived liveliness of the environment. We found that the participants tend-

Table 4. Means of the Negative Atmosphere Ratings on 5-Point Likert Scale from "Strongly Disagree" to "Strongly Agree"

Contrast and Colour Combination per Adjective		Mean	Contrast and Colour Combination per Adjective		Mean
Lifeless	Low contrast – Cool[a]	3.85	Depressing	Low contrast – Cool[a]	3.33
	Med contrast – Grey[a]	3.27		Med contrast – Grey	2.76
	High contrast – Warm	2.06		High contrast – Warm	2.00
	Med contrast – Warm	2.91		Med contrast – Warm	2.58
	High contrast – Grey[a]	3.36		High contrast – Grey	2.55
	High contrast – Cool[a]	3.39		High contrast – Cool[a]	3.15
	Med contrast – Cool[a]	3.48		Med contrast – Cool[a]	3.09
	Low contrast – Grey[b]	4.21		Low contrast – Grey[a]	3.48
	Low contrast – Warm	2.15		Low contrast – Warm	2.94
Dark	Low contrast – Cool[a]	3.70	Narrow	Low contrast – Cool	2.91
	Med contrast – Grey	2.94		Med contrast – Grey	2.70
	High contrast – Warm	1.52		High contrast – Warm	2.42
	Med contrast – Warm	2.79		Med contrast – Warm	2.58
	High contrast – Grey	2.48		High contrast – Grey	2.45
	High contrast – Cool[a]	3.09		High contrast – Cool[a]	3.03
	Med contrast – Cool	3.00		Med contrast – Cool	2.82
	Low contrast – Grey[b]	4.00		Low contrast – Grey[a]	3.58
	Low contrast – Warm	2.88		Low contrast – Warm	2.70
Gloomy	Low contrast – Cool[a]	3.67	Uncomfortable	Low contrast – Cool[a]	3.27
	Med contrast – Grey	2.94		Med contrast – Grey	2.67
	High contrast – Warm	1.85		High contrast – Warm	2.15
	Med contrast – Warm	2.67		Med contrast – Warm	2.52
	High contrast – Grey	2.64		High contrast – Grey	2.79
	High contrast – Cool[a]	3.21		High contrast – Cool	2.70
	Med contrast – Cool[a]	3.18		Med contrast – Cool	2.85
	Low contrast – Grey[a]	3.91		Low contrast – Grey[a]	3.42
	Low contrast – Warm	2.85		Low contrast – Warm	2.45
Blurry	Low contrast – Cool	2.79	Subdued	Low contrast – Cool[a]	3.73
	Med contrast – Grey	2.39		Med contrast – Grey[a]	3.30
	High contrast – Warm	1.88		High contrast – Warm	1.88
	Med contrast – Warm	2.42		Med contrast – Warm	2.97
	High contrast – Grey	2.61		High contrast – Grey[a]	3.48
	High contrast – Cool	2.58		High contrast – Cool[a]	3.18
	Med contrast – Cool	2.55		Med contrast – Cool[a]	3.27
	Low contrast – Grey[a]	3.24		Low contrast – Grey[a]	3.97
	Low contrast – Warm	2.58		Low contrast – Warm	2.33

[a]Rated adjective mean is above the neutral (3.00) and agreed in varying degrees
[b]Rated adjective mean is above the agree (4.00)

Table 5. Atmosphere Adjectives Correlate with the Luminance Contrast of Images

Lively	Lifeless	Exciting[a]	Depressing[c]	Dynamic	Subdued
Bright	Dark	Roomy[b]	Narrow[b c]	Transparent[a b c]	Blurry
Intimate[a]	Gloomy	Uncomfortable[c]			

[a]Marks not significant adjectives for luminance contrast; [b]Marks not significant adjectives for colour categories; [c]Marks statistically different adjectives for gender.

ed to agree on certain adjectives for particular luminance contrast groups and colour categories. The experiment results showed no effect of luminance contrast for "lifeless", "exciting", "transparent", and "intimate" descriptions of atmosphere. Only for the negative adjectives means were above 3.00 (neutral), in other words participants have agreed upon the negative atmosphere descriptions in relation to luminance contrast. Low luminance contrast should be avoided to prevent "dark", "gloomy", "uncomfortable", "depressing", "narrow", "subdued", and "blurry" perceived atmosphere results. However positive adjectives ("lively", "bright", and "dynamic") were disagreed upon in all contrast categories, suggesting the other aspects of the room design should be considered as influencing these atmosphere results. When both studies are compared the design of the room and/or the usage of electric light in the scene appears as a factor to be considered. This study examined a single living room, and the fact that the environment adjectives "roomy", "narrow", and "transparent" were not found among the colour variations may have something related with the room's dimensions and material properties.

Another finding was that cool colours were significantly different in comparison with warm colours for the "lively", "lifeless", and "bright" adjectives. No significance could be found for other atmosphere adjectives nor any difference when compared to grey colours. For the remaining eleven adjectives plus the "bright" adjective, participants agreed on the warm living room condition while disagreeing on positively associated adjectives for the grey option, and vice versa for the negative adjectives.

This study has demonstrated the extent of interaction between perceived atmosphere and the observer. A high or low contrast environment can be associated with positive atmosphere descriptions, but may also be perceived negatively depending on the colour category. The adjectives found to be significant varied based on luminance contrast, colour, their combinations, and the gender of observers, see Table 5. The variation seen across different conditions suggests that atmosphere is an influencing phenomenon rather than a determining factor in how an environment is perceived.

Since luminance contrast values are relative to display properties, numerical results or histograms of calibrated images were not included in this study. Instead, luminance contrast was grouped into low, medium, and high categories, ensuring that the findings remain applicable across varying displays and image sets in future research. This approach allows for greater comparability in subsequent studies examining different lighting conditions or room designs. It is also important to consider the broader context in which people construct their homes. As previous research suggests, residents must work within material, sensory, and social constraints to shape their living environments [26, 27]. This study's methodology contributes to understanding how these constraints impact atmosphere perception and offers practical applications for interior design and architecture. Probing deeper into these dynamics can improve the way we communicate and design spaces with the necessary atmospheres, enhancing both functionality and emotional resonance.

Examining a single living room was a limitation of this study, yet it provided a focused and controlled environment to explore the interaction of light, colour, and materials. Future studies could build on these findings by exploring luminance contrast and colour perception across different architectural contexts and lighting conditions. The application of AI-based image analysis and machine learning models could provide predictive tools for assessing perceived atmosphere based on luminance and colour properties. Additionally, integrating these findings into virtual reality simulations with real-time adjustments to illumination and material properties could further validate and expand on the role of luminance contrast in shaping interior environments. These advancements could contribute to more adaptive design strategies, ensuring that

interior spaces are both functionally effective and emotionally engaging.

6. DISCLOSURE STATEMENT

The authors report there are no competing interests to declare.

REFERENCES

1. Vercell, K. From function to fantasy in the new American home // Home Cultures, 2023, Vol. 20, # 1, pp. 19–42. https://doi.org/10.1080/17406315.2023.2206764.

2. Maki, K. Relationship between interior preferences and personal attributes // Proceedings of the Department of Environment, Architectural Institute of Japan, 2018, Vol. 83, # 752, pp. 811–819. https://doi.org/10.3130/aije.83.811.

3. Moore, J. Placing home in context // Journal of Environmental Psychology, 2000, Vol. 20, pp. 207–217. https://doi.org/10.1006/jevp.2000.0178.

4. Böhme, G. Atmospheric architectures: The aesthetics of felt spaces // Schwarzpaul, E. (ed.) Atmospheric architectures: The aesthetics of felt spaces, 1st ed., Bloomsbury, 2017.

5. Arnkil, H., Anter, K.F., Klarén, U. Colour and light: Concepts and confusions / Aalto University, 2012.

6. Jacobson, M., Silverstein, M., Winslow, B. The Good House: Contrast as a design tool / Taunton Press, 1990.

7. Griffero, T. Architectural affordances: The atmospheric authority of spaces // Tidwell, P. (ed.) Architecture and atmosphere / Tapio Wirkkala-Rut Bryk Foundation, 2014, pp. 15–47.

8. Vogels, I. Atmosphere metrics: Development of a tool to quantify experienced atmosphere // Law, E., Van den Hoven, E. (eds.) Probing experience from assessment of user emotions and behaviour to development of products, Springer, 2008, pp. 47–58.

9. Stokkermans, M., Vogels, I., de Kort, Y., Heynderickx, I. Relation between the perceived atmosphere of a lit environment and perceptual attributes of light // Lighting Research and Technology, 2018, Vol. 50, # 8, pp. 1164–1178. https://doi.org/10.1177/1477153517722384.

10. Flynn, J.E., Spencer, T.J., Martyniuk, O., Hendrick, C. Procedures for investigating the effect of light on impression: Simulation of a real space by slides // Environment and Behaviour, 1997, Vol. 9, # 4, pp. 491–510. https://doi.org/10.1177/00139165779400330.

11. Engelke, U., Stokkermans, M.G.M., Murdoch, M.J. Visualizing lighting with images: Converging between the predictive value of renderings and photographs // Human Vision and Electronic Imaging, 2013, Vol. XVIII, pp. 8651–86510L. https://doi.org/10.1117/12.2008465.

12. Kim, D.H., Mansfield, K. Creating positive atmosphere and emotion in an office-like environment: A methodology for the lit environment // Building and Environment, 2021, Vol. 194, 107686 p. https://doi.org/10.1016/j.buildenv.2021.107686.

13. Schielke, T. Validity of simulations for lighting and brand image evaluation // Lighting Research and Technology, 2016, Vol. 48, # 4, pp. 473–490. https://doi.org/10.1177/1477153515589116.

14. Caivano, J.L. Black, white, and greys: Are they colours, absence of colour or the sum of all colours? // Colour Research and Application, 2022, Vol. 47, # 2, pp. 252–270. https://doi.org/10.1002/col.22727.

15. Einhäuser, W., König, P. Does luminance-contrast contribute to a saliency map for overt visual attention? // European Journal of Neuroscience, 2003, Vol. 17, # 5, pp. 1089–1097. https://doi.org/10.1046/j.1460–9568.2003.02508.x.

16. Kauffmann, L., Ramanoël, S., Peyrin, C. The neural bases of spatial frequency processing during scene perception // Frontiers in Integrative Neuroscience, 2014, Vol. 8, p. 37. https://doi.org/10.3389/fnint.2014.00037.

17. Sekuler, R., Blake, R. Perception / McGraw-Hill, 2002.

18. Westheimer, G. The Fourier theory of vision // Perception, 2001, Vol. 30, # 5, pp. 531–541. https://doi.org/10.1068/p3193.

19. Rockcastle, S., Andersen, M. Measuring the dynamics of contrast and daylight variability in architecture: A proof-of-concept methodology // Building and Environment, 2014, Vol. 81, pp. 320–333. https://doi.org/10.1016/j.buildenv.2014.06.012.

20. Rockcastle, S., Amundadottir, M.L., Andersen, M. Contrast measures for predicting perceptual effects of daylight in architectural renderings // Lighting Research and Technology, 2016, Vol. 0, # 1, pp. 1–22. https://doi.org/10.1177/1477153516644292.

21. Budak, V.P., Zheltov, V.S., Meshkova, T.V. Experimental study of the new criterion of lighting quality based on analysis of luminance distribution at Moscow Metro stations // Light & Engineering, 2020, Vol. 28, # 3, pp. 98–105.

22. Budak, V.P., Zheltov, V.S., Meshkova, T.V. Lighting quality criteria based on the luminance spatial-angular distribution // Proceedings on Computer Graphics and Lighting Engineering, 2021, Vol. 1.

23. Glass, G.V., Peckham, P.D., Sanders, J.R. Consequences of failure to meet assumptions underlying the fixed effects analyses of variance and covariance // Review of Educational Research, 1992, Vol. 42, pp. 237–288.

24. Harwell, M.R., Rubinstein, E.N., Hayes, W.S., Olds, C.C. Summarizing Monte Carlo results in methodological research: The one- and two-factor fixed effects ANOVA cases // Journal of Educational Statistics, 1992, Vol. 17, # 4, pp. 315–339. https://doi.org/10.2307/1165127.

25. Lix, L.M., Keselman, J.C., Keselman, H.J. Consequences of assumption violations revisited: A quantitative review of alternatives to the one-way analysis of variance "F" test // Review of Educational Research, 1996, Vol. 66, # 4, pp. 579–619. https://doi.org/10.2307/1170654.

26. Pink, S. (ed.) In and out of the academy: Video ethnography of the home // Applied Visual Anthropology, a guest edited issue of Visual Anthropology Review, 2004, Vol. 20, # 1, pp. 82–88.

27. Miller, D. (ed.) Home possessions: Material culture behind closed doors, 1st ed. / Routledge, 2001. https://doi.org/10.4324/9781003085607.

Ipek Yalcin,
M. A. in Lighting Design. She graduated from Bilkent University in Ankara, Turkey, with a B. A. (Hons.) in Interior Architecture and Environmental Design. She earned an M. A. in Lighting Design from Edinburgh Napier University in Edinburgh, Scotland, because of her studies in exhibition design and lighting. She is currently interested in studying vision and perception in relation to contemporary aesthetics like atmosphere and design quality. Additionally investigating potential avenues for future research based on novel methods for image analysis

Nilgun Olgunturk,
Associate Professor in the Interior Architecture and Environmental Design Department, Faculty of Art, Design, and Architecture at Bilkent University, Ankara, Turkey. She has studied in the US and Italy, and worked on research projects in the UK. She has 25 years of research and experience on colour perception, colour preference, and colour use in architecture and interior architecture. Dr. Olgunturk is an active member in the CIE, the AIC, the ISCC, the Colour Group Great Britain, and the UIA, Chamber of Architects of Turkey

Light & Engineering
Vol. 33, No. 4, pp. 27–34, 2025

https://doi.org/10.33383/2024-097
Svetotekhnika # 2, 2025, pp.15–21

ANALYSIS OF PHYSIOLOGICAL COLORIMETRIC SYSTEMS OF TRICHROMATS

George V. Boos, Andrei A. Grigoryev*, and Victoria A. Rybina

National Research University Moscow Power Engineering Institute (NRU MPEI), Moscow, Russia
*E-mail: *aag.2010@yandex.ru*

ABSTRACT

Criteria for determining whether a physiological colorimetric system[1] belongs to the colour space of basic colorimetry have been formulated. A method for assessing the correspondence of an arbitrary colour space to the physiological space of the CIE 1931 standard colorimetric observer is presented. Studies of CIE-recommended colorimetric spaces – CIEPO06, Judd, Mac-Adam, and several other well-known systems – revealed that they are non-physiological for the CIE standard observer. The error in the colour-matching functions of the physiological LMS_{phys} system, caused by the uncertainty in the position of the reference colour stimulus *S* within the Nyberg triangle, has been quantified.

Keywords: colour-matching functions, colorimetric systems, dichromats, trichromats, protanopes, deuteranopes, statistical theory, comparison fields

1. INTRODUCTION

All existing methods for evaluating the quantitative and qualitative characteristics of floodlighting installations and their components (light sources and luminaires) rely on experimental studies to establish colour equality between two comparison fields. These experiments are essential for determining the colour-matching functions (CMFs) of colorimetric systems, which form the basis of all lighting engineering calculations.

According to Schrödinger [1, 2], the task of defining CMFs for any colorimetric systems is addressed within basic colorimetry, which is grounded in the Young – Helmholtz theory and Grassmann's laws [3]. The work of Maxwell and Schrödinger demonstrated that the colour space (CS) of basic colorimetry is a three-dimensional affine space where the coordinates of points, directed segments, and their lengths are defined, but neither distances nor angles between these segments are specified. For visual representation, Grassmann and later Schrödinger introduced a vector colour space, which is widely used in colorimetry.

Basic colorimetry is founded on the theory that the human visual system, under photopic vision, perceives responses from three types of cone photoreceptors with partially overlapping spectral sensitivity curves, Fig. 1, (*a*). This overlap makes it impossible to measure even the relative spectral sensitivities of the three cone types through direct colour-matching function assessment experiments. Indirect methods, such as using dichromats instead of trichromats [4, 5], inducing artificial colour blindness in receptors [6], and others, rely on hypotheses with limited applicability. These approaches have led to discrepancies in the measured sensitivity distributions of *L-, M-, S-* cones reported by different authors. Despite these variations, the colour spaces constructed from these *L, M,* and *S* sensitivity functions are termed as "physiological" by their authors.

[1] In Russia, there is a concept of a physiological colorimetric system in which the colour-matching functions correspond to the spectral sensitivities of the *L*-, *M*- and *S*-cone types.

Since the vector colour space (CS) constructed from the basic colorimetry CS is linear [2], Grassmann's laws [3] imply that the number of equivalent colorimetric systems is infinitely large. This property of CS is erroneously extended to the physiological CS of basic colorimetry. According to Meisel [7], a physiological CS is defined as one where the spectral sensitivities of the three receptors in the average human eye with normal vision of trichromat coincide with the CMFs of that CS.

As demonstrated in [8], individual spectral sensitivity curves of *L*-, *M*-, *S*- receptors vary significantly among trichromats. Consequently, their averaged values differ across observer groups and deviate from the reference *L, M, S* sensitivities, established for reference receptors. In our view, this is one reason for the proliferation of distinct physiological CS proposed by various authors. A second cause lies in the use of dichromats to derive spectral sensitivity functions for trichromats. As shown in [8], this approach introduces substantial errors in determining the $\overline{l}(\lambda)$ function.

Based on the Young – Helmholtz theory, Grassmann's laws, and visual physiology data [3], it's possible to formulate criteria that should be met by the physiological CS of an arbitrary set of trichromat's observers. All trichromatic CSs in basic colorimetry are related by means of linear transformations, which makes their analysis most convenient within the framework of the standardized CIE colorimetric system [9]. The XYZ system is particularly advantageous, as colour luminance is defined by a single coordinate, *Y*.

1.1. Criteria for Belonging of a Physiological Colorimetric System to the Colour Space of Basic Colorimetry

There are next criteria to belong to CS of basic colorimetry:

1. In the photopic vision range (luminance $L_v \geq 10$ cd/m²) signals from all *L, M, S* receptors in the physiological colour space must be greater than zero. This criterion is uncontested among lighting engineers, and many proposed physiological systems satisfy it.

2. The luminance sensation elicited by positive *L, M, S* receptor signals cannot be negative. Thus, the luminance coefficients of the physiological CS must also be positive.

3. A physiological CS must account for the positive luminance sensations of real colours in individuals with colour vision deficiencies. Specifically, it must explain the experimentally confirmed fact that protanopes, deuteranopes, and tritanopes exhibit distinct but always positive spectral luminous efficiency.

4. Since the transformation of a chromaticity diagram from one colorimetric system to another is projective, the chromaticity coordinates of all real colours must lie within the reference colour stimuli triangle (RCST) in both the physiological CS and any other colorimetric system derived via projective transformation.

The authors of "physiological" colorimetric systems analysed the obtained functions in relation to only some of the requirements mentioned above, what is not enough for a truly physiological system. Experimental data in [8] demonstrate that even when trichromats analysing, the formulated criteria are not always met in the reference colorimetric system.

This discrepancy arises because CMFs derived from specific trichromatic observer groups may differ markedly in shape and peak positions from those of the Guild and Wright observer set, which the CIE established as the reference for constructing the RGB and XYZ systems. Consequently, a colorimetric system deemed "physiological" for an author's observer group may not qualify as such for the CIE reference trichromats.

The value of developing niche "physiological" CS is limited unless they align with the reference RGB and XYZ systems. Thus, defining a CS that is truly physiological for these CIE-standardized systems is critical. Only such a CS can be universally recognized as the physiological colour space of trichromats.

The significance of determining CMFs for a trichromat's physiological colorimetric system lies in its ability to account for chromatic adaptation of *L, M, S* receptors in a physiologically valid manner. This is critical for modern colour difference spaces such as OSA-UCS, DIN99d, CAM02-UCS, CAM16, and others, which rely on these principles.

2. RESEARCH METHOD

In accordance with CIE recommendations, authors of physiological colour spaces typically characterize their systems using transition matrices that

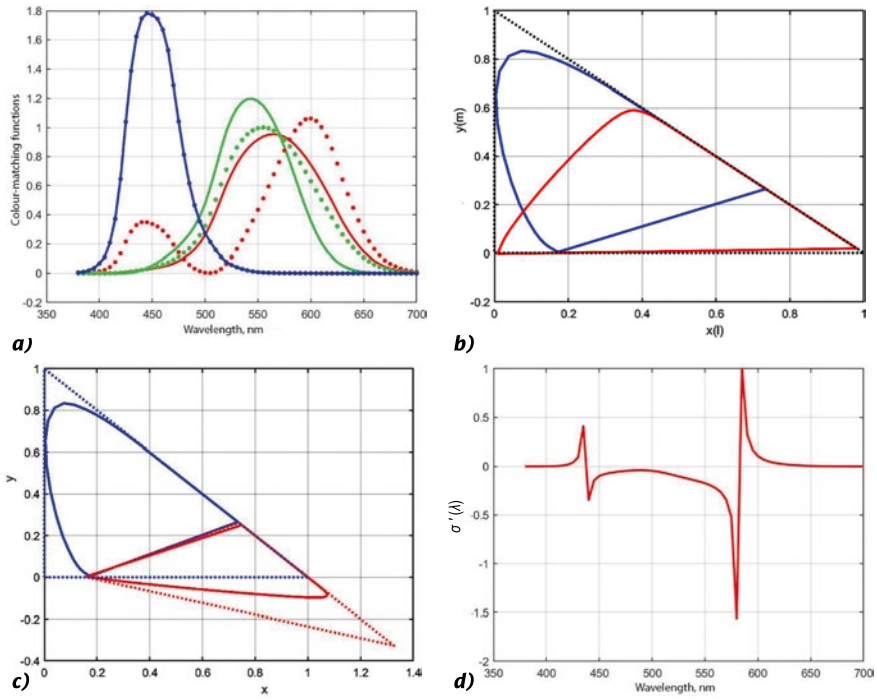

Fig. 1. Plots for the CIEPO06 and XYZ colorimetric systems: *a*) colour-matching functions; *b*) chromaticity diagram in the reference colour space; *c*) chromaticity diagram of CIEPO06 (red) within the XYZ (blue); *d*) $\sigma'(\lambda)$.

convert their CS's CMFs into the standard XYZ system. However, full specifications of physiological CS, including CMFs, transition matrices, and luminance coefficients, are rarely provided.

Furthermore, instead of transition matrices from physiological CS to XYZ system, authors often provide coefficient matrices that convert the relative spectral sensitivities of the physiological CS receptors into colour-matching. functions of XYZ system. While there is no inherent issue with this approach, since the equal-energy illuminant "E" is centred in the chromaticity diagram (a principle used in constructing the XYZ system), it remains straightforward to derive forward and inverse transition matrices between the physiological CS and XYZ system using these coefficients.

The critical problem lies in the fact that deriving such transition matrices does not validate the physiological nature of these CS. According to Grassmann's laws, infinitely many equivalent colorimetric systems exist, but only one corresponds to the physiological colour space of the reference trichromat. For example, the CIE 1931 RGB system is undeniably a trichromat colorimetric systems, yet it fails to describe a physiological colour space because receptor responses in this system assume negative values, violating Criterion 1. Similarly, the XYZ system cannot qualify as physiological, as "dichromats" lacking the "X" or "Z" receptors exhibit unchanged relative luminous efficiency compared to trichromats, contradicting experimental data and Criterion 3.

The core of the proposed methodology involves analysing known physiological CS for compliance with the criteria outlined above. If any criterion, evaluated in the reference XYZ system, is not satisfied, the colorimetric system in question cannot represent the physiological colour space of the standardized trichromat adopted as the reference.

3. RESULTS

In 2006, CIE Technical Committee 1–36 published a report [10], recommending the use of the physiological colour space (cone fundamentals) CIEPO06, for which the following matrix, converting the relative *L, M, S* colour-matching functions to the XYZ system, was provided in 2019 [5]:

$$\begin{pmatrix} X \\ Y \\ Z \end{pmatrix} = \begin{pmatrix} 1.9473 & -1.4144 & 0.3647 \\ 0.6899 & 0.3483 & 0 \\ 0 & 0 & 1.9348 \end{pmatrix} \begin{pmatrix} L \\ M \\ S \end{pmatrix}. \quad (1)$$

This transformation (1) enables the derivation of transition matrices from the LMS system to XYZ system and vice versa, as well as the chromaticity coordinates of the *L, M, S* reference colour stimuli in *X, Y, Z*:

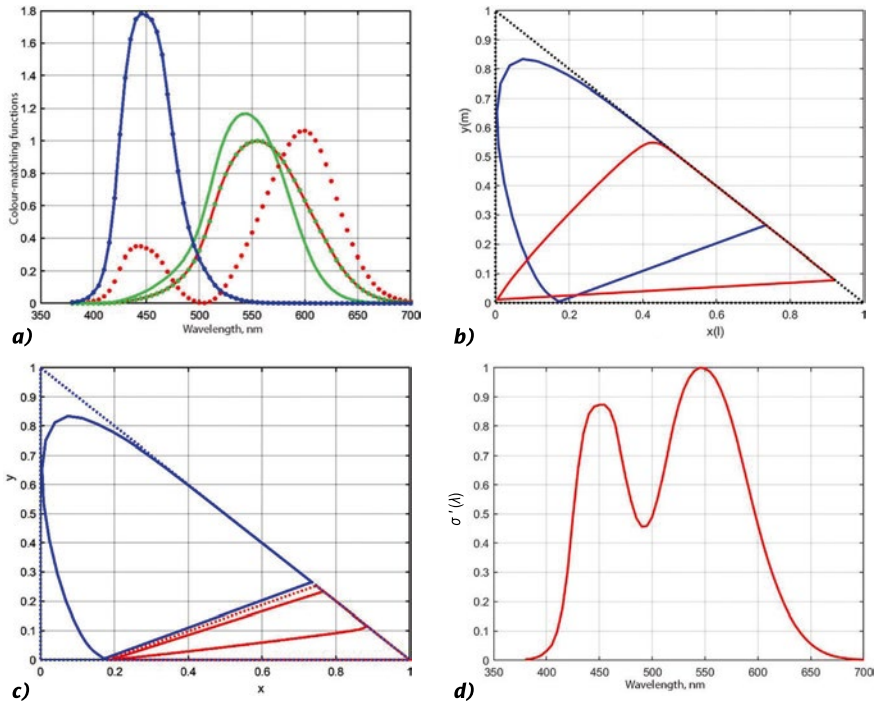

Fig. 2. Plots for the Judd and XYZ colorimetric systems: *a*) colour-matching functions; *b*) chromaticity diagram in the reference colour space; *c*) chromaticity diagram (red) within the XYZ (blue); *d*) $\sigma'(\lambda)$

$$(L\ M\ S) = (X\ Y\ Z)\begin{pmatrix} 0.205244 & -0.497222 & 0 \\ 0.833449 & 1.403485 & 0 \\ -0.038693 & 0.093737 & 1 \end{pmatrix},$$

$$(X\ Y\ Z) = (L\ M\ S)\begin{pmatrix} 1.997938 & 0.707823 & 0 \\ -1.18646 & 0.292177 & 0 \\ 0.188522 & 0 & 1 \end{pmatrix}, \quad (2)$$

$$\begin{pmatrix} x_L\ y_L\ z_L \\ x_M\ y_M\ z_M \\ x_S\ y_S\ z_S \end{pmatrix} = \begin{pmatrix} 0{,}738401 & 0{,}261599 & 0 \\ 1{,}326716 & -0{,}326716 & 0 \\ 0{,}158619 & 0 & 0{,}841381 \end{pmatrix}.$$

Fig. 1, (*a*) shows the colour-matching. functions of the XYZ system (dashed curves) and CIEPO06 LMS systems (solid curves), while Fig. 1, (*b*) displays their chromaticity diagrams in the reference colour space. Using the methodology from [3, 8, 11], the *l, m* chromaticity diagram for CIEPO06 was calculated, Fig. 1, (*c*). In the XYZ system, the luminance coefficient of the *Y* reference colour stimulus is 1, while those of the other two reference colour stimuli are zero. Thus, *Y* coordinate of the sum of the tristimulus values, $\sigma'(\lambda)$ [23], transformed into XYZ system from CIEPO06 (or another system), must remain positive for all real colours, as it is proportional to the perceived luminance. This *Y* coordinate can be calculated based on the known values of the converted in CS *X, Y, Z* chromaticity coordinates $Y'(\lambda)$ for real colours *l, m* in the CIEPO06 CS, Fig. 1, (*c*), and the CMF $\overline{y}(\lambda)$ derived via the transition matrix (2) for the LMS system of CIEPO06**,** Fig. 1, (*a*).

$$y'(\lambda) = \frac{Y'(\lambda)}{\sigma'(\lambda)},$$

$$\sigma'(\lambda) = \frac{Y'(\lambda)}{y'(\lambda)},$$

where $Y'(\lambda)$ represents the wavelength-dependent *Y* coordinate of monochromatic radiation, obtained by using equation (2).

Since matrix (2) was designed by the CIEPO06 authors to ensure $Y'(\lambda) = \overline{y}(\lambda)$,

$$\sigma'(\lambda) = \frac{\overline{y}(\lambda)}{y'(\lambda)}.$$

Fig. 1. (*d*) plots $\sigma'(\lambda)$ for CIEPO06.

Calculations $\sigma'(\lambda)$ reveal that, according to CIEPO06, monochromatic radiation at λ in range (440–580) nm is perceived by the standard trichromat with negative luminance. Fig. 1, (*c*) further shows that non-monochromatic colours with chromaticity coordinates below the alychne (x-axis) also exhibit negative luminance. This confirms that the CIEPO06 CS is not a physiological colorimetric system for the trichromat, corresponding to the CIE 1931 XYZ and RGB systems.

The best results among the analysed systems were obtained for Judd's colorimetric system [3], with reference colour stimuli's chromaticity coordinates in XYZ system:

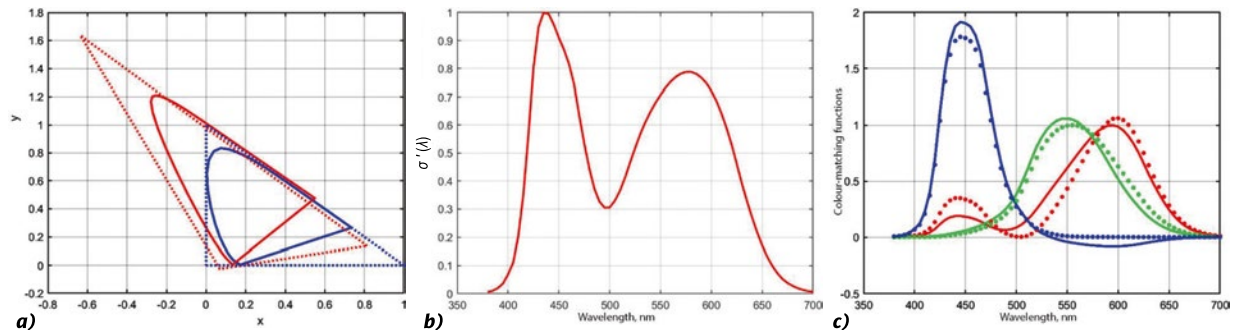

Fig. 3. Plots for the König and Dieterici colorimetric system: *a*) chromaticity diagram of the König and Dieterici colorimetric system (red) within the XYZ system (blue); *b*) $\sigma'(\lambda)$; *c*) colour-matching functions for the König and Dieterici colorimetric system

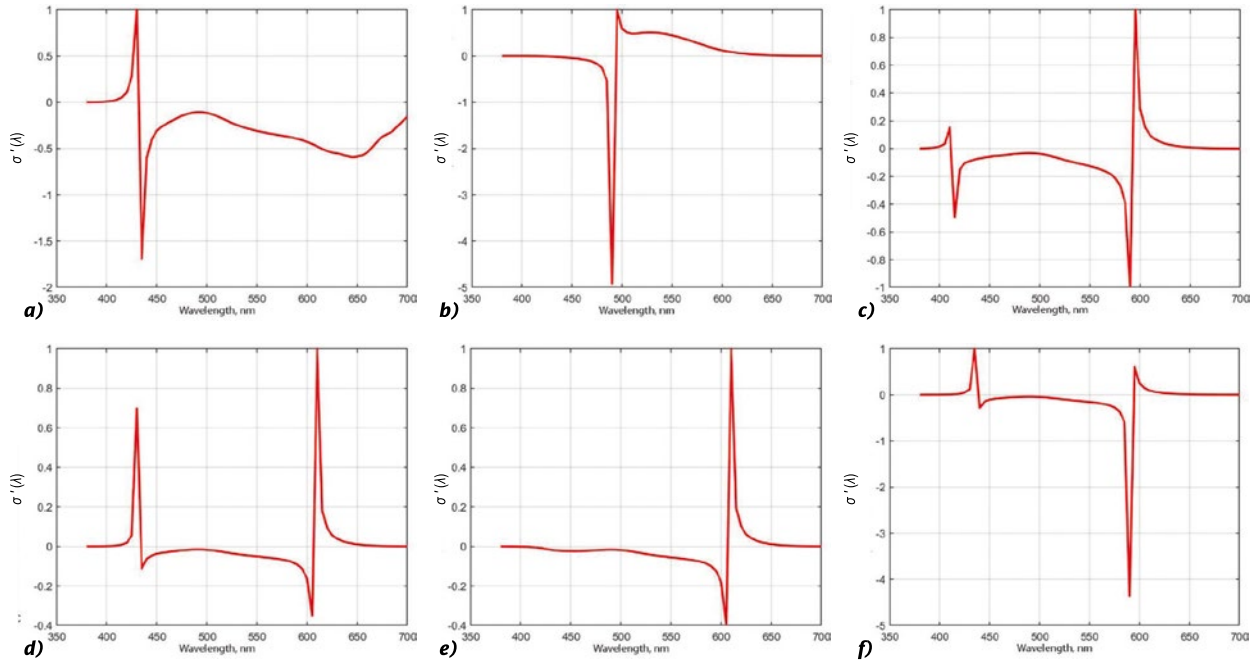

Fig. 4. Transformation of $\sigma'(\lambda)$ into the XYZ colorimetric system for the colorimetric systems of: *a*) Pitt [14], *b*) Stiles [15], *c*) Szekeres [16], *d*) Yustova [4], *e*) Mac-Adam [17], *f*) Kustarev [18]

$$(L,M,S)=\begin{pmatrix} 2{,}96 & -2{,}17 & 0{,}22 \\ 1 & 0 & 0 \\ 0 & 0 & 1 \end{pmatrix},$$

these yield the following transition matrices between *X, Y, Z* and *L, M, S* CMFs:

$$\left.\begin{aligned} (L,M,S)&=(X,Y,Z)\begin{pmatrix} 0 & -0{,}46 & 0 \\ 1 & 1{,}36 & 0 \\ 0 & 0{,}1 & 1 \end{pmatrix} \\ (X,Y,Z)&=(L,M,S)\begin{pmatrix} 2{,}95 & 1 & 0 \\ -2{,}17 & 0 & 0 \\ 0{,}22 & 0 & 1 \end{pmatrix} \end{aligned}\right\}.$$

Results for Judd's colorimetric system, analogous to those for CIEPO06, are shown in Fig. 2.

Judd's colorimetric system satisfies all physiological criteria except Criterion 3, placing the *S* and *M* reference colour stimuli on the alychne renders protanopes (lacking *L* receptors) blind in this system. Additionally, Judd's colorimetric system implies identical luminous efficiency for deuteranopes and trichromats, contradicting experimental data in Judd's own work [3]. Thus, Judd's colorimetric system is also non-physiological for the CIE 1931 standard observer.

Similar calculations chromaticity diagrams and $\sigma'(\lambda)$ were performed for 10 other colorimetric systems, Table 1.

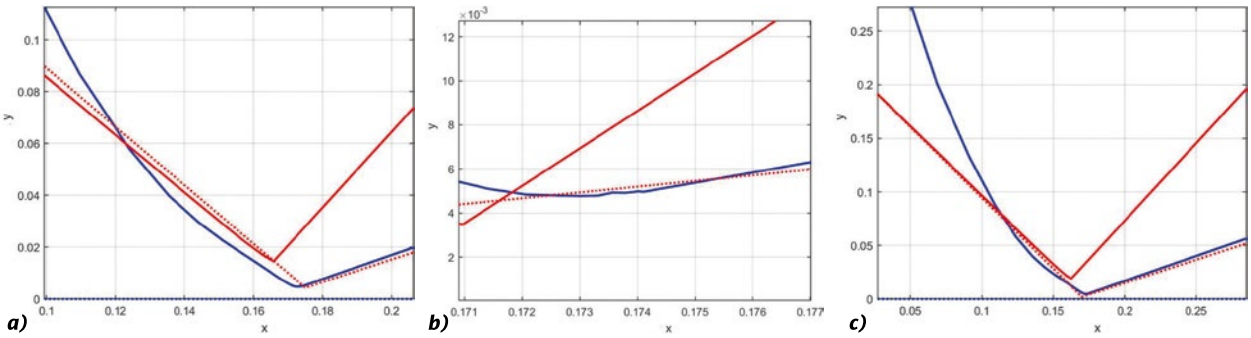

Fig. 5. Chromaticity diagrams (solid curves) and reference colour stimuli triangle (dashed curves), magnified for the colorimetric systems of: *a*) Thomson and Wright [19], *b*) Fedorov [6], *c*) Sperling [20]

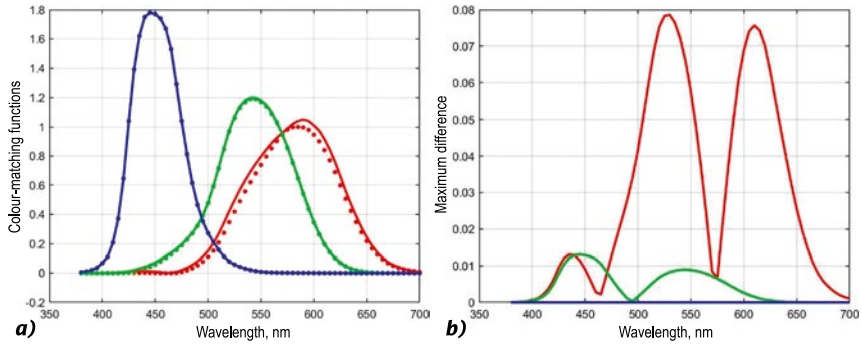

Fig. 6. Maximum (solid curves) and minimum (dashed curves) values of the colour-matching functions of the LMS_{phys} colorimetric system – *a*, maximum differences between the CMFs – *b*

For König and Dieterici colorimetric system [13], negative values of the $\overline{s}(\lambda)$ function at $\lambda >$ 535 nm, Fig. 3, indicate its non-physiological property for the trichromat in XYZ system.

4. DISCUSSION

Fig. 4 shows $\sigma'(\lambda)$ calculations for six colorimetric systems from the Table 1, including MacAdam's colorimetric system [17], recommended by the CIE and Russian standard [12] for evaluating light source colour rendering. Negative luminance values for some real colours indicate that, from the reference XYZ system perspective, none of these systems qualify as physiological.

The last three colorimetric systems in the Table 1, like König and Dieterici, have a positive ***y***-coordinate for the *M* reference colour stimulus, ensuring $\sigma'(\lambda) > 0$ across the visible spectrum. However, they cannot be fully deemed physiological, as their CMFs assume negative values at certain wavelengths.

Fig. 5 magnifies the chromaticity diagrams of the XYZ system (solid blue curves) and three colorimetric systems from the table (solid red curves).

Since all three colorimetric systems RCST (red dashed lines) intersect the *X, Y, Z* chromaticity diagram, their colour-matching functions exhibit negative values at specific wavelengths:

- Thompson and Wright's colorimetric system: $\overline{l}(\lambda) < 0$ at $\lambda < 470$ nm.
- Fedorov's colorimetric system: $\overline{m}(\lambda) < 0$ at $\lambda = (400–405)$ nm.
- Sperling's colorimetric system: $\overline{l}(\lambda) < 0$ at $\lambda = (495–540)$ nm.

CONCLUSIONS

The conducted study demonstrates that the analysed colorimetric systems are not physiological for the CIE 1931 standard colorimetric observer. Reference [8] presents the development of the LMS_{phys} colorimetric system, which eliminates the shortcomings of the reviewed systems. The chromaticity coordinates of its reference colour stimuli are listed in the table's final row, with the following distinguishing features:

1. *L* reference colour stimulus in LMS_{phys} system is a real colour with *x, y, z* chromaticity coordinates (0.7346657271, 0.2653342729, 0) [21].

2. Positive luminance coefficients: All reference colour stimuli in the XYZ system have strictly positive luminance coefficients, as their *y* coordinates lie above the alychne.

Table 1. The Chromaticity Coordinates of the Reference Colour Stimuli of Ten Colorimetric Systems within the XYZ System

№	Authors	*L*		*M*		*S*	
		x_l	y_l	x_m	y_m	x_s	y_s
1	König, A., & Dieterici, C [13]	0.814	0.136	–0.636	1.636	0.069	–0.026
2	Pitt, F. H. G [14]	0.745	0.257	10.991	–9.74	0.16	0.004
3	Stiles, W. S [15]	0.788	0.213	1.118	–0.115	0.175	–0.017
4	Szekeres, G. A [16]	0.736	0.264	1.458	–0.456	0.174	0.002
5	Yustova, E. N [4]	0.748	0.252	1.65	–0.65	0.174	0.002
6	MacAdam, D. L [17]	0.747	0.253	1.75	–0.759	0.178	0
7	Kustarev, A. K [18]	0.737	0.2653	1.43	–0.43	0.173	0.0045
8	Thomson, L. C., Wright, W. D [19]	0.747	0.253	–5.94	6.91	0.175	0.0044
9	Fedorov, N. T [6]	0.825	0.175	–1.22	2.22	0.156	0.0005
10	Sperling, H. G [20]	0.746	0.252	–5.66	7.713	0.17	0.002
	LMS_{phys} system [8]	**0.7347**	**0.2653**	**–5.2457**	**6.2457**	**0.1692**	**0.0011**

3. Reference colour stimuli triangle**:** The LMS_{phys} system RCST fully encloses the XYZ system chromaticity diagram without intersecting it, ensuring positive colour-matching functions for all real colours perceived by trichromats.

The aforementioned features of the LMS_{phys} system enable the description of all known colour-matching. phenomena for the XYZ system trichromat within the framework of basic colorimetry, the Young-Helmholtz theory, and Grassmann's laws. However, it cannot be asserted that the CMFs of LMS_{phys} system precisely align with the physiological system of Guild and Wright's observers. The reason lies in the inability to definitively determine the position of the *S* reference colour stimulus from Guild and Wright's experimental data. Nyberg [22] proposed a method to define the region of possible chromaticity coordinates for the *S* reference colour stimulus, based on Criteria 1–3 outlined earlier in this article. This region forms a triangle of very small area. As shown by calculations in [4, 21], the position of the *S* reference colour stimulus has negligible impact on the $\overline{m}(\lambda)$, $\overline{s}(\lambda)$ colour-matching functions and only weakly affects $\overline{l}(\lambda)$, though deviations remain. The work in [8] reduced the area of the Nyberg triangle by more than half, enabling a more precise estimation of the maximum deviation between LMS_{phys} system CMFs and those of the physiological system corresponding to the RGB and XYZ systems. Fig. 6, (*a*) illustrates, for each wavelength, the maximum (solid curves) and minimum (dashed curves) values of the CMFs across all possible positions of the *S* reference colour stimulus. Fig. 6, (*b*) shows the absolute differences between these values, providing an assessment of the maximum calculation errors.

Differences in Fig. 6 stem from *S*-reference colour stimulus uncertainty, not discrepancies with XYZ system. All colorimetric systems with *S* within the Nyberg triangle align with XYZ system calculations to 5–6 decimal places. That is sufficient to ensure physiological colorimetric systems errors are negligible compared to experimental noise. Except for points on the alychne, any *S* position within the Nyberg triangle satisfies all criteria. Placing *S* reference colour stimulus at the triangle's geometric centre (as in LMS_{phys} system) is statistically justified.

REFERENCES

1. Schrödinger, E. Grundlinien einer Theorie der Farbenmetrik im Tagessehen. I. Mitteilung // Annalen der Physik, vierte Folge, 1920, Bd. 63 (21), ss. 397–426.

2. Schrödinger, E. Grundlinien einer Theorie der Farbenmetrik im Tagessehen. II. Mitteilung // Annalen der Physik, vierte Folge, 1920, Bd. 63 (21), ss. 427–456.

3. Judd, D. B., & Wyszecki, G. Colour in Science and Technology (P.F. Artyushin, Ed.) // Mir, 1978. *(Original work published in English as Colour in Business, Science, and Industry, 1975, John Wiley & Sons, New York, London, Sidney, Toronto),* 592 p.

4. Yustova, E.N. Spectral Sensitivity of Eye Receptors // Proceedings of the USSR Academy of Sciences [Doklady Akademii Nauk SSSR], 1950, Vol. 74, # 6, pp. 1069–1072.

5. Stockman, A. Cone fundamentals and CIE standards // Current Opinion in Behavioural Sciences, 2019, Vol. 30, pp. 87–93.

6. Fedorov, N.T., Fedorova, V.I. Research on Colour Vision // Izvestiya Akademii Nauk SSSR, Series VII: Mathematics and Natural Sciences, 1935, # 10, pp. 1431–1450.

7. Maizel, S.O. Fundamentals of Colour Science // Moscow, Leningrad: Gostekhizdat, 1946, 128 p.; 2nd ed. M.: Librokom Publishing House, 2010, 128 p.

8. Boos, G.V., Grigoryev, A.A., Rybina, V.A. Research into Monochromatic Colour Vision Thresholds and Determination of the Trichromatic Colour-Matching Coefficients // Light & Engineering Journal, 2022, Vol. 30, # 2, pp. 89–19; DOI: 10.33383/2021-106.

9. Proceedings of the 8th Session of the CIE // Cambridge, England, 1931, pp. 19–29.

10. CIE 170–1:2006. Fundamental chromaticity diagram with physiological axes – Part 1 // Vienna, CIE Central Bureau, 2006.

11. Meshkov, V. V., Matveev, A.B. Fundamentals of Lighting Engineering: Vol. 2. Physiological Optics and Colorimetry (2nd ed.) // Energoatomizdat, 1989, 430 p.

12. Russian standard: GOST R 8.827–2013. State System for Ensuring the Uniformity of Measurements: Method for Measuring and Determining the Colour Rendering Index of Light Sources.

13. König, A., Dieterici, C.Z. Die Grundempfindungen in normalen und anomalen Farben Systemen und ihre Intensitats-Verthielung im Spectrum // Zeitschrift für Psychologie und Physiologie der Sinnesorgane, 1892, # 4, ss. 241–347.

14. Pitt, F.H.G. The Nature of Normal Trichromatic and Dichromatic Vision // Proceedings of the Royal Society B: Biological Sciences, 1944, Vol. 132 (866), pp. 101–117.

15. Stiles, W.S. Separation of the "Blue" and "Green" Mechanisms of Foveal Vision by Measurements of Increment Thresholds // Proceedings of the Royal Society B: Biological Sciences, 1946, Vol. 133 (873), pp. 418–434.

16. Szekeres, G.A. New Determination of the Young-Helmholtz Primaries // J. Opt. Soc. Am. 1948, Vol. 38, # 4, pp. 350–363.

17. Mac-Adam, D.L. Chromatic Adaptation // J. Opt. Soc. Am. 1956, Vol. 46, # 7, pp. 500–513.

18. Kustarev, A.K. The reference colour stimuli of the physiological colour system [Referentnyye tsvetovyye stimuly fiziologicheskoy tsvetovoy sistemy] // Svetotekhnika, 1965, # 6, pp. 5–11.

19. Thomson, L.C., Wright, W.D. The Convergence of the Tritanopic Confusion Loci and the Derivation of the Fundamental Response Functions // J. Opt. Soc. Am. 1953, Vol. 43, # 10, pp. 890–894.

20. Sperling, H.G. Case of Congenital Tritanopia with Implications for a Trichromatic Model of Colour Reception // J. Opt. Soc. Am. 1960, Vol. 50, # 2, pp. 156–163.

21. Boos, G.V., Grigoriev, A.A. On the chromaticity coordinates of the reference colour stimuli of the colorimetric system of the *L, M, S* [O koordinatakh tsvetnosti opornykh tsvetovykh stimulov kolorimetricheskoy sistemy *L, M, S*] // Svetotekhnika, 2016, # 3, pp. 30–34.

22. Nyberg, N.D. Determination of the position of the reference colour stimuli of blue colour in the chromaticity triangle // Proceedings of the USSR Academy of Sciences (Doklady Akademii Nauk SSSR), 1949, Vol. 65, # 2, pp. 159–162.

23. Budak, V.P., Grigoriev, A.A., at al. Basics of Light and Engineering / Moscow, NRU MPEI, 2023, 534 p.

George V. Boos,
Ph. D. and Member of the Russian Academy of Natural Sciences. In 1986, he graduated from the Moscow Power Engineering Institute (MPEI). At present, he is the President of MSK BL GROUP, Head of the Light and Engineering subdepartment of NRU MPEI. He is Recipient of the State Prize of the Russian Federation for Architectural Lighting of Moscow, the Chairman of the Science and Engineering Board Svetotekhnika and of the editorial board of the Svetotekhnika/Light & Engineering Journal

Andrei A. Grigoryev,
Doctor of Technical Sciences, Professor. In 1981, he graduated from the Moscow Power Engineering Institute (MPEI). At present, he is the Professor of the Lighting Engineering subdepartment of NRU MPEI, the Head of the Vision Functions Research Group at Sergey Vavilov Russian Lighting Research Institute (VNISI)

Viktoria A. Rybina,
Ph. D. In 2018, she graduated from NRU MPEI. At present, she is a Associate Professor of the Light and Engineering subdepartment of NRU MPEI and researcher of the Vision Functions Research Group of Sergey Vavilov Russian Lighting Research Institute (VNISI)

Light & Engineering
Vol. 33, No. 4, pp. 35–43, 2025

https://doi.org/10.33383/2025-004
Svetotekhnika # 3, 2025, pp. 46–51

LIGHT-GRAPHIC DESIGN IN WAYFINDING OF THE HISTORICAL CENTRE OF SAINT PETERSBURG

Olga A. Vul[1] and Daniil F. Nikandrov[2]

Peter the Great St. Petersburg Polytechnic University (SPbPU), Russia
E-mails: [1]zaret-olga@yandex.ru, [2]dan.nikandrov@gmail.com

ABSTRACT

The article introduces the concept of "light-graphic design", which reveals the synthetic aspects of lighting design that combine informational illumination, graphic design, and urban wayfinding. The authors examine the results of 2018 discussions on terminological changes in the field of lighting design, as presented in publications of the "Svetotekhnika" journal. The study analyses the application of light-graphic design in the structure of the historical centre of St. Petersburg, highlighting existing issues such as the lack of systematization in light signage, light pollution caused by advertising and decorative lighting, and the inconsistency between architectural lighting and the perception of light-graphic information. The authors argue for the necessity of developing a unified wayfinding system based on the synthesis of light and graphics. They emphasize the importance of creating a unified graphic design code to facilitate orientation in the urban environment.

Proposed solutions to these problems outline the main directions for the development of light-graphic design, using urban wayfinding in the protected historical and cultural zones of St. Petersburg as an example. These include structuring innovations in light infographics and existing informational signs, implementing light projection technology, introducing interactive markers into the urban environment, utilizing animated light-graphics, employing light installations and art objects as landmarks, and, finally, creating light scenarios and routes as tools for visual orientation that ensure an organic perception of the urban context.

Key aspects of the research include the modernization of light-graphic tools in the development of tourist routes and the identification of architectural landmarks during night time, as well as the potential use of light routing in the design of urban park spaces.

The authors identify promising directions for the development of light-graphic design in the historical centre of St. Petersburg, justifying the need for a comprehensive light wayfinding system as a significant component of the city's informational environment.

Keywords: lighting design, informational lighting, light wayfinding, visual communications, light graphics, light scenarios, urban environment, historical centre of Saint Petersburg

1. INTRODUCTION

Considering the features of the informational environment in a modern metropolis, light and graphics are two main means that are ensuring spatial orientation in the dark. Light sources are primary guiding reference points during night time. Means of artificial lighting are vital for ensuring safe and comfortable visibility in the evening city, for illuminating architectural objects, squares, embankments, and urban parks. Alongside lighting, the informational environment of the modern metropolis is shaped by graphic design. Graphic signs are the most widely used means for visual communication and information transmission in the city. The fun-

damental tasks of visual-communicative systems are to ensure the "legibility" of the city and effective orientation within it [1]. One of the significant means of visual communication in the city is urban wayfinding, which is formed through the system of signs in the visual environment.

The issues related to the study of urban wayfinding are currently gaining additional relevance due to the need to address the problems of citizens' orientation in the transforming environment of the metropolis. Urban wayfinding objects, as carriers of light and colour-graphic information, are intended to provide comfortable perception of the surrounding space. As a result of analysing informational lighting in the urban environment, the demand for a synthesis of the fields of lighting and graphic design becomes apparent.

The purpose of the study is to identify the role of light-graphic design as a key component of the informational environment of the historical centre of Saint Petersburg in the context of urban wayfinding development.

The objectives of this article are:

- To explore the synthesis of light and graphics, considered as key aspects of the urban wayfinding system;
- To define the concept of "light-graphic design" as a significant component of contemporary design research;
- To analyse light-graphic design as a component of informational lighting in metropolises based on existing design solutions;
- To identify existing problems of light-based signage in the historical centre of Saint Petersburg;
- To examine possible ways of developing light-graphic design in urban wayfinding.

2. TERMINOLOGY

The concept of "lighting design", which characterizes the active development of architectural environment design at the turn of the 20th and 21st centuries, includes a multitude of semantic components that require dedicated terms. Discussion articles addressing the formation of lighting design and the evolution of terminology in this field – from "light architecture" to "lighting design" – were published in the journal "Svetotekhnika" in 2018, forming a field of scientific interaction in this area. For instance, S.N. Siziy associates the emergence of the term "light architecture" with the necessity of synthesizing light and architecture [2]. Y.B. Aizenberg characterizes lighting design as a synthetic field at the intersection of lighting technology and architecture [3]. N.V. Bystryantseva considers lighting design as an interdisciplinary sphere associated not only with architecture, but also with environmental and industrial design, closely interwoven into the informational space of the modern city [4]. V.P. Budak and N.I. Shchepetkov, summarizing the discussion, assert that lighting design is a new branch of architecture – "comprehensive in its typology of objects, a promising and fascinating field of professional, creative and scientific activity in shaping the living environment" [5].

Despite the broad range of discussed issues, the discussion did not examine in detail a significant subdivision of lighting design – informational lighting, which synthesizes light and graphics. As informational lighting has by now developed into an integral part of the urban environment, its further advancement requires the expansion of the terminological apparatus for future interdisciplinary studies. Special attention should be given to the formulation of concepts that describe the interaction between lighting and graphic design.

The necessity of interaction between graphic design and architectural environment design in creating urban visual communications is emphasized in the works of M.A. Silkina [6]. The terms "light graphics", "light-graphic drawing", and "light-graphic compositions" are elaborated in the monograph Urban Lighting Design by N.I. Shchepetkov [7]. Techniques of light-graphic design in informational lighting are presented in the book Light Art Installations by V.V. Mironenkov. He uses the term "light-graphic language" to describe an expressive tool for informing and communist propaganda of citizens in the USSR [8]. However, the cited scientific works consider only individual aspects of a direction that shapes the modern urban environment and which is referred to in this study by the term "light-graphic design".

Let us examine in more detail the semantic content of the proposed term. Its most important aspect is the synthesis of lighting and graphic design. Thus, light-graphic design can include the application of light-based means in environmental identity – typography, infographics, motion graphics – forming a characteristic group of graphic design objects complemented by lighting tools. This group includes information boards and advertising signs,

where signs such as text, pictograms, logos, and linear graphic images accentuated with light serve as the main graphic components. The second group includes environmental objects and situations characterized using light as the primary tool, sometimes accompanied by graphic means: light shows, festive lighting scenarios for buildings and streets, decorative use of illuminated typefaces, and elements of architectural light graphics. The block diagram, Fig. 1, presents the results of an analysis of the use of lighting and graphic means in urban informational lighting.

The identification of conventional groups that determine the dominant role of either graphics or light in various environmental situations and in relation to different urban objects overall demonstrates the tendency toward the convergence of lighting and graphic approaches in design practice, their interpenetration, which highlights the relevance of the term "light-graphic design". Thus, in this study, light-graphic design is defined as a synthesis of light and graphics in the development of the informational space of the modern city, ensuring an integrated approach to shaping the architectural environment.

Light, used as a medium for transmitting information in the metropolis, is a key instrument of communication and message transmission [9]. When analysing the informational system created through light-graphic design, it is necessary to distinguish its areas of application in the city by identifying three categories: light signage, light commercials, and decorative lighting. It is important to note that the latter two categories can serve as auxiliary components of the first, becoming light-based landmarks. Accordingly, light wayfinding is the defining category of informational lighting in the metropolis [10] and is of greatest interest from the perspective of light-graphic design. The study of light wayfinding problems becomes the most appropriate analytical tool for identifying the directions of development of the light-graphic communication system of Saint Petersburg as a whole.

3. PROBLEM STATEMENT

The study of light-graphic design as a part of informational lighting in the historical centre of Saint Petersburg, based on on-site observation and analytical methods, has made it possible to identify several problems in the organization of light-based wayfinding. The research also highlights the necessity of its systematization and the development of a structured, stylistically unified light wayfinding system.

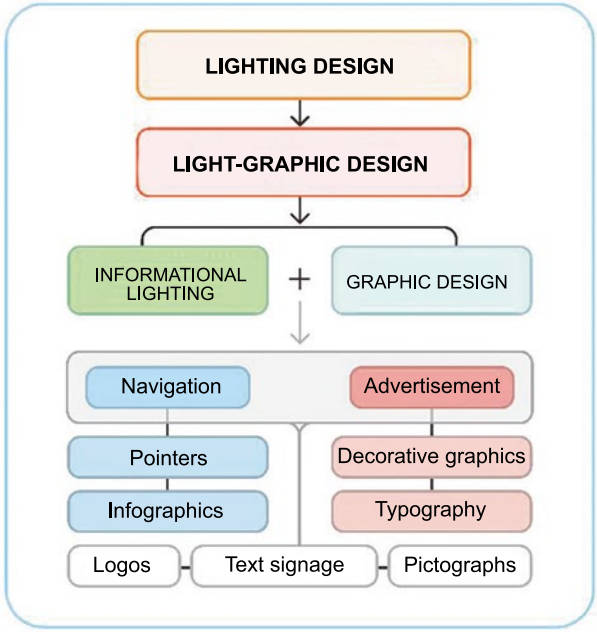

Fig. 1. Block diagram of application of light and graphic means used in information lighting of the city (illustration: D.F. Nikandrov, O.A. Vul)

Currently, the centre of Saint Petersburg is characterized by a lack of systematization and poor legibility of light-based wayfinding elements. Various modes of transport rely on different visual-communicative and symbolic systems, Fig. 2, (*a*). For instance, metro stations are identified by illuminated boxes and "M" light signs, whereas surface public transport stops lack any light-based identification. Light-graphic signage in the form of texts, signs, pictograms, and inscriptions is typically present in cultural, commercial, and gastronomic institutions of private business, Fig. 2, (*b*), but it is rarely applied to public and budget institutions such as schools, clinics, and administrative buildings.

Informational lighting is placed on advertising carriers of varying shapes and heights, which complicates orientation and becomes a source of both light and informational pollution – especially along major thoroughfares, including Nevsky Prospekt, Fig. 2, (*c*). Due to the predominance of illuminated advertising, the city's address and transport wayfinding elements often appear dim and difficult to read. Tourist light signage, which informs visitors about landmarks and cultural heritage sites, is mostly limited to backlit maps and a few illuminated panels near some museums, Fig. 2, (*d*).

Fig. 2. *a* – various navigation systems for the underground and ground transportation of St. Petersburg; *b* – light graphic navigation in the cultural cluster "New Holland"; *c* – light and information pollution on Nevsky Prospekt; *d* – typical information stand with a map of St. Petersburg (photo: D.F. Nikandrov)

Recently popularized in Saint Petersburg, gobo projectors that display static images onto sidewalks or building walls are often used for advertising purposes and are poorly integrated into the urban context, Fig. 3, (*a*). However, in some cases, the identification of historical sites within the metropolis can effectively support the wayfinding system – for example, the illuminated portrait of Dostoevsky on the wall of the writer's museum-house, Fig. 3, (*b*).

The city currently faces a deficit of illuminated orientation reference points. Meanwhile, on festive days, the urban environment becomes oversaturated with random light-graphic forms and installations, Fig. 4. The decoration of streets and buildings with graphically inconsistent garlands, patterns, and figures often leads to visual chaos, structural clutter,

Fig. 3. *a* – light projection advertising with signs (photo: D.F. Nikandrov); *b* – light projection-portrait on the building of the Dostoevsky House-Museum (source: https://kgainfo.spb.ru/)

and light pollution. This issue is also addressed in an article by A.G. Khadzhin and G.S. Matovnikov using the example of Moscow [11].

Such decorations frequently distract attention from not only the informational, but also the architectural components of the urban environment, which is particularly noticeable in the tourist areas of the historical centre – Nevsky Prospekt, Palace Square, and the Griboedov Canal embankment.

Without the use of mobile navigators, pedestrians who are unfamiliar with Saint Petersburg city environment will find it difficult to visually orient themselves during night time. No specific solutions have been proposed for direct orientation or the formation of pedestrian light-based routes. Many architectural sights and monuments are hard to identify due to the absence of illuminated information plaques or stands. The city fabric lacks informational links between key landmarks, pathways, and transport infrastructure nodes. The existing light-graphic wayfinding system does not include interactive elements that allow users to interact with the urban environment, such as accessing information via QR codes. Furthermore, light-based signage and routing are not implemented in the parks of Saint Petersburg's historical centre – from small gardens like Yusupov Garden to the larger parks such as Yekateringof Park and the Central Park of Culture and Leisure on Yelagin Island. This shortcoming may negatively impact visitation during the autumn-winter season.

Thus, the analysis of the existing lighting environment reveals a critical lack of a unified light wayfinding system in the centre of Saint Petersburg. This is further compounded by the insufficient lighting of current informational elements and the

Fig. 4. Festive light-graphic forms in the historical centre of St. Petersburg (photo: D.F. Nikandrov)

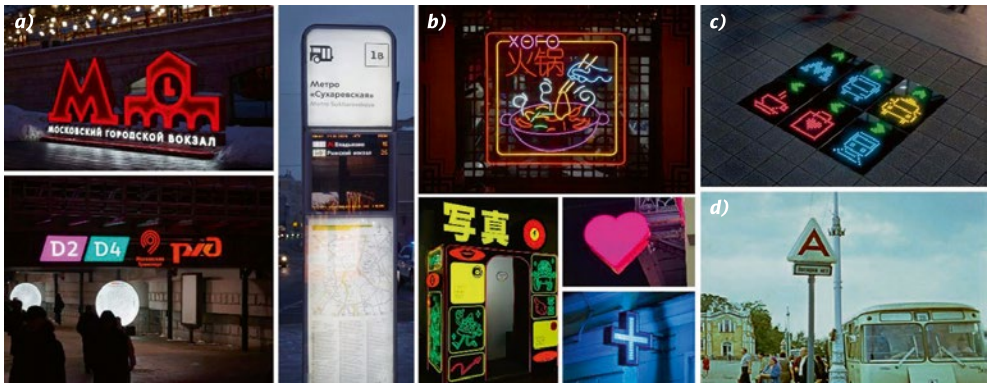

Fig. 5. *a* – design code of public transport navigation in Moscow (photo: D.F. Nikandrov); *b* – pictograms as a means of light-graphic design in St. Petersburg navigation (photo: D.F. Nikandrov); *c* – light navigation in the surface of the earth by Aira; *d* – typical self-illuminated bus stop sign in Leningrad, Novy Peterhof station, 1972 (photo – Erhard Kranz)

oversaturation of illuminated advertising and decorative lighting, which hinder spatial orientation. At the same time, the use of light-based means in wayfinding represents a crucial direction for the development of Saint Petersburg's information system – especially considering the region's climate and the short daylight hours in the autumn-winter period [12]. To qualitatively improve Saint Petersburg's light-information environment, it is necessary to develop a typology of possible developmental pathways, with a focus on effective innovations that meet the demands of the present day.

4. SOLUTIONS

Let us consider the typology of the main solutions for the development of light-graphic design in the urban wayfinding of the historical centre of St. Petersburg.

4.1. Systematization of Light-Graphics

First and foremost, it is necessary to systematize and further develop the already existing solutions. Current wayfinding system in St. Petersburg includes illuminated steles, LED displays, and stands with informational maps and schemes. These are usually located near metro stations and city landmarks. The most relevant path for applying light-graphic design is the introduction of a unified design code for this wayfinding system, like the example set in Moscow, Fig. 5, (*a*). The practice of using light infographics in wayfinding – such as pictograms, maps, symbols applied both indoors and outdoors, Fig. 5, (*b*), – also requires unification into a coherent and recognizable design code system. Developing these codes would positively impact the public transport wayfinding system, potentially including light-graphic designs at stops according to transport types, following the Leningrad practice, Fig. 5, (*c*), as well as creating lighting scenarios for informing about vehicle movement.

A light-graphic language of concise and recognizable pictograms, signs, and labels used in the design of municipal and state institutions, social service facilities, cultural sites, tourist attractions, and commercial areas will help optimize visual information delivery during night time, significantly speeding up its perception. Informational plaques, stands, and illuminated QR codes can serve as im-

Fig. 6. *a* – projection navigation of the "GES-2" House of Culture in Moscow (photo: D.F. Nikandrov); *b* – "Strana Sveta" video mapping show on Palace Square in St. Petersburg (photo: Vladimir Cherenkov; source: https://vk.com/wall-222526013_1173); *c* – "Magic Carpets" – Interactive Street video projection, Bangkok, 2018, by Miguel Chevalier (photo: https://www.miguel-chevalier.com/work/magic-carpets-bangkok-2018)

portant additions to light infographics, enabling access to extra details about historical sites, Fig. 5, (*d*). In the spring and summer seasons, it's possible to use information panels embedded into the pavement, allowing visitors to navigate the city "by looking down", without the need for maps or mobile navigation, Fig. 5, (*e*).

4.2. Light Projection Signage

Light projection technology is increasingly used in St. Petersburg, primarily for advertising and information lighting. However, there is a growing trend toward its application in wayfinding [12].

Projection signage can be seen in modern museums such as the General Staff Building of the Hermitage and "GES-2" in Moscow, Fig. 6, (*a*). Wayfinding projections can appear not only as text, pictograms, or graphic signs, but also as full-fledged artistic graphics or photographs related to themes or individuals associated with the place, Fig. 6, (*c*). The potential of using projections in wayfinding has yet to be fully explored, especially regarding their interactive capabilities. For example, video mapping – the art of projecting light onto environmental objects, Fig. 6, (*b*) – can serve not only as part of a show but also as a tool for communication, informing, and managing human flows [13]. As lighting designer Roger Narboni said, "light projection creates a world of clearly distinguishable signs, symbols, and graphic images that successfully complement the lighting itself" [14]. This creates a synthesis of virtual and real spaces in the architectural and landscape environments of the city, Fig. 6, (*c*). Thus, light projection signage is one of the most promising areas for developing urban communication.

Fig. 7. *a* – "Take Flight!" light-graphic installation by Ralph Westerhof (source: https://ralfwesterhof.nl/work/take-flight/); *b* – "Drawn in Light" light-graphic installation by Ralph Westerhof, Amsterdam (source: https://ralfwesterhof.nl/work/drawn-in-light/); *c* – light landmark "ballerina" near the second stage of the Mariinsky Theater (photo: D.F. Nikandrov)

Fig. 8. *a* – city square and concert hall in Moscow City MIBC (source: Gorproject); *b* – projection lighting of Ishoj Station in Copenhagen, lighting design by AF Lighting (source: https://lightonline.ru/news/svetotechnika/7–2013/Lighting_ Station_in_Copenhagen. html); *c* – event space using light graphics – Bridgelife Neighborhood Park by Lab D+H (source: https://mooool.com/en/bridgelife-neighborhood-park-by-lab-dh.html); *d* – Guryevsky Park of Light, light-graphic installations (source: Guryevsky municipality community – VK, dot.bureau – Dmitry Chebanenko)

4.3. Light Forms and Installations as Landmarks for Orientation

As mentioned earlier, decorative and event lighting can serve not only as city embellishments during holidays, but also as orientational aids. Volumetric light forms and installations placed on streets and squares, as discussed in the article by V.G. Karpenko and N.I. Shchepetkov [15], can function as "light beacons" and place identifiers, Fig. 7, (*a*). For tourist wayfinding, it is possible to implement a system of light landmarks for significant sites and heritage objects, including technologies of augmented and mixed reality, Fig. 7, (*b*), [16]. These landmarks can form routes made up of light-graphic installations in the form of architectural objects, recognizable environmental details, signs of city identity, and images or characters associated with St. Petersburg, Fig. 7, (*c*).

4.4. Light Scenarios and Routes

The light design of the contemporary urban environment often includes light-dynamic scenarios used both on festive occasions and in everyday life. A clear example of such a scenario is the City Square and Concert Hall at Moscow City, Fig. 8, (*a*), where the theme of time is expressed through spatial development of light graphics on multiple planes – facade lines synchronized with music, illuminated panels embedded into the square's surface, and dynamic gobo projections.

This design approach could also be relevant for transforming historic and modern public spaces in St. Petersburg – such as Sennaya, Troitskaya, and Birzhevaya squares. The main goal in designing light routes is to create a unified visual orientation system linking infrastructure objects, landmarks, city embankments, and park landscapes. Establishing the previously discussed light landmarks makes it possible to form attraction centres, Fig. 8, (*b*), and develop festive light routes across symbolic locations in St. Petersburg that reflect the spirit of specific events, such as the Day of the Siege Lifting, Navy Day, or City Day. Lighting design in park environments, in turn, promotes the use of parks and boulevards during dark hours, especially in colder seasons. It can emphasize the historical identity of the city's parks and support the development of special event clusters, Fig. 8, (*c*). Examples of such interactive park scenarios include the 800th Anniversary Park in Nizhny Novgorod, the Park of Light in Guryevsk, Fig. 8, (*d*), and park zones in Almetyevsk. In St. Petersburg, these ideas could be applied to linear park spaces like Konnogvardeisky Boulevard.

The conducted analysis of possible development paths for light-graphic design in urban wayfinding of St. Petersburg's historical centre reveals both the need to systematize existing solutions and the demand for innovations. Creation a unified light wayfinding design code appears to be a key element in enhancing the city's visual communication. Systematization of the pictogram language, integrating

modern lighting technologies and dynamic informational elements into urban infrastructure, and utilizing historically established light symbols demonstrate the potential for a harmonious synthesis of tradition and contemporary design. This approach will not only ensure functionality, but also elevate the aesthetic quality of urban wayfinding.

Thus, a comprehensive implementation of the proposed directions for light-graphic design development will contribute to the creation of a comfortable and visually appealing urban environment, enhancing user interaction with the wayfinding system of St. Petersburg.

5. CONCLUSION

The definition of the term "light-graphic design" proposed in this study presents it as a synthetic field that combines both lighting and graphic components. The significant intersection of these disciplines in the design of wayfinding systems, informational support, decorative architectural lighting, and urban environment organization makes this concept an essential element of contemporary design research.

The role of light-graphic design in the city's informational space lies in ensuring the high legibility of graphical information and providing comfortable orientation during night time. The analysis of light-graphic design use in the informational lighting of a metropolis – using the historical centre of Saint Petersburg as an example – reveals several challenges that require modern design solutions. The explored directions for the development of light-graphic design in urban wayfinding outline a trajectory for lighting design that impacts transportation, tourism, and social services. The authors identify the necessity of creating a coherent system of light-graphic signage and implementing a design code aimed at enhancing the tourist potential of Saint Petersburg's central areas and improving the overall legibility of the urban environment.

To improve the city's wayfinding system, it is crucial to conduct further research in the field of light-graphic design. Introducing the term "light-graphic design" and defining it as a direction in the development of urban visual communications is necessary for systematizing studies of the metropolis's informational environment. The proposed definition becomes an integral part of design theory and contributes to a comprehensive approach to the development of light-graphic elements in the urban environment. Future studies should focus on developing a detailed typology and expanding the conceptual framework of this field.

REFERENCES

1. Lynch, K. The image of the city / M.: Stroyizdat, 1982, 328 p.

2. Sizyi, S.N. The current state and prospects of the development of lighting design [Sovremennoe sostoyanie i perspektivy razvitiya svetodizayna] // Svetotekhnika, 2018, # 3, pp. 72–78.

3. Aizenberg, Yu.B. Discussion on the problem of lighting design [Diskussiya po probleme svetovogo dizayna] // Svetotekhnika, 2018, # 5, pp. 79–83.

4. Bystryantseva, N.V., Ovcharov, A.T., Novakovsky L.G. Discussion on the problems of lighting design [Diskussiya po problemam svetovogo dizayna] // Svetotekhnika, 2018, # 4, pp. 80–93.

5. Budak, V.P., Shchepetkov, N.I. Discussion on the problem of lighting design [Diskussiya po probleme svetovogo dizayna] // Svetotekhnika, 2018, # 6, pp. 74–76.

6. Silkina, M.A. Environmental and graphical aspects of the formation of navigation visual and communicative systems [Sredovye i graficheskie aspekty formirovaniya navigatsionnykh vizual'no-kommunikativnykh system] // Science, education, and experimental design. Proceedings of the MARCHI: Proceedings of the international scientific and practical conference. Collection of articles, Moscow, April 09–13, 2012. Moscow: Moscow Architectural Institute (State Academy), 2012, pp. 295–300.

7. Shchepetkov, N.I. Light design of the city [Svetovoy dizayn goroda] / M.: "Architecture-S", 2006, 320 p.

8. Mironenkov, V.V. Light propaganda and artistic installations [Svetovye agitatsionno-khudozhestvennye ustanovki] / Moscow: Plakat, 1983, 64 p.

9. Cherkasov, G.N., Popova, D.D. Modern areas of light and colour application in architecture // Light & Engineering, 2021, Vol. 29, # 4, pp. 90–99.

10. Silkina, M.A. The history of forming visual-communicative components of a night city light medium // Light & Engineering, 2015, Vol. 23, # 3, pp. 4–9.

11. Khadzhin, A.G., Matovnikov, G.S. A controversial history of pedestrian space lighting in Moscow // Light & Engineering, 2021, Vol. 29, # 4, pp. 64–78.

12. Nikandrov, D.F., Vul, O.A. Features of the use of light projections in the navigation system of a modern megalopolis, ISI Science Week: proceedings of the All-

Russian Conference, April 1–4, 2024 at 4 p.m. 4. / St. Petersburg: POLYTECHNIC PRESS, 2024, 271 p.

13. Barchugova, E.V., Rochegova, N.A. Video mapping from presentation to architecture // Light & Engineering, 2016, Vol. 24, # 4, pp. 25–30.

14. Narboni, R. Lighting public spaces: new trends and future evolutions // Light & Engineering, 2020, Vol. 28, # 2, pp. 4–16.

15. Karpenko, V.E., Shchepetkov, N.I. Light forms in urban environment // Light & Engineering, 2021, Vol. 29, # 4, pp. 6–15.

16. Karpenko, V.E. Augmented reality and virtual reality in light installations and night urban environment // Light & Engineering, 2022, Vol. 30, # 5, pp. 47–55.

Olga Alexandrovna Vul,
Ph. D. in Pedagogy, Associate Professor at Higher School of Design and Architecture, Institute of Civil Engineering, Peter the Great St. Petersburg Polytechnic University (SPbPU), member of Russian Designers Association and the Union of Artists of Russia. Research interests are creation of lighting scenarios for residential and public interiors, development of lighting art objects in an urban environment, methods of designing individual lighting equipment, sketching in design activities

Daniil Filippovich Nikandrov,
Master degree student of Higher School of Design and Architecture at Peter the Great St. Petersburg Polytechnic University (SPbPU), lighting designer of MARTINI RUS, St. Petersburg. Research interests are lighting design, communicative design, light navigation, information lighting, light scenarios, light as a means of communication

Light & Engineering
Vol. 33, No. 4, pp. 44–49, 2025

https://doi.org/10.33383/2025-002
Svetotekhnika # 3, 2025, pp. 27-31

LED STREET LIGHTING

Irina V. Sokolova

National Research Moscow State University of Civil Engineering (NRU MGSU), Russia
E-mail: SokolovaIV@mgsu.ru

ABSTRACT

LED lighting devices are widely used for lighting in modern cities**.** That type of illumination offers many advantages over traditional lighting systems. This is, first of all, high energy efficiency and a service life increased by 50 times. This article is devoted to the study of the development and improvement of LED outdoor street lighting technology. The article provides a brief history of the development of LED lighting technology. Examples of LED lighting devices are provided for various applications of LED lighting. Specific types of LEDs used in lighting fixtures in various areas of outdoor LED lighting have been studied. The advantages of LED lighting compared to other types of electrical lighting are presented.

Keywords: LED, light engineering, outdoor street lighting technology, utilitarian lighting, architectural lighting, energy efficiency, durability

1. INTRODUCTION

The history of street lighting is a continuous search for more and more efficient light sources from light oil street lamps to modern efficient street lighting technologies [1]. One of such resource of electrical street lighting is the devices based on light emitting diodes (LED lighting). Light emitting diode (LED) is a semiconductor device that converts electrical current into visible radiation. The principle of LED operation is based on the phenomenon of electroluminescence when an electric current is passing through a semiconductor material that causes the emission of photons.

2. EXPEREMENTAL RESEARCH IN THE FIELD OF LED LIGHTING

Experimental physicists first observed such a light phenomenon more than 100 years ago, but could not explain it. Many scientists have been engaged in research in this area, including Russian scientist Oleg Losev [3]. He conducted experiments back in the 30s of the 20th century. He revealed a glow at the point of contact between two materials – steel and carborundum. In 1927, he received a patent for his invention, which he called "The light relay", Fig. 1. American engineer from General Electric company, Nick Holonyak, invented the world's first practical LED in 1962. However, the crystal also only had a red glow. It was the result of mixing gallium arsenide with gallium phosphide. George Craford invented the first yellow LED in 1972. Blue, green, purple LEDs appeared in the early 90s. The light from the first LEDs was too weak.

Their efficiency left much to be desired – only 1–2 lumens per watt, which was almost an order of magnitude lower than traditional incandescent lamps. Only 30 years later, in the mid-90s, this figure was already 30 lumens per watt, and by the end of the millennium – up to 60 lumens per watt [4]. They were used as an indicator, such as in calculators. In 1996, the Japanese company Nichia Chemical Industries developed technology for creating an inexpensive white LED. They used blue light – the cheapest and most efficient colour to produce be-

cause of its short wavelength. The blue light was directed into compounds called luminophores which absorbed some of the blue light and emitted yellow light. When yellow and blue light were mixed, white light was obtained. That's because the shade of white emitted depends on the blend of yellow and blue. The LEDs, developed by Nichia, had a correlated colour temperature (CCT) about 8000 K on the Kelvin scale, meaning they emitted more than 45 % blue light and appeared harsh on the eyes. For comparison, most HPSL (High-Pressure Sodium Lamps) with a "warm" orange-yellow hue have CCT in range (2700–3000) K. Fig. 2 shows the correlated colour temperature of LED lamps.

LED lamps began to be produced on an industrial scale since about 2006. LEDs have become widely used for lighting: chandeliers, spotlights, strips for hidden interior lighting, and street lighting. By the end of the 20th century, LED lights became one of the fastest-growing lighting technologies. LEDs have become popular in a variety of applications, from electronic device screens to LED luminaires for indoor and outdoor lighting. Energy-efficient LED street lighting has been gradually introduced in the cities of Europe and around the world since 2006. This innovation has reduced energy consumption up to 70 % compared to traditional lighting technologies. The important circumstance is that it is easy to control and program [5]. For example, Copenhagen has installed thousands of energy-efficient LED street lights that can be controlled and adjusted remotely, based on traffic patterns and other factors. Copenhagen has implemented a smart lighting project that integrates motion and light sensors with city data networks. The system allows you to automatically adjust lighting depending on weather conditions, time of day, and level of activity on the streets. This helps to reduce energy consumption and improve safety. The system also allows you to monitor the status of lamps in real time, which simplifies their maintenance.

LED lighting has a wide range of colours and lighting effects. With the help of coloured LED lighting, unique light installations have begun to be created in urban public places. Barcelona has begun using wireless LED street lights made by Spanish energy giant Endesa, which operate on timers and energy-saving motion sensors. The introduction of such street lights has reduced energy costs by 1/3. About 30 % of street lighting in the USA was converted to LEDs in 2016. Chicago saves $10 Million in Annual Energy Costs with LED Lighting.

3. LED LAMPS FOR STREET LIGHTING

Since 2010, a program for introducing street LED lighting has been launched in Russia, which is associated with the opening of the Optogan LED lamp assembly plant in St. Petersburg [6]. In the Russian Federation, LED lamps are produced for lighting roads of federal, regional and local importance, for architectural lighting, and for holiday lighting. Several generations of LED street lamps have appeared in Russia thanks to the progress in the field of LED technologies. First generation lamps are characterized by a specific luminous efficiency in the range of (80 – 100) lm/W. Second generation, already achieves higher luminous efficiency, exceeding 120 lm/W. In recent years third-generation LED lamps, characterized by a specific luminous efficiency of (140–150) lm/W, have found widespread use. Luminaires start to appear on the market that offer even higher luminous efficiency, exceeding (150–170) lm/W. New models are more energy efficient and cheaper than previous ones. Innovative solutions such as intelligent remote control, network communication, and thermal recognition systems are being implemented. In 2024, the volume of the Russian LED lamp market grew by 6.6 billion rubles. The global outdoor LED lighting market is expected to grow by 14.57 % over the next five years. At the same time, since 2016, the share of traditional lighting equipment has decreased by 10 %. Currently, the widespread introduction of energy-saving lighting technologies is the official strategy of the state. The main directions of development of LED outdoor lighting in the Russian Federation are utility lighting fixtures (streets, roads, public spaces), architectural lighting fixtures, and fixtures for festive decoration. For road lighting of different categories (highways, main roads, streets, alleys) trunk-type LED lamps are used. They are also used to light car parks, petrol stations, railway crossings, stadium areas, supermarkets, and house territories. Lighting fixtures must ensure traffic safety on highways, roads, streets, squares, tunnels, and alleys. Lighting of motorways is associated with such factors as the category of the road, traffic intensity, and the brightness of the road surface. Table 1 shows several examples of utility lighting fixtures used in the Russian Federation.

Table 1. The Examples of Street and Road Lighting (Utility Lighting)

Purpose of the device	Example of a lighting device	Technical specifications
City streets, roads of classes A1-A4, B1-B2, streets of rural settlements, territories of public improvement facilities, bridges		CCT: 2 700 K – 4 000 K Luminous flux: 5250 lm – 17250 lm Protection rating: IP66 IC type: LED Colour rendering index: 80 variety of device body colours
Streets and roads of urban and rural settlements, gas stations, car parks ground pedestrian crossings		CCT: 2700 K – 4000 K Luminous flux: 12700 lm – 39200 lm Protection rating: IP66 IC type: LED Colour rendering index: 80 ariety of device body colours
Pedestrian streets of urban settlements territories of public improvement facilities of urban settlements		CCT: 2700 K – 4000 K Luminous flux: 12700 lm – 39200 lm Protection rating: IP66 IS type: LED Colour rendering index: 80 variety of device body colours

High-intensity white LEDs are used in luminaires for illuminating roads, squares, and parking lots [7]. White cool glow light provides neutral illumination, high brightness and clarity. It promotes good visibility and does not distort the colour of surrounding objects. Such lamps are used wherever maximum visibility and safety are required and are suitable for most public spaces.

A special place in street lighting is occupied by architectural and artistic lighting (illumination) of buildings and urban areas [8]. High-quality lighting decor has today become an integral part of the design of the building facade as well as landscape design. This type of lighting is a combination of functional qualities and decorativeness. According to its type, architectural lighting can be flood, local (accent), contour, and background. Flood (general) lighting completely illuminates the facade and does not disrupt the overall perception. This type of lighting is used to make the illuminated object look the same as it does during daylight hours. For flood lighting, powerful ground spotlights are used, installed on stands or nearby buildings. This type of lighting is used mainly for historical buildings. Local lighting is used to highlight architectural elements of a building: arches, columns, pilaster, capitals. Contour lighting highlights the contours of a building and its large elements. This type of lighting is most often done with LED strips and linear lights. Background lighting reveals the contours of a building by illuminating its background. It is provided by diffused light luminaires. The building lighting is designed in conjunction with the lighting of the surrounding space and nearby public roads. Table 2 shows examples of different types of architectural lighting.

Light sources for architectural lighting must meet the following technical requirements:

CCT (4000–6000) K for cold white surfaces;

CCT (2300 – 3500) K for warm colour surfaces;

Protection class IP not less than 65;

Colour rendering index for multi-coloured surfaces not less than 80;

Powerful lamps (more than 150 W) are installed in a protective casing to protect against blinding the driver.

Table 3 shows the examples of LED luminaires used for architectural lighting of buildings.

Lighting standards vary depending on the location and significance of the illuminated object. For example, the average brightness for illuminating a public building in a wide city area range from 10 cd/m^2 to 30 cd/m^2, depending on the type of architectural lighting chosen. In the case of buildings that are cultural heritage sites, located in the surrounding areas, the average luminance is usually be-

Table 2. The Examples of Architectural Lighting of Buildings

Flood lighting	Contour lighting	Local lighting	Background lighting
		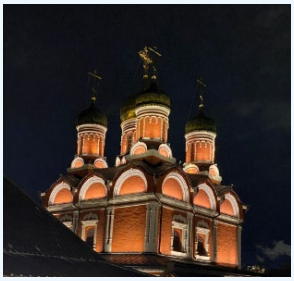	

Table 3. The Examples of Lamps for Architectural Illumination of Buildings

Purpose of the device	Example of a lighting device	Technical specifications
Lighting of facades of buildings, structures, public facilities		Colour rendering: 90 R_a CCT: 3000 K – 4000 K Degree of protection: IP68
Lighting of building facades, including contour lighting of individual architectural elements, road structures	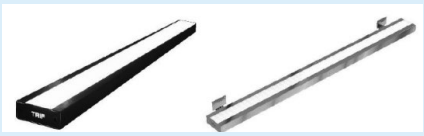	Colour rendering: 85 R_a CCT: 3000 K – 4000 K Degree of protection: IP68
Narrowly targeted lighting of decorative elements of the facades of buildings, structures, and public facilities		Colour rendering: 90 R_a CCT: 3000 K – 4000 K Degree of protection: IP68

tween 3 cd/m² and 10 cd/m². In addition, architectural lighting must be designed so, that the lighting installations do not create a dazzling effect for vehicle drivers and pedestrians.

Festiv illumination is a festive decorative lighting intended only for decorating streets, squares, buildings, structures and landscape elements without the need to create a certain level of illumination. The difference between festive lighting (illuminations) and utilitarian and architectural lighting is that the light sources themselves are the objects of consideration. Equipment for holiday lighting can be divided into large groups of light sources: contour (flexible neon, duralight), area (light curtains) and figures (trees, animals).

Flexible neon is an LED strip (110 or 120 diodes/m) enclosed in a matte silicone or PVC shell. The entire space between the LEDs is filled with a waterproof compound, making the glow uniform and "soft" along the entire length of the wire. Flexible neon can be cut in multiples of 1cm and 2.5cm – this way you can easily adjust the length to suit the requirements of the project. Flexible neon is used for decorative lighting of parts of buildings, bridges, and for decorating trees. It can be of different colours and shades: cold white, blue, yellow, red, orange, green.

Durus light is a transparent PVC tube containing LEDs inside. Due to the transparency of the tube, each LED remains visible and a point glow effect is achieved. "Flexible neon" is often used in the ad-

Fig 1. Russian scientist Oleg Losev (1903–1942)

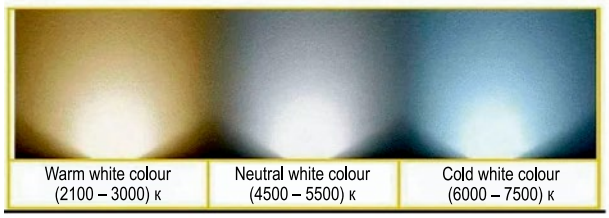

Fig. 2. Correlated colour temperature of LED lamps

a) *b)*

Fig. 3 Light sources for festive lighting: *a)* duralight; *b)* flexible neon

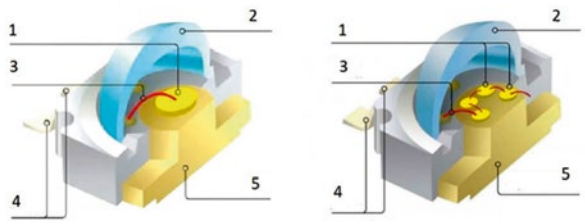

a) *b)*

Fig. 4. The design schemes of SMD (*a*) and COB (*b*) LEDs: 1 – semiconductor crystal; 2 – lens; 3 – contact wire; 4 – contact; 5 – heat dissipating body elements

vertising field: to design inscriptions, logos or illuminate signs. Duralight can be used for decorative lighting of building facades, entrance lobbies, windows, doors, columns, as well as for creating light figures. It bends easily and can take different bends and shapes. Both backlight options can have different brightness and glow colours. They can operate from the network and be controlled using an external controller programmed for various lighting effects. Fig. 3 shows the examples of duralight and flexible neon.

4. TYPES OF LEDs FOR STREET LIGHTING

The following types of LEDs are used for street lighting: SMD (Surface-Mounted Device) LEDs; COB (Chip on Board) LEDs; Multi-chip LEDs [9,10].

SMD LEDs are mounted on the surface of the printed circuit board. They are characterized by high light output, compact size and durability. Their disadvantage is the difficulty of repair.

COB LEDs are several crystals mounted on a single board and coated by the phosphor, which ensures uniform light distribution. Their advantages are high brightness and uniform light emission. Disadvantages are higher cost and limited replacement options. They are using in high-power street lamps that require high luminous intensity.

Multi-chip LEDs consist of multiple LED crystals, placed side by side and working together to produce a powerful light output. They are highly efficient and have the ability to control the light temperature. Disadvantages – the need for high-quality heat dissipation and more complex control. They are used to illuminate large objects such as highways and parks. The design schemes of SMD and COB LEDs are shown in Fig. 4.

One of the latest advances in LED lighting is the introduction of organic light emitting diodes OLEDs. These are very thin, rigid or flexible sheets no thicker than 1.8 mm, visually similar to films, Fig. 5. They emit soft, diffused light over their entire surface. Their light emitting layer consists of carbon and hydrogen compounds without any other components. Organic LEDs can emit light of different colours, while when turned off, they are almost completely white and transparent. OLEDs are environmentally friendly and energy efficient. They comply with government programs adopted in many countries of transition to energy efficient technologies.

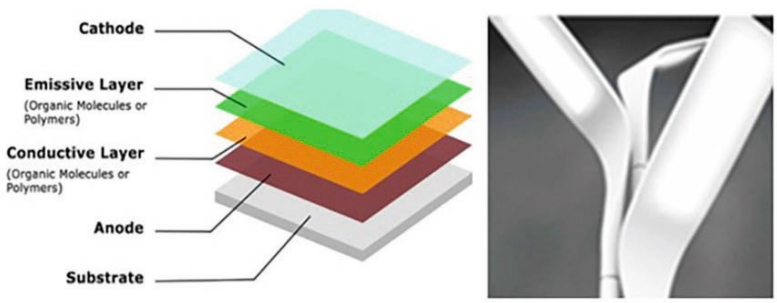

Fig. 5. OLED light emitting diode composition and the appearance of OLED lamp

One of the promising areas in the development of LED devices is the use of phosphors based on quantum dots. In any case, LED lighting technology will continue to develop with increasing energy efficiency and decreasing equipment prices.

CONCLUSIONS

LED street lighting has become widespread because it has a number of significant advantages compared to other types of lighting:

– LED lighting is more energy efficient in comparison to traditional lighting technologies, energy consumption is 70 % lower;

– The quality of lighting with LED lamps is higher due to the absence of flicker. LED lamps operate at voltage drops from 80 V to 300 V and at temperatures from –50 °C to +60 °C. This property is especially important for applications such as street lighting. LED lamps do not require warming up after switching on. 100 % of the light flux is delivered immediately;

– The lifespan of the selected LED is designed to last approximately 100 000 hours or approximately 20 years. This is approximately 6 times the lifespan of traditional street lights;

– Exposure to LED light is as safe as exposure to daylight or any other electrical light source**;**

– LED lighting is also very versatile, capable of producing a wide range of colours and lighting effects, and can be easily controlled and programmed using smart city technologies;

– LED street lighting is programmable, which is manifested primarily in the ability to adjust its brightness.

REFERENCES

1. Sokolova, I.V. Gas Lighting in the History of Lighting Technology // Light &Engineering, 2024, Vol. 32, # 1, pp. 107–113.

2. What is LED chip? Understanding the Basics and Types // URL: https//polluxteam.com/mag/led-chip (Accessed: 12 November 2024).

3. Rabinovich, O., Yunovich, A. On the discovery of semiconductor light sources (to the history of the creation of LEDs) [Ob otkrytii poluprovodnirovyx istochnikov syeta (k istorii sozdaniya syetodiodov)] // Svetotekhnika, 2014, # 3, pp. 40–45.

4. 25th Anniversary of the White LED Nichia innovation that changed the world // URL: https:// www.ledinside.com/ node/ 32252 (Accessed: 10 November 2024).

5. Goswami, A.D., Chakraborty, S. Road lighting standards evolution and future development of smart street lighting based upon users // Light & Engineering, 2023, Vol. 31, # 5, pp. 106–117.

6. Optogane and Philips Start Production of LEDs for Streets // URL: https: ria.ru/20130402/502121401.html (Accessed: 12 November 2024).

7. Savikova, T.N., Krachenko, A.I., Kolesnik, Y.N., Seliverstova, D.I. Current state and development prospects of lighting devices based on white LEDs [Sovremennoe sostoyanie i perspektivy razvitiya osvetitel nyx ustrojstv na osnove belyh svetodiodov] // Vestnik GGTU named after P.O. Suhoi, 2020. # 3, pp. 45–49.

8. Zaporenko, S.Y. Features of festive architectural lighting of facades of cultural objects [Osobennosti-prazdnichnogo-arhitekturnogo-osveshcheniya-fasadov-obektov-kultury] // Sovremennoe-stroitelstvo-i-arhitektura 2020, # 1 (17), pp. 6–14.

9. Esteki, M., Khajehoddin, SA., Safaee, A., Li, Yu. LED systems applications and LED driver topologies: a review // IEEE ACCES eISSN: 2169–3536, 2023, Vol. 11, pp. 38324–38358.

10. Types of LEDs, parameters, marking // URL: https://terra-led.ru/reviews/detail/vidy-svetodiodov-parametry-markirovka/?ysclid=m4h8ngy2ba356103624 (Accessed: 12 November 2024).

Irina V. Sokolova,
Ph. D., Associate Professor. In 1980, she graduated from NRU MGSU with specialty in Civil Engineering. Her research interest is building design and construction physics

Light & Engineering
Vol. 33, No. 4, pp. 50–56, 2025

https://doi.org/10.33383/2024-096
Svetotekhnika # 3, 2025, pp. 59–63

CALCULATION AND EVALUATION OF THE EFFECTIVENESS OF LIGHTING THE CONSTRUCTION SITE WITH FLOODLIGHTS OF VARIOUS CAPACITIES

Elena A. Korol and Evgeniy N. Degaev

National Research Moscow State University of Civil Engineering (NRU MGSU), Russia
E-mails: degaev@inbox.ru, professorkorol@mail.ru

ABSTRACT

Working in the dark requires quality lighting of the construction site. To illuminate large open spaces, floodlights are used to create a powerful directional luminous flux, which improves visibility of working areas, reduces the risk of occupational injuries and improves overall safety at the construction site. Analysis of construction organization projects developed in period of 2014–2024 years revealed that almost all projects determine the number of floodlights for outdoor lighting of construction sites for incandescent lamps using the specific power method. Due to the fact that incandescent lamps are prohibited at the legislative level, LED floodlights are actually used on construction sites in violation of project requirements. This can affect the quality and safety of work, as well as increase the cost of lighting. The results of the study showed that the method of specific power provides at the required level of average illuminance on the horizontal plane, but can only be considered as a preliminary calculation and in the projects of construction organization should not use them, because the method does not take into account other mandatory lighting characteristics that determine the safety of work at the construction site. For the device of general illumination of the studied construction site preferable are floodlights with a capacity of 70 W in the number of 28 pcs. Other LED floodlights turned out to be more than (1.04–4.64) times more expensive to operate and maintain.

Keywords: illumination modelling, specific power method, construction site lighting, LED floodlights, visibility of work areas, occupational safety

1. INTRODUCTION

The global trend of increasing housing construction is associated with population growth and urbanization. This leads to an increase in demand for housing and the development of the construction industry. Different countries have their own particularities and challenges in this area, but the general trend is to increase the volume and pace of construction. Working at night is one of the most common approaches to increase the speed of construction. Working at night requires quality lighting of the construction site [1]. To illuminate large open spaces, floodlights are used to create a powerful directional light stream, which improves the visibility of working areas, reduces the risk of occupational injuries and improves overall safety at the construction site [2].

The current regulatory documentation[1] allows the use of general-purpose incandescent lamps, high-pressure sodium lamps, high-pressure metal halide lamps, high-pressure mercury lamps, xenon lamps, LEDs and LED modules. Until 2011, construction organizations widely used incandescent

[1] Russian standard: GOST 12.1.046–2014 "System of labour safety standards. Construction. Norms of lighting of construction sites"

lamps as the cheapest source of light, but now the use of incandescent lamps of 100 W and above is legally restricted. In the last decade, LED floodlights are mainly used for outdoor lighting of construction sites, which are a rational choice due to their economy, durability, safety and environmental friendliness [3].

The issues of LED lighting in recent years have attracted the attention of both domestic and foreign researchers. This is due to the growing interest in environmentally friendly and energy-efficient lighting technologies.

In the studies of domestic and foreign authors consider various aspects of the use of LED lighting fixtures and floodlights in different operating conditions of their impact on the electrical grid, human health, and the environment. Researchers analyse the advantages and disadvantages of LED technologies, and offer recommendations for their use and efficiency improvement [4–8].

Although the problems of LED lighting are widely considered in scientific research, the issue of the correctness of calculating the number of floodlights for a construction site requires more in-depth study. Thus, El Korany Tamer, Eldosouky Adel, and Azzam Rawan from Tanta University (Egypt) conducted a study of the actual placement of floodlights on construction sites and came to the conclusion that the actual distribution of lamps is an order of magnitude higher than the standard illumination at various points of the facility. The authors propose using smaller tilt angles, leading to greater coverage of surfaces with light, which minimizes the number of floodlights [4].

Gordeeva V.V. and Shamin K.V. suggest using the developed program "TechnicalLight" to optimize the placement of lighting sources on construction sites. The authors note that the development of the product takes into account the requirements for the construction of calculation models and the program can be used by designers, as well as in the educational process in the discipline "Life Safety", but the choice of light sources should be guided by economic indicators [5].

In his research, Kazarin V.E. analysed the calculation of lighting by the specific power method using LED lighting devices and found that reference and regulatory documents do not contain data on the specific power values of LED lamps and modern lighting devices, as well as on the values of the utilization factor and the coefficient of unevenness [6].

The current regulatory documentation does not establish strict requirements in the choice of method for calculating the number of floodlights, so, in the design documentation, the method of specific power is using, because it is the simplest. However, nowhere is it specified what coefficient to use to take into account the light output of LED floodlights, so the construction management projects continue to provide calculations for known light sources for which this coefficient was previously established by regulatory documentation. When analysing the construction organization projects developed in period of 2014–2024 years, it was found that almost all projects determine the number of floodlights for outdoor lighting of construction sites is made for incandescent lamps, which since 2011 have been banned for use. On the sites themselves, LED floodlights are used mainly, as incandescent lamps are not available, so the number and placement of floodlights raises questions. In addition, the power density method does not take into account the uniformity of illumination and the gloss factor, which are mandatory characteristics for safety at the construction site.

The purpose of this work is to investigate the possibility of using the power density method to calculate the number of LED floodlights and the choice of their power with consideration of economic efficiency.

Scientific novelty of the work is to clarify the method of specific power to calculate the lighting of construction sites using LED floodlights, taking into account their light output.

Practical significance of the work is to determine the total economic costs associated with the purchase, installation and operation of LED floodlights of different power. The results of the study can be useful in practice for designers, builders and lighting specialists working on construction sites.

2. METHODS

Regulatory requirements for the level of general illumination of a construction site have been significantly tightened in the current editions of regulatory documents, which determines the choice of construction organizations in favour of LED floodlights with high energy efficiency. Thus, since 2014 it has been established that the general uniform lighting should be used if the standardized value of illumi-

Table 1. Illumination and Maximum Permissible Specific Installed Capacities of the General Lighting of the Construction Site[1]

Visual work category	Type of work	Average illumination in the horizontal plane, lx	Uniformity of illumination U_0, relative units, not less	Gloss coefficient R_G, relative units	Maximum allowable specific power, W/m², not more than
XVI	General monitoring of the production process	10	0.25	55	0.8

[1] Document RF: SP 52.13330.2016 "Natural and artificial lighting"

nance does not exceed 10 lx[2] (was 2 lx)[3]. In other cases, and in addition to the general uniform lighting should be provided for general localized lighting or local lighting. Table 1 presents the main normative characteristics of general illumination of the construction site, which are the initial data for calculations.

To calculate the required number of floodlights with incandescent or discharge lamps for general illumination of the construction site in the projects of construction organization widely used method of specific power of lamps:

$$N = \frac{mE_pS}{P}, \qquad (1)$$

where m is the coefficient depending on luminous efficacy of the luminaire, W/(lx·m²); $E_p = K \cdot E_n$ (K is the safety factor; E_n is the standardized minimum illuminance, lx); S is the illuminated area, m²; P is the lamp power, W.

A construction site with an area of 11024 m² used in the construction of a 12-storey apartment building in Moscow was chosen as the object. For the study, LED floodlights with power from 30 W to 480 W were selected, which are widely available on the market and used on construction sites. Lighting characteristics of the projectors are presented in Fig. 1 and Table 2.

[2] Standard RF: GOST 12.1.046–2014 "System of labor safety standards. Construction. Norms of lighting of construction sites"

[3] Standard RF: GOST 12.1.046–85 "System of labour safety standards. Construction. Norms for lighting of construction sites"

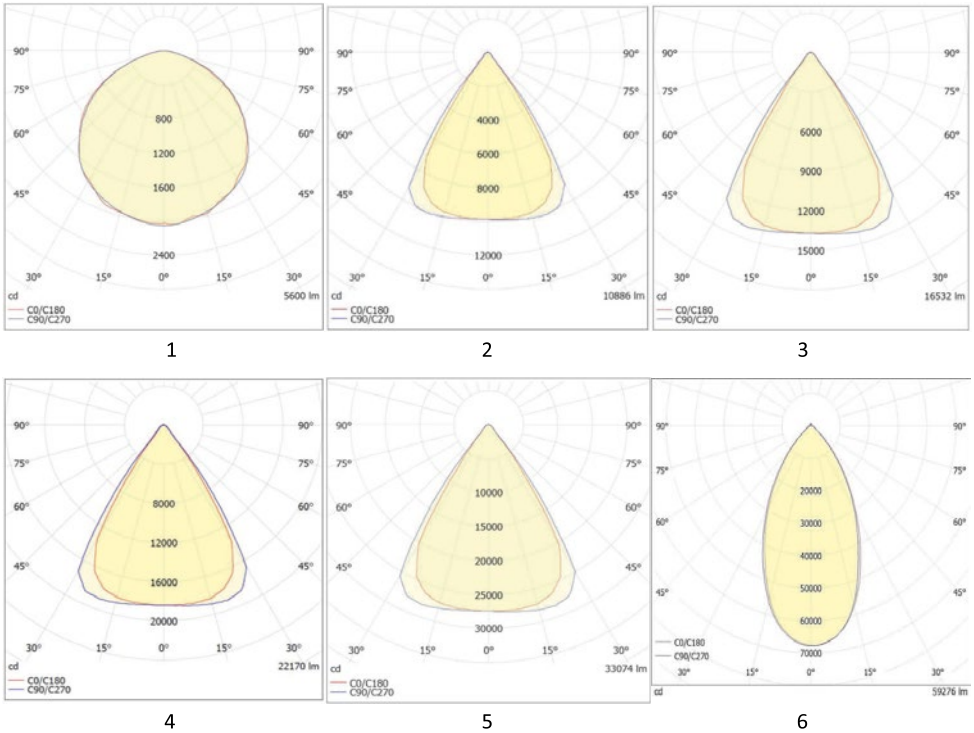

Fig. 1. Luminous intensity curves of LED floodlights with a power of 70 W (1), 100 W (2), 150 W (3), 200 W (4), 300 W (5) and 480 W (6)

Table 2. Lighting Characteristics of the Studied LED Floodlights

Floodlight power, W	Luminous flux, lm	Luminous efficacy, lm/W	The angle of the light beam, angle degree	CCT, K	Coefficient *m*, W/(lx·m²)
30	2400	80.0	120	4000	0.0125
50	4050	81.0	120	4000	0.0123
70	5600	80.0	120	4000	0.0125
100	10886	108.9	60	5000	0.0092
150	16532	110.2	60	5000	0.0091
200	22170	110.9	60	5000	0.0090
250	32500	130.0	60	5000	0.0077
300	33074	110.3	60	5000	0.0091
400	52000	130.0	60	5000	0.0077
480	69277	144.3	60	5000	0.0069

3. RESULTS

According to the available characteristics and formula (1), the required number of LED floodlights of different power (for general illumination of the construction site (E_n = 10 lx)) are calculated:

$N_{30} = 59.7 \approx 60$ pcs; $N_{50} = 35.4 \approx 36$ pcs;

$N_{70} = 25.6 \approx 26$ pcs; $N_{100} = 13.2 \approx 14$ pcs;

$N_{150} = 8.7 \approx 9$ pcs; $N_{200} = 6.5 \approx 7$ pcs;

$N_{250} = 4.4 \approx 5$ pcs; $N_{300} = 4.3 \approx 5$ pcs;

$N_{400} = 2.8 \approx 3$ pcs; $N_{480} = 2.1 \approx 3$ pcs.

To verify the calculations obtained by the specific power method, we will use the computer program DIAlux evo, which is based on photon maps constructed on the basis of stochastic ray tracing, followed by a final acquisition procedure (synthetic iteration according to the global illumination equation), which is more accurate than the specific power method and takes into account the illuminance uniformity and the gloss ratio, which affect the safety of the works [9]. The simulation results are presented in Figs. 2–5. As a solution, the program proposed and arranged 16 LED floodlights with a power of 100 W and 15 m masts, Fig. 2.

According to the accepted rule of rounding upwards, in calculating by the method of specific power, a difference of 2 floodlights was received. Indeed, with 14 floodlights average illuminance of the construction site will be 10 lx, however, to ensure uniformity of illumination 16 floodlights should be used. Computer modelling established the need for 6 floodlights with a power of 300 W, Fig. 3.

If the height of the masts is 30 meters, the average illumination will be 10.7 lx, the minimum illumination will be 2.7 lx, which corresponds to the uniformity of illumination U_0 of 0.25 units. A smaller number of floodlights is also unable to provide uniformity of illumination. Thus, when calculat-

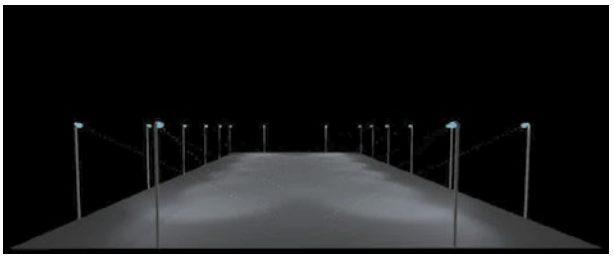

Fig. 2. Simulation results of general lighting of the construction site in DIALux evo with 100 W LED floodlights

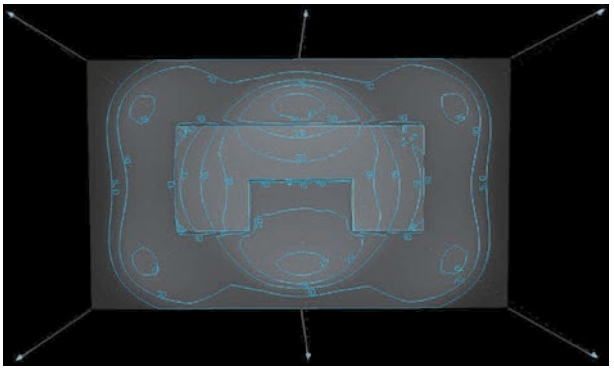

Fig. 3. Simulation results in DIALux evo of the total illumination of the construction site with 300 W LED floodlights

Table 3. Information on the Cost of Purchasing and Using LED Floodlights with a Power of (30–480) W

Floodlight power, W	The average cost of one floodlight, rub.	Required number of searchlights and masts, pcs	The cost of purchasing floodlights, rub.	Total floodlight power, kW	Cost of electricity, rub/kW	The operating time of the floodlights at night during the year, h	Electricity costs, rub	Required height of the lighting mast, m	The average cost of one lighting mast, rub	Cost of purchasing masts and lighting poles, rub
1	2	3	4	5	6	7	8	9	10	11
30	2100	54	113400	1.62	6.99	4161	47118	8	15500	837000
50	3560	34	121040	1.70	6.99	4161	49445	8	15500	527000
70	6450	28	180600	1.96	6.99	4161	57007	8	15500	434000
100	8000	16	128000	1.60	6.99	4161	46537	15	140000	2240000
150	10240	10	102400	1.50	6.99	4161	43628	20	215000	2150000
200	12500	8	75000	1.60	6.99	4161	46537	25	284000	2272000
250	14390	6	86340	1.50	6.99	4161	43628	30	357000	2142000
300	16000	6	96000	1.80	6.99	4161	52354	30	357000	2142000
400	85000	4	340000	1.60	6.99	4161	46537	40	665000	2660000
480	100000	4	400000	1.92	6.99	4161	55844	40	665000	2660000

ing the method of specific power, the difference was found for all LED floodlights, except for 400 W and 480 W, Fig. 4.

It is worth noting that it is necessary to take into account the fact that some of the light may be shaded during the construction of the building. For example, if you use 3 floodlights with a power of 400 W or 480 W, erecting a building higher than the light masts will lead to a lack of lighting on one side of the site. To ensure illumination of the object throughout the entire construction cycle, it is necessary to install 4 floodlights of 400 W or 480 W, placing them in the corners of the site at a height of 40 m, Fig. 5.

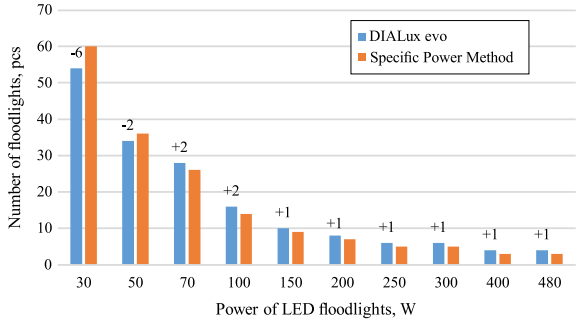

Fig. 4. The results of determining the number of light sources in the DIALux evo and the specific power method, indicating the difference between the floodlights quantity

When selecting the capacity of floodlights should take into account their economic efficiency, which is characterized by the lowest costs of purchase, installation and operation in comparison with other floodlights [5, 10, 11]. Table 3 summarizes the cost information, which will be required to calculate the total costs of each variant of floodlights.

From the results, Fig. 6, it follows that the lowest costs of the construction organization will be incurred in the case of the purchase and use of LED floodlights with a capacity of 70 W (672 thousand rub.) when working during the year in 3 shifts of 8 hours.

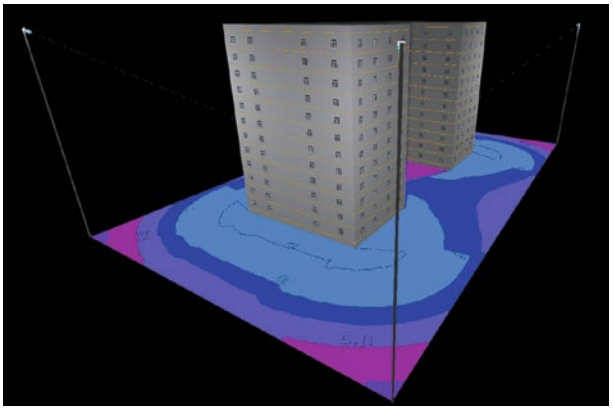

Fig. 5. Simulation results in DIALux evo of the total illumination of the construction site with 480 W LED floodlights

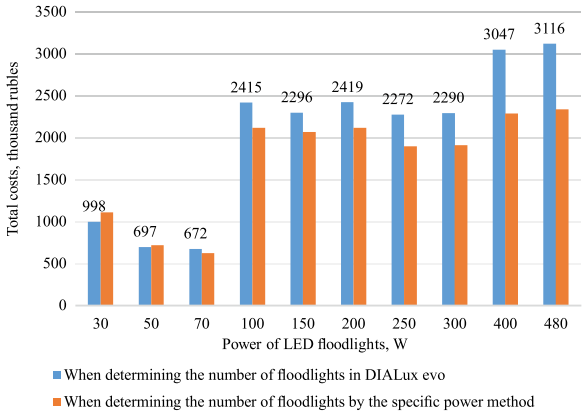

Fig. 6. Total costs for purchasing and using LED floodlights with a power of (30–480) W

Thus, for the device of general lighting of the construction site under study, floodlights with a power of 70 W in the number of 28 pcs. are preferable. Other LED floodlights were more expensive in operation and maintenance by more than (1.04–4.64) times.

4. DISCUSSION

The results of the study showed that the method of specific power can be used only for approximate determination of the number of floodlights. The use of the calculation results of this method in the construction organization projects does not provide the required lighting characteristics of illumination of the construction site, determining the safety of work performance. The difference in the results of determining the number of light sources was found for all considered LED floodlights, except for 400 W and 480 W. The power density method provides the average illumination of the construction site with the required number of floodlights, but the safety factor of 1.3 does not provide uniformity of illumination at the level of 0.25 units. Lighting uniformity plays a key role in workplace safety, reducing the risk of accidents and injuries.

LED floodlights with 70 W are the most energy efficient, which is characterized by the lowest total cost of purchase and operation. Other LED floodlights were more expensive in operation and maintenance more than (1.04–4.64) times.

The results of computer simulation clearly visualize the object, while providing the required lighting characteristics, so the use of DIALux evo or other similar software products should become mandatory for the organization of the construction site.

REFERENCES

1. Smirnova (Meshkova), T.V., Boos, G.V., Budak, V.P., Ilyina, E.I. Evaluation of lighting quality based on visibility // Light & Engineering, 2023, vol. 31, # 4, pp. 4–13; DOI: https://doi.org/10.33383/2022-096.

2. Onososen Adetayo, Musonda Innocent, Onatayo Damilola, Saka Abdullahi, Adekunle Samuel, Onatayo Eniola. Drowsiness Detection of Construction Workers: A Proactive Approach to Accident Prevention Leveraging Yolov8 Deep Learning and Computer Vision Techniques // Preprints.org (www.preprints.org), Posted: 10 October 2024; DOI: https://doi.org/10.20944/preprints202410.0764.v1.

3. Solovyov, K.A. Lighting fittings and the history of the development of artificial lighting in Russia [Osvetitel'naya armatura i istoriya razvitiya iskusstvennogo osveshcheniya v Rossii] // Svetotekhnika, 2022, # 3, pp. 12–18.

4. Kuzmenko, V.P. Investigation of the influence of LED floodlights on the processes of managing the quality of electric energy and energy efficiency [Investigation of the influence of LED floodlights on the processes of electric energy quality and energy efficiency management] // Omsk Scientific Bulletin, 2021, # 2(176), pp. 15–19; DOI: https://doi.org/10.25206/1813-8225-2021-176-15-19.

5. Gordeeva, V.V., Shamin, K.V. Program for optimizing the placement of lighting sources at construction sites [Programma optimizacii razmeshcheniya istochnikov osveshcheniya na stroitel'nyh ploshchadkah] // Software engineering: modern trends in development and application: collection of materials of the 3rd All-Russian conference dedicated to the 55th anniversary of South-West State University, Kursk, March 11–12, 2019, Kursk: Closed Joint-Stock Company "University Book", 2019, pp. 117–121.

6. Kazarin, V.E. Improving the methodology for calculating the lighting by the specific power method of LED lighting devices for agricultural enterprises and organizations [Sovershenstvovanie metodiki rascheta osveshcheniya metodom udel'noj moshchnosti svetodiodnymi svetovymi priborami sel'skohozyajstvennyh predpriyatij i organizacij] // Bulletin of the Altai State Agrarian University, 2019, # 2 (172), pp. 172–176.

7. Boos, G.V., Grigoryev, A.A. New approach in the determination of qualitative characteristics of outdoor il-

lumination installations // Light & Engineering, 2016, Vol. 24, # 1, pp. 51–57.

8. Shmarov, I.A., Brazhnikova, L.V., Soloviev, A.K. Safety of using LED lighting according to the EU Scientific Committee and Russian studies [Bezopasnost' primeneniya svetodiodnogo osveshcheniya po dannym nauchnogo komiteta Evrosoyuza i rossijskih issledovanij] // News of higher educational institutions. Technology of the textile industry, 2019, # 4 (382), pp. 196–202.

9. Shcherbakov, A.S., Frolov, V.A. Matrix transformations for effective implementation of radiosity algorithm using graphic processors // Light & Engineering, 2019, Vol. 27, # 2, pp. 105–110.

10. Stolyarevskaya, RI. Forecasting the technical resource of lamps with LEDs [Prognozirovanie tekhnicheskogo resursa svetil'nikov so svetodiodami] // Svetotekhnika, 2017, # 3, pp. 70–75.

11. Budak, V.P., Zheltov, V.S. Mathematical modelling in light and engineering education // Light & Engineering, 2023, vol. 31, # 6, p. 22–28; DOI: https://doi.org/10.33383/2022-095.

Elena A. Korol,
Doctor of Technical Sciences, Professor of the Department of Housing and Communal Complex at Moscow State University of Civil Engineering (NRU MGSU); Corresponding Member of the Department of Building Sciences of the Russian Academy of Sciences

Evgeniy N. Degaev,
Ph. D., Associate Professor of the Department of Housing and Communal Complex at Moscow State University of Civil Engineering (NRU MGSU)

Light & Engineering
Vol. 33, No. 4, pp. 57–65, 2025

https://doi.org/10.33383/2025-007
Svetotekhnika # 3, 2025, pp. 34–39

VERTICAL DAYLIGHT FACTOR AS A CRITERION FOR GENERAL DAYLIGHTING IN EDUCATIONAL AUDITORIUMS

Nina A. Molchina* and Alexei K. Solovyov**

National Research University Moscow State University of Civil Engineering (NRU MGSU)
*E-mails: *nina_mour@mail.ru, **kafedraarxitektury@yandex.ru*

ABSTRACT

High-quality daylighting plays a crucial role in creating a comfortable environment in educational auditoriums. It is well known that insufficient daylighting adversely affects both: students' health and academic performance. The existing methods for designing and evaluating daylighting focus on ensuring the minimum acceptable levels of horizontal illuminance (Daylight Factor, *D*) required for visual tasks. However, it is equally important to provide comfortable general daylighting in auditoriums.

Currently, requirements for general daylighting are not systematized. This article proposes a structured approach to defining the functions of daylighting as general lighting in indoor spaces and criteria for assessing comfortable general lighting. These proposals aim to refine the requirements not only for daylighting but also for electrical lighting in future design projects. The authors continue to investigate the relationship between measurable photometric parameters, obtained using a luxmeter, and qualitative lighting criteria such as light saturation, uniformity, and contrast.

The article presents the results of studies conducted in several auditoriums at the National Research Moscow State University of Civil Engineering (NRU MGSU) with side lighting openings, all serving the same functional purpose but differing in room and opening characteristics. An evaluation of *D* levels was carried out using the existing methodology, alongside an assessment of saturation through the ratio of the coefficient of daylight cylindrical illuminance (CDCI) to Daylight Factor (*D*). Additionally, the distributions of the coefficient of daylight vertical illuminance (CDVI) in four planes relative to the light opening and the coefficient of daylight spherical illuminance (CDSI) in characteristic cross-sections were analysed.

It was found that the CDVI in the plane oriented towards the wall opposite the light opening remains nearly constant in absolute values across all points of the characteristic cross-section of the room. Suggestions are provided for assessing contrast and light saturation in rooms using the CDVI.

Keywords: quality of daylighting, general daylighting, spherical illuminance, cylindrical illuminance, indoor light environment, side daylighting, light saturation in rooms, the coefficient of daylight vertical illuminance (CDVI), the coefficient of daylight cylindrical illuminance (CDCI), lighting uniformity, lighting contrast

1. INTRODUCTION

"Quality should be embedded in technology, not proven by control," said William Deming, the 20th-century scientist and specialist in quality management. His words are also applicable to the formation of the quality of the daylight environment in the premises.

In educational spaces where concentration, attention, and engagement are required from all participants in the process, daylighting plays a particularly important role. It is known that insufficient, low-quality daylighting negatively affects the results of students [1].

At the same time, major changes are taking place within universities today: new educational technologies are emerging, the educational environment is changing, the material and technical base is being updated, education itself is becoming more flexible and adaptive, and the importance of cross-disciplinary relations is increasing [2].

But how exactly can we incorporate the quality of daylighting into the design of classrooms? Light, which the famous architect Le Corbusier called a "building material", plays a key role in creating a comfortable educational environment. In the professional environment of designers and architects, there is a term "light space" [3], which emphasizes the importance of light as a formative element of space.

According to regulatory requirements, daylighting should ensure the fulfilment of visual tasks, be uniform and eliminate the discomfort associated with the blinding effect. However, the question remains: how to make the lighting like this? What criteria should be applied to the projected "light space" and what quantitative parameters should be used to describe it?

In the context of increasing attention to public health, the impact of the urban environment on it and the comfort of the internal environment of buildings under construction, outlined in the Construction Industry Development Strategy and the Decree on the National Development Goals of the Russian Federation for the period up to 2030 and for the future up to 2036, these issues are becoming particularly relevant [4, 5]. Today, the systematization of the requirements and parameters of the quality of daylighting is necessary to form a correct technical specification for lighting in the context of the transformation in the construction industry associated with the transition to the registry principle and the parametric rationing system [2].

This article presents the results of a study on the search for numerical parameters of the quality of daylighting, which continues the authors' research cycle on the issue of assessing the saturation of rooms with daylight [6, 7, 8]. The authors aim to find a physical quantity measured by a conventional luxmeter that characterizes the quality indicators of the room's day lightening, is able to describe the light field in the room and correlate with the psychophysical assessment of observers, as well as having an accessible engineering calculation method in the future.

The requirements for the quality of the light environment depend on the function of the space under study and on the direction of the luminous flux. In this study, classrooms of higher educational institutions with lateral light openings at the line-of-sight level, located on the left side relative to the blackboard, were considered.

2. METHODS

The main functions of daylighting arise from its differences from electrical lighting – humans need sunlight and its unique spectral composition. It has been proven that insufficient daylight affects the hormonal background and cognitive abilities of people, and especially children. A space flooded with daylight has a positive effect on a person's psycho-emotional state. Therefore, when forming functional requirements for the interior, it is advisable to set the following tasks for daylighting to increase the level of satisfaction and functionality of the daylight environment:

– Orientation in space;

– Ensuring communication with the external environment;

– Creating a uniform and daylight-saturated indoor environment.

The formation of comfortable general daylighting is seen as the most important for spaces where the line of sight is not fixed for its functional purpose, for example, in rooms designed for human communication.

It seems that the criteria for ensuring the listed functions of daylighting can be **saturation of light**, c**ontrast of light,** and **uniformity of lighting** in the room.

In this approach, daylighting is considered as a factor ensuring the quality and comfort of the indoor environment.

The comfort of the environment is an indicator that can only be assessed by the consumer, in this case by an observer. The scale of this assessment may be the degree of satisfaction with the space. The Daylight factor (D) parameter, being normalized today, has no confirmed connection to the observer's subjective assessment of the daylight scene in the room. At the same time, it is possible to predict the degree of satisfaction at the design stage, as well as the functionality of daylighting, that is a sufficiency of daylighting to perform visual work in a specific room of the projected object in the future

could improve the quality of the projected spaces and the compliance with the functions inherent in these spaces.

An analysis of foreign studies on this issue shows that attempts are being made to define new relative criteria for evaluating daylighting, in addition to and in addition to the existing indicator *D* (daylight factor), which is an analogue of the coefficient of daylight illuminance in Russian standards, as well as physical criteria for evaluating the light environment as a whole, formed indoors. For example, the British standard requires an increase in *D* standards if a room combines several functional spaces by 1 %. The UDI indicator has also been added to the standards, which takes into account the function of time and shows the availability and levels of daylight during working hours, for example, school hours. In Poland, in addition to *D*, the illumination of the ceiling and walls is estimated. Also, in European standards, there is a separation of the fields of performing a visual task and the fields of the background from the field of the task [1].

A study by scientists Antonello Durante and Kevin Kelly from the Dublin University of Technology is also of interest, who are investigating the relationship between perceived lighting adequacy (PAI) and the average illumination of indoor surfaces (MRSE), an assessment of illumination within the framework of a new design methodology focused on ambient and target lighting [9].

Their predecessor, Peter Boyce, and co-authors argue that a paradigm shift is actually needed using new interior design methods that prioritize lighting the space rather than the horizontal working plane [10].

This approach essentially suggests estimating the brightness of the room's surfaces, which is closer to estimating the light field in a room than to estimating the illumination level at a point on the work surface according to *D*. Among the problems of implementation, the authors cite the complexity of measurements and the lack of evidence that the proposed indicator is related to people's satisfaction and their perception of the amount of light in the room [9].

An experimentally proven correlation with the psychophysical assessment of the saturation of a room with light by an observer is the spatial characteristic of the light field – cylindrical illumination and the indicator of saturation with daylight of rooms proposed in previous studies by the authors of this article [11]. This is the CDCI/*D* ratio, where CDCI is the coefficient of daylight cylindrical illumination.

According to the authors' research, it is acceptable to measure cylindrical illumination as the average vertical illuminance on 4 sides, but this approach still involves a large number of measurements, which makes it difficult to use this criterion.

When an observer evaluates the overall illumination of a room, he looks at the surfaces and the surrounding three-dimensional objects, their brightness, the ratio of the brightness of different surfaces, the contrast of the plane of the light system and the walls. The more the brightness of the window differs from the brightness of the walls, the faster the feeling of gloominess of the room will come with a decrease in outdoor illumination. It should be added that the observer can evaluate the general lighting of the room from different points of the space, doing different functional tasks. Here it seems advisable to apply the approach used in the design of sports facilities, where the illumination should satisfy different functional processes (athletes, spectators, filming) with an unstable line of sight and a moving object of discrimination. For such spaces according to SR 440.1325800.2023 "Sports constructions. Daylighting and electrical lighting design" the vertical illuminance, created by electrical light sources, is evaluated. The plane and location of the point in height depend on the sport type. Returning to the daylight illumination of classrooms with side light openings, it is interesting to evaluate the average illumination and brightness of surfaces, which is described in studies [9, 10], through vertical illuminance in planes differently oriented relative to the light barrier.

The authors conducted a series of studies in classrooms of the NRU MGSU with the same functional purpose, similar dimensions in plan, but different colours of decoration and the location of the side light openings. It should be noted that the windows in all classrooms were located on the left. All measurements were made with simultaneous measurements of the external horizontal illumination in a completely cloudy sky.

2.1. Research # 1

The first research was conducted in the standard class for practical lessons of the National Research University of Moscow State University (auditori-

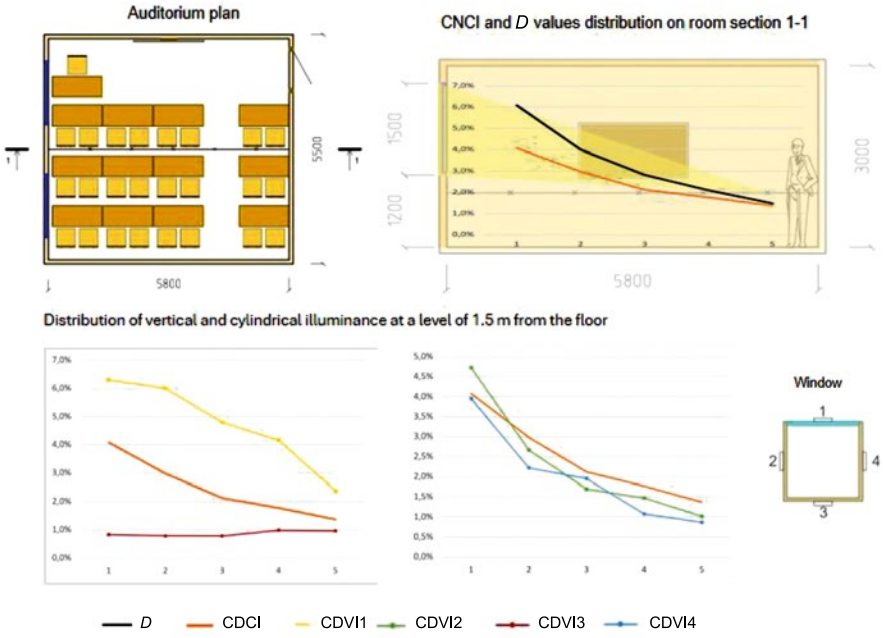

Fig. 1. Measurement results in auditorium # 1

um # 1). The task was to consider the distribution lines along the characteristic section of the room of 4 vertical illuminance E_i in mutually perpendicular planes. It's known that the average value of them corresponds to the value of the cylindrical illuminance E_c (1). Since we are talking about daylighting, the study considered relative values, representing the ratio of indoor illuminance (vertical and cylindrical) to outdoor horizontal illuminance (E_{out}): the coefficient of daylight vertical illuminance CDVI and the coefficient of daylight cylindrical illuminance CDCI.

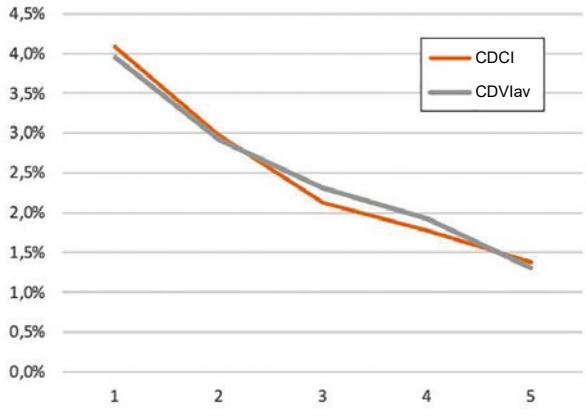

Fig. 2. Comparison of the distribution patterns of D and CDVI average value ($CDVI_{av}$) by control points in auditorium # 1

$$CDCI = CDVI_{av} = \frac{\sum_{i=4} CDVI_i}{4} = \frac{E_{v1}/E_{out1} + E_{v2}/E_{out2} + E_{v3}/E_{out3} + E_{v4}/E_{out4}}{4} \quad (1)$$

Measurements of outdoor illuminance, horizontal and vertical illuminance were carried out with an authorized Testo 545 47989–11Z luxmeter. Cylindrical illuminance was measured at a height of 1.5 meters from the floor with a PRC Krochmann luxmeter with a special cylindrical frosted glass nozzle. Horizontal illuminance was measured at the level of the conditional working surface h = 0.8 m, vertical illuminance – at the level of 1.5 m. Measurements were carried out at 5 points of the characteristic section of the room in the area of the wall between two light openings, the room plan is shown in Fig. 1.

The walls of the room are painted yellow, the floor is light brown, and the ceiling is white plaster. Subjectively, the light saturation of a room with absolute cloud cover is estimated as low.

Based on the results of the analysis of the graphs, shown in Fig. 1, the following conclusions can be drawn:

1. D at the point furthest from the light source is 1.5 % and meets the requirement of SR52.13330.2016 Daylight and electrical lighting: $D\text{exp} \geq D\text{req} = 1.2$ %;

2. CDCI /D indicator in the centre of the room is 0.75, which is lower than the recommended values

in [1] CNCI /*D* = [1–1.3], that is, the saturation of the room with light is insufficient;

3. The values of vertical illuminance in the plane directed at the light source exceed the values of cylindrical illuminance by an average of 1.5–2 times.

4. The values of vertical illuminance on surfaces directed at walls that are perpendicular to the light source are close to cylindrical illuminance character at the central point. The differences between the average of the values of CDVI2 and CDVI4 and CDCI are 14 %;

5. The values of vertical illuminance in the surface directed at the wall opposite the light source vary by no more than 0.2 % throughout the characteristic section and average is 0.9 %;

3. The deviation of the values of the average vertical illuminance on the 4 sides from the CNCI values is on average 1.5 %, at points 3 and 4 it is 8.6 %, Fig. 2.

2.2. Research # 2

In the research # 1, the vertical illuminance is of the greatest interest on the surface oriented to the wall opposite the light opening CDVI3. Its value does not change with distance rising from the wall and, as a result, can provide an accurate estimate of the overall illuminance level in the room. The value of CDVI3 is influenced exclusively by reflected and re-reflected light fluxes, and at point 5 it is mainly from the walls of the room. At other points, reflection from the floor and ceiling is added. This indicator provides a numerical estimate of the brightness of the walls.

Indeed, all walls appear to be equally bright when observing the surface of the walls of a small room, for example, a classroom from a point where the light source does not enter the field of vision with sufficiently uniform illumination, no matter where the observer is in the room. But if you look at the window, the walls will appear darker against the background of a bright light source.

Fig. 3. Photos of auditoriums # 2 and # 3

The differences in the characters of CDVI1 and CDVI3 make it possible to evaluate the contrast of daylighting in the future: it can be assumed that the brighter the light output, the greater the difference between these values will be.

How do the characters and levels of CDVI1 and CDVI3 differ for rooms of similar size and colour with a different arrangement of light openings? Research # 2 was devoted to finding an answer to this question.

Two classrooms were compared, in which auditorium # 2 is an auditorium identical in size to the room and light openings of auditorium # 1, but with a different wall colour – light green.

Auditorium # 3 is also an auditorium for practical exercises, of similar size in plan, painted in light green, but the windows are located above the line of sight.

The measurements were carried out in December during the daytime at sufficiently low levels of outdoor illuminance during the same period of the day for both audiences.

Subjective assessment of the room # 2: low light saturation, gloomy. Room # 3 is subjectively more

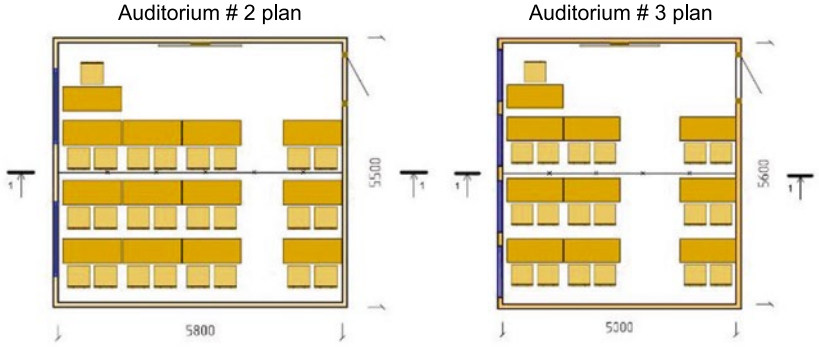

Fig. 4. Auditorium plans # 2 and # 3

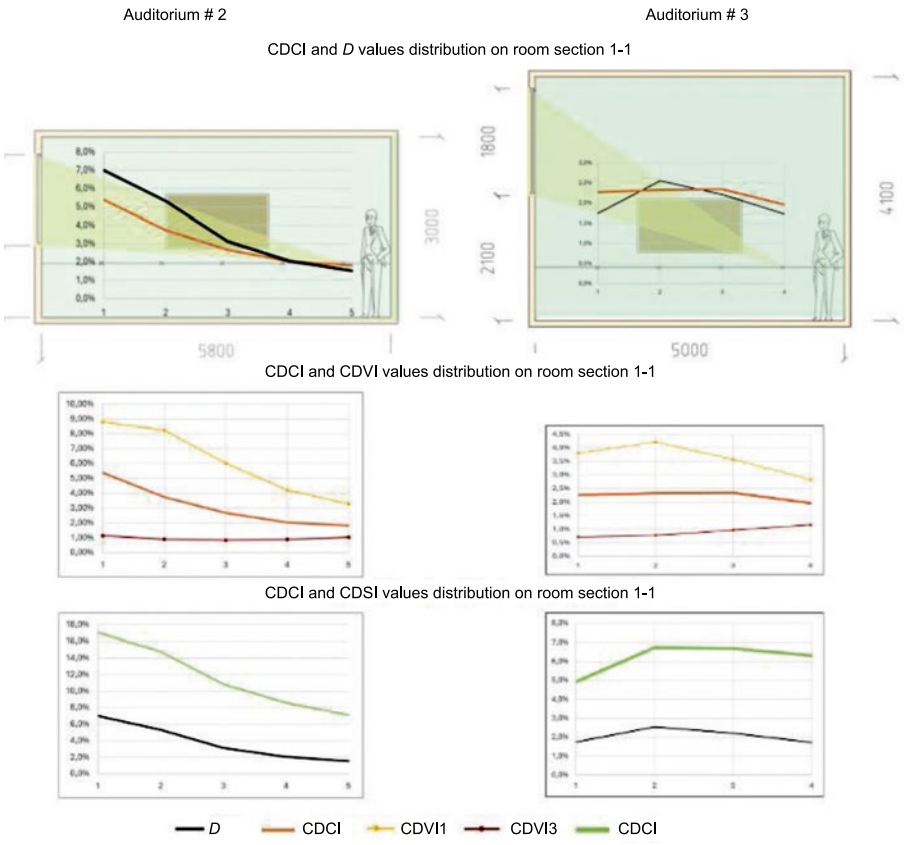

Fig. 5. Measurement results for classrooms # 2 and # 3

saturated with light than room # 2, but the windows located above the line of sight create a feeling of a "well", which significantly reduces the comfort level of the audience, Figs. 3, 4. The subjective assessment was carried out by the authors of the study and the student assistants of the experiment.

The values of *D*, CDCI, CDVI1, and CDV3 were measured in 5 points of the room' s characteristic section. As well as relative spherical illumination (CDSI – coefficient of daylight spherical illuminance) at the work surface level was measured. This value was added to the analysis as a potential criterion for lighting quality and lighting contrast. At the end of the 20th century, Russian lighting scientists conducted a large number of researches to assess the quality of lighting using the spatial characteristics of the light field, on the basis of which methods were proposed to improve the quality of lighting in the workplace and the general levels of combined lighting in industrial enterprises of various industries [12]. Among others, the lighting contrast was evaluated using the M.M. Gutorov formula:

$$m_{4\pi} = \left|\vec{\varepsilon}\right| / E_{4\pi}, \qquad (2)$$

where $\vec{\varepsilon}$ is the light vector, $E_{4\pi}$ is the spherical illuminance.

Spherical illuminance was measured using a special frosted glass photometric head with a PRC Krochmann luxmeter.

The measurement results are summarized in comparative graphs, shown in Fig. 5.

The *D* value at the point furthest from the light source is 1.5 % and 1.7 % for rooms 2 and 3, respectively, and meets the requirement of SR52.13330.2016 $D_{\text{meas}} \geq D_{\text{req}} = 1.2$ %. Comparing the daylighting of classrooms by *D* alone provides a similar assessment of the daylight environment.

The CDCI/*D* value for room # 2 in the centre of the room is 0.86, which is lower than the values recommended in [1], and in auditorium # 3 the CDCI/*D* value = 1.06, which corresponds to a sufficient level of light saturation and correlates with a subjective assessment of saturation.

The value of CDVI3, as well as in the first study, remains close to the value of 1 % for the entire characteristic section, showing minor deviations (despite the values of CDVI1 and CDCI different from the 1st study). In auditorium 3, the values of CDVI3 increase by 0.5 % (from 0.7 % to 1.2 % in absolute terms as they move away from the light source).

Table 1. Numerical Ratio of the Studied Characteristics

	D (point 5)	CDCI/*D*	*D*/CDSI	CDVI3/CDSI	CDVI3/*D*	CDVI1/*D*	CDVI3/CDVI1	CDVI1/CDSI
Auditorium # 1	1.5 %	0.75			0.28	1.70	0.16	
Auditorium # 2	1.5 %	0.86	0.29	0.08	0.27	1.93	0.14	0.56
Auditorium # 3	1.7 %	1.06	0.33	0.14	0.44	1.62	0.27	0.53
Value difference between auditoriums # 3 and # 2	1.14	1.24	1.15	1.87	1.64	0.84	1.95	0.96

The values of spherical illumination at all points significantly exceed the values of all other measured values and exceed the *D* values by an average of 3 times for room # 2 and 3.5 times for room # 3.

3. RESULTS

So, what value can show the subjective difference in classrooms 2 and 3: auditorium 3 feels more saturated with light, it has lower contrast, but there is a feeling of a "well" because of the windows located above the line of sight.

The numerical ratios that can characterize the qualitative indicators mentioned earlier are summarized in Table 1.

The last line shows the difference (in number of times) between the values obtained at the point in the centre of auditorium # 2 and # 3, since only in them all the specified values were measured.

The *D* values correspond to the norm and vary by 14 %, and generally allow us to conclude that it is acceptable to perform visual work in the audience according to its functionality.

The CDCI/*D* ratio shows that in terms of light saturation, auditorium # 3 is the best, which corresponds to the subjective assessment of the room.

If we replace the modulus and direction of the light vector in formula 1 with the value of a constant in the characteristic section of the value CDVI3 (directed at the wall opposite the light source), then we can make an attempt to estimate the contrast at the central point of the room as the ratio CDVI3/CDSI. This indicator differs for the audience # 2 and # 3 by almost 2 times.

The CDVI3/CDVI1 ratio gives similar results. For rooms # 1 and # 2, the value changes slightly, but for room 3 it exceeds the previous ones by 2 times, as well as the ratio of CDVI3/CDSI.

The ratio of CDVI3/*D* is also significant. It also demonstrates sensitivity to changes in the location of light sources, but less than the previous indicators. The advantage of this criterion, is

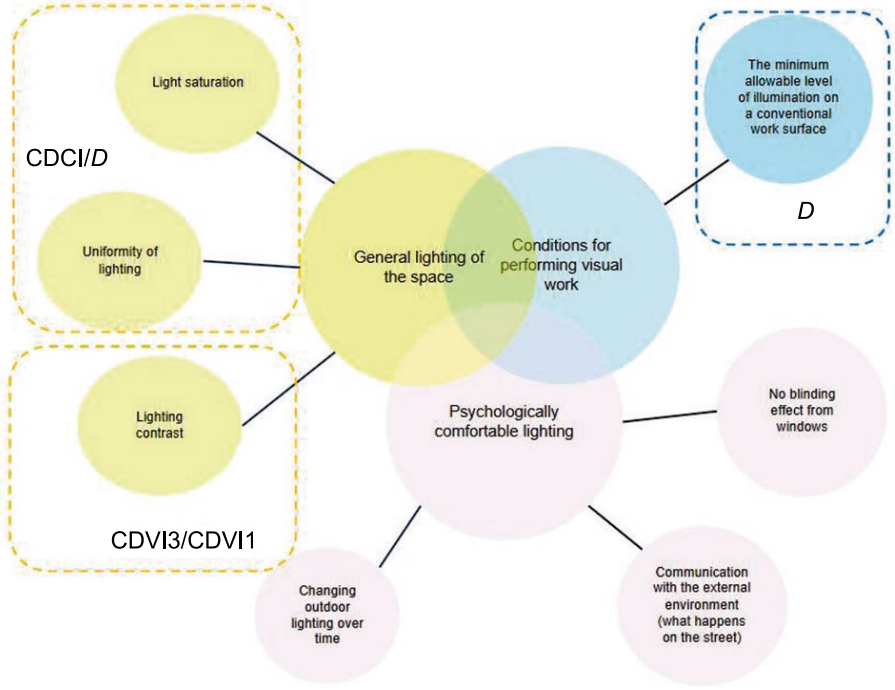

Fig. 6. Relationship of criteria, requirements and parameters of daylight quality

that to evaluate it, you will need to add only one parameter – CDVI3.

The question of the method of calculating this value, which is formed by reflected and re-reflected light, remains open. At point 5, located 1 m from the wall, the brightness of the wall and, accordingly, the reflected component can be estimated according to Lambert's law, if we imagine the wall as a luminous rectangle onto which direct light from a light source fall.

CONCLUSIONS

The conducted research has shown that the coefficient of daylight illuminance (*D*) does not allow us to fully assess the differences in the characteristics of the general lighting of rooms. Although this indicator ensures that the conditions necessary for visual work are met, it is not enough to create a comfortable light environment. It is important for a person not only to successfully perform visual tasks, but also to perceive the surrounding space as a whole, so that it evokes positive emotions, which improves a person's condition and increases labour productivity. Thus, to assess the overall lighting environment of a room, additional criteria such as saturation, contrast, and uniformity of illumination must be taken into account, Fig. 6.

Creating a universal parameter capable of integrating all these aspects into one value seems to be a difficult task, but we aim to find an approach that will bring us as close to this goal as possible. In the previous article, the authors proposed a simple and familiar method for calculating the direct component of the CDVI [2]. The next task is to find a method for calculating the reflected component of the CDVI.

The results of the study demonstrate the possibility of using the value of CDVI3 to assess contrast. To assess saturation, it is advisable in the future to consider replacing cylindrical illuminance and CDCI with an average value of CDVI2-CDVI4.

However, more research is needed. It is necessary to develop functional, technological, and psychological requirements for general lighting. This requires a more detailed gradation of the functions of the light system.

Combining the criteria listed in the article into a single system for assessing the quality of daylighting will allow us in the future to form requirements for the parameters of the room and light openings in conjunction with a subjective assessment of the overall lighting and formulate requirements for electrical lighting, taking into account the characteristics of the emerging daylighting pattern.

REFERENCES

1. Novikova, I.I., Zubtsovskaya, N. A., Lobkis, M. A., Ivleva, G.P. Hygienic rationing of daylighting: problems, tasks, international experience (review article) // Population health and habitat – ZniSO, 2020, # 3(324), pp. 10–15.

2. Zvonov, I.A., Kashirina, N.V., Molchina, N.A. Educational and technological conditions as a factor of university environment development // Real Estate: Economics, Management, 2024, # 1, pp. 63–66.

3. Nasybullina, R., Samogorov, V. Light space: The evolution of the role of natural light in architecture [Lightspace: Evolyutsiya roli yestestvennogo sveta v arkhitekture] / Ekatirinburg, TATLIN, 2020, 136 p.

4. Strategy for the development of the construction industry and housing and communal services of the Russian Federation for the period up to 2030 with a forecast up to 2035 // URL: http://static.government.ru/media/files/AdmXczBBUGfGNM8tz16r7RkQcsgP3LAm.pdf (accessed 03/31/2025).

5. Decree on the National Development Goals of the Russian Federation for the period up to 2030 and for the future up to 2036 // URL: http://kremlin.ru/events/president/news/73986 (accessed 03/31/2025).

6. Molchina, N.A., Solovyov, A.K. Prospects and methods of rationing the quality of daylighting in rooms with side light openings [Perspektivy i metody normirovaniya kachestva yestestvennogo osveshcheniya v pomeshcheniyakh s bokovymi svetovymi proyemami]// Svetotekhnika, 2023, # 6, pp. 12–17.

7. Molchina, N.A. The influence of reflected light on the assessment of the quality of daylighting in rooms with vertical windows // Light & Engineering, 2024, Vol. 32, # 1, pp. 39–44.

8. Muraviova, N.A., Soloviev, A.K., Stetsky, S.V. Comfort light environment under natural and combined lighting: method of their characteristics definition with subjective expert appraisal using // Light & Engineering, 2018, Vol. 26, # 3, pp. 124–131.

9. Durante, A., Kelly, K. Investigating mean room surface existence values for office lighting // Lighting Research & Technology, 2022, Vol. 54, # 7, pp. 657–673.

10. Boyce, P., Cuttle. K., Kelly, K., Raynham, P. The ambient lighting manifesto // Light Lines (Newsletter of the Society of Light and Lighting), 2020, # 3, pp. 6–7.

11. Molchina, N.A., Magera, T.N. Daylight Quality Assessment of Rooms with Lateral Daylighting by the Room Light Saturation Criterion // Light & Engineering, 2023, Vol. 31, # 6, pp. 29–34.

12. Solovyov, A.K. Theory of the light field and improvement of visual work conditions [Teoriya svetovogo polya i uluchsheniye usloviy zritel'nogo truda] // Building Sciences, 2009, # 5, pp. 470–474.

Nina A. Molchina,
lecturer of the Department of Architectural and Structural Design and Environmental Physics, National Research University Moscow State University of Civil Engineering

Alexei K. Solovyov,
Prof., Dr. of Technical Sciences. He graduated in 1965 from Moscow Institute named after V.V. Kuibyshev. At present, he is the Professor of the Department of Architectural and Structural Design and Environmental Physics, National Research University Moscow State University of Civil Engineering. He is a Member of the European Academy of Sciences and Arts and the editorial board of the "Svetotekhnika/Light & Engineering" Journals, has the titles of "Honorary Builder of the Russian Federation" and "Honoured Worker of the Higher School of Russia"

Light & Engineering
Vol. 33, No. 4, pp. 66–72, 2025
https://doi.org/10.33383/2025-012
Svetotekhnika # 3, 2025, pp. 53–57

IMPACT OF INSOLATION REQUIREMENTS ON THE QUALITY OF THE ARCHITECTURAL ENVIRONMENT

Lyubov A. Solodilova

Moscow State University of Civil Engineering (NRU MGSU)
Moscow Architectural Institute (State Academy MArkhI)
E-mail: usepo@mail.ru

ABSTRACT

The relevance of the topic of the article is caused by the low quality of the architectural environment, which is determined among other things by the requirements for sufficient insolation not only of residential premises in houses, but also in the territories adjacent to them. However, more and more often there are demands to abolish the concept of insolation, leaving only the concept of illumination, which is caused by investment interests to increase the density of buildings not only by a simple increase in the number of storeys, but also by a reduction of insolation gaps between buildings. It is quite obvious that such ill-conceived decisions can adversely affect not only the health of subsequent generations, but also the gene pool of the nation as a whole. At the same time, the already low architectural quality of the mass dwelling will finally become unsuitable for a full life. In this regard, the purpose of this study is a chronological analysis of the impact of insolation requirements on the calculated building density standards and the evolution of the aesthetic appearance of mass housing at different time stages. To achieve the goal, tasks have been set related to the loss of privacy and scale to humans in the environment, the identification of insufficient greenery and places of quiet rest in an open space, which leads to the facelessness and monotony of the spatial pattern of new construction. A hypothesis has been put forward about the need to switch from multi-storey construction to low-rise buildings of comparable density with the obligatory preservation of insolation standards, which will help ensure a high aesthetic and sanitary-hygienic quality of development.

The issues of insolation, and accordingly the quality of mass residential development, were considered in the works of individual scientists and research teams, published in 2004–2023 in free print on the pages of the electronic e-library and the databases of Russian Science Citation Index (RSCI), Scopus, and Web of Science.

The results of search queries include 104 links with a sample of 20 articles, the analysis of which was carried out taking into account the following main directions: the history of changes in the standards for ensuring insolation of premises in residential buildings and in the territories they formed, as well as the effect of the duration of insolation on building density injection and, as a result, deterioration of the architectural appearance of mass residential development.

The prevailing trends in reducing the time of insolation in residential premises and in playgrounds, together with the growing number of square meters per unit of territory, led to a deterioration in the quality of life in areas of new housing construction. The transition from multi-storey to low-format high-density residential buildings will help improve the architectural appearance of mass housing.

Keywords: building density, architectural appearance, quality of living environment, insolation of premises, lighting of premises

1. INTRODUCTION.

The architectural quality of the living environment is largely determined by the standards for the duration of insolation and natural illumination [1]. Insolation, as a way to improve the living environment with direct sunlight, was adopted in Soviet and world architectural and construction practice back in the 20s of the last century [2]. However, with the advent of a market economy in Russia, the standard of insolation time is constantly being adjusted towards its reduction, and this is especially noticeable in the densely populated cities of modern Russia. This happens, according to some experts, in order to create expressive architectural solutions and, in the opinion of others, in the absence of the need to maintain the norms in their former form, since people have learned to fight against tuberculosis bacillus and other microbes with more effective drug methods [3, 4].

In the current conditions, it is necessary to understand whether insolation norms are really excessive or the true reason lies in the rampant desire of investors to maximize building compaction in order to make a profit.

2. METHODS

Analysis of the works, published in period of years 2004–2023 on the pages of the electronic library RSCI, Scopus, and Web of Science databases and devoted to the history of regulatory requirements for insolation of residential premises and territories, seems to us especially relevant today, given the practical concealment and informative inaccessibility of the impact of these changes on the architectural quality of mass housing even for professionals [5].

The search for the maximum parameters of sanitary rationing began in Russia from the first post-revolutionary years in response to the poor quality of development with its crowded courtyards-wells, in which the sun was extremely insufficient and the need, dampness, and diseases seemed to be an integral part of these walls themselves. Already in the 1920–30s in the studies of Erisman F.F., Voeykova A.I., Gershun A.A., Nikolskiy A.S., Vetoshkin S.I., Belikova V.K. the first attempts are made to determine the calculated indicators of good sanitation of premises in 'indicative' housing complexes and social cities, communal houses and houses of 'transitional type', and later in residential complexes, which was supposed to emphasize the importance of the favourable impact of insolation in the context of political transformations [6, 7].

Since late 1940s the development of methods for calculating the biological norms of insolation for residential premises was carried out by G.M. Frank, N.M. Danzig, V.K. Galanin, and others [8]. Such scientists as Belinskiy V.A., Rudnitskiy A.M., Tvarovskiy M., Boldyrev N.G., Shchepetkov N.I., Popovskiy Yu.B., Danilyuk A.M., Meshkov V.V., Sapozhnikov R.A., Garadzha M.P., Metennaya L.M., Steinberg A. Ya., Zelenko A.U., Ershov A.V., and others were engaged in geometric methods of solar calculation. In 1963–1977 the works of Dashkevich L.L., N.M. Gusev, Dunaev B.A., Obolenskiy N.V., Bakharev D.V., Maslennikova D.S. Sukhanov I.S., Vasilyev B.F., and others were devoted to the extensive theoretical issues of insolation [9, 10]. In addition to the hygienic and psycho-aesthetic effects of insolation on humans, studies on light-climatic zoning are known, which are reflected in the works of Soviet and foreign scientists Kalitin N.N., Baburin K.E., Khoroshilov P.I., Kireev N.N., Krista Van Santen, Ulriki Brandi, Christoph Geismar-Brandi [11–13].

As a result of numerous studies in 1963, SN 427–63[1] was issued, which first streamlined urban density and later adopted SN 1180–74. Both documents regulated the same hygienic requirements for rationing continuous insolation lasting at least 3 hours. Subsequently, SN 41–58[2] was published, which in 1962 was replaced by SNiP II-K2–62[3] that determined the building density of the quarter in accordance with the number of floors. At the same time the possibilities of building consolidation were considered due to the superstructure of houses. This was reflected in SNiP II-60–75[4] (SNiP II-60–75**).

Of course, the requirements of continuous insolation significantly limited the freedom of developers and already in SP # 2605–82 the concept of inter-

[1] SN 427–63 Sanitary standards and rules for ensuring insolation of premises of residential and public buildings and residential buildings in populated areas

[2] SN 41–58 Rules and norms of planning and development of cities

[3] SNiP II-K 2–6 2 Planning and development of populated areas. Design standards

[4] SNiP II-60–75, SNiP II-60–75** Planning and development of cities and towns and rural settlements

mittent insolation is introduced, as a result of which the building density begins to grow. Later intermittent insolation becomes the only norm for subsequently adopted SNiP 2.01–8907, TSN 23–303–98 (including for MGSN 2.05–97 and 2.05–99), SanPiN 2.1.2.1002–00 and SanPiN 2.2.1/2.1.1.1076–01. In the introduced SNiP 2.07.01–89* we find instructions to calculate the density in human units of the population per hectare of territory (people/ha) in accordance with regional (republican) standards. Moreover, the standard duration of exposure is already 2.5 h instead of 3 h, and in TSN 23–303–98, it is reduced to 1.5 h, depending on window orientation and number of rooms [14].

Modern SanPiN 1.2.3685–21[5] provides the maximum insolation duration of 2.5 h only for the northern zone (northern of 58° N), for the central zone (58° N – 48° N) – 2 h, and for the southern zone (southern of 48° N) – 1.5 h. In order to increase the building density, the estimated dates of insolation previously indicated in March and September, have been moved to April 22 and August 22, when the sun is already enough, and for winter time, when the sun is so necessary, the norms of insolation have not been established at all [15]. If we compare the time of insolation, for example, in Sweden and the Netherlands, strictly speaking in the Russian equivalent it should approach to 2.5 h. It is also necessary to emphasize the importance of taking into account the opinions of professional doctors, and especially in conditions of increasing building density, threats arise in connection with the emergence and spread of new viruses and infections, in particular COVID-19 [16].

3. RESULTS

Despite the fact that over the past half century insolation standards have more than halved, from (3–4) h to (1.5–2) h, it still continues to be practically the only barrier that restrains the growth of building density, measured in thousands of square meters per hectare of territory (thousand m^2/ha). This partly explains the insistence on abolishing insolation, limiting itself only to lighting requirements. The dwindling norms of insolation led to massive multi-storey buildings without balconies and loggias, which became synonyms for the functional warrens. In this regard, it is of interest to analyse the effect of building density on the evolution of the aesthetic appearance of mass housing at different time stages.

3.1. The Stage of the Revolutionary Avant-Garde of 1920–1930

In this time of constructivism, rationalism, and traditionalism, the work of hygienic justification of insolation and illumination was limited mainly to the search for optimizing the internal microclimate of premises due to, for example, the best geometry of tape openings and their relationship to the floor area (house-commune of the Textile Institute, House URALOBLSOVET, etc.) [7]. Although even then the attempts were made to increase the density of development, including multi-level use of land (urban planning projects of L. Khidekel).

3.2. The stage of monumental socialist classicism of 1930–1952

At this time, it is not so much the saving of land resources that comes to the fore, but the new aesthetics of preserving and returning the historical traditional features of post-constructivism and the Stalin Empire (Art Deco).

3.3. The Mid 1960–1970

In that time, there is a rather long time period of Soviet modernism, which lasted until 1990 of the 20th century (industrial architecture), and is characterized by the ubiquitous processes of unification and typification of housing construction. Refusal of closed well development leads to line setting of large-block and later – panel typical houses with a meridional location, which contributes not only to improving the hygienic qualities of the housing, but also to reducing the length of engineering communications. In the current conditions of strictly valid technical standards, architects actually could not influence the architectural and spatial appearance of housing, in part therefore they came to grips with the design of inter-house territories, such functionally extensive and still attractive in comparison with the compensatory development carried out under the Renovation Programs [17]. The gradual-

[5] SanPiN 1.2.3685–21 Sanitary rules and regulations 'Hygienic standards and requirements for ensuring the safety and (or) harmlessness for humans of habitat factors' (as amended on December 30th, 2022)

Table 1. Parameters of the Building Density

No.	Document	Building density in thousands of building area in sq. m/ha in accordance with the number of storey				
1	SN 41–58	4	5	8	9	12
		2.2–2.7	2.4–3.0	2.9–3.4		–
2	SNiP II-K.2–62	2.6–2.8	2.8–3.2	3.4–3.8	3.6–4.2	–
3	SNiP II-60–75	4.6	5.3	6.200	6.6	6.9
4	SNiP II-60–75**	5.0	5.8	6.800	7.2	7.5

ly growing density of development determined the economic efficiency of rationing insolation with a general decrease in its duration. Some parameters of the building density – the ratio of the floor area of buildings to the total area of territories in hectares (m^2 / ha) – valid until the beginning of the 90s of the last century, are given in the Table 1.

3.4. At the End of the Last Century

And if in the 90s of the last century the architectural appearance of residential buildings in Russia began to change rapidly towards pseudo-historicism and postmodernism, then later we can observe an absolutely functional architecture of mass housing devoid of any individual features [18].

3.5. The Beginning of 21st Century

Already in the early 2000s the building density was adopted in accordance with the Urban Planning Code of the Russian Federation adopted in 1998 and the maximum building parameters of the Land Use and Development Rules and the established (basic, auxiliary and conditionally permitted) regulations for the use of land and capital construction facilities, taking into account the urban zoning of the territory, Fig. 1, which was reflected in the updated edition of the Code of Rules SP 42.13330.2011 and SP 42.13330.2016[6] [19].

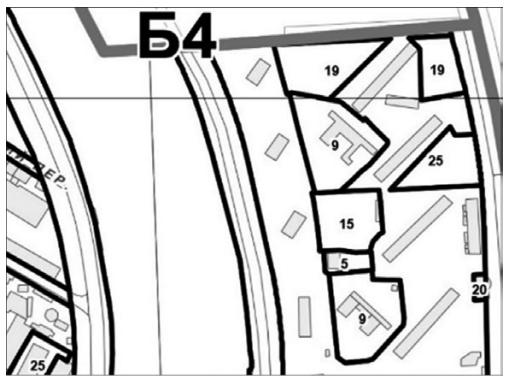

Fig. 1. Fragment of the map of the territorial zones' boundaries indicating the maximum building density: ▭ is the boundaries of territorial zones; numbers, for example 25, is the building density in thousands of square metres per hectare

Since 2017, changes have come into force, in accordance with which the insolation of playgrounds and sports grounds is reduced, which led to a further increase in building density. The next stage was the implementation of SP 476.1325800.2020[7], according to which the maximum design building density of the quarter should not exceed the established 25 thousands square meters per hectare, but it is allowed to take up to 40 thousands m^2/ha.

And finally, in order to meet the requirements of the Federal Law 'Technical regulations on the safety of buildings and structures', the 'DOM.RF Fund' in accordance with the 'Standard for the integrated development of territories' developed a joint venture XXX.1325800.20XX[8], in which the density of residential and multifunctional buildings for the largest cities is (35.0–60.5) thousands m^2/ha (for large city – (30.0–55.0) thousands m^2/ha). At the same time for low-rise buildings in the largest cities the building density of (5.25–22.0) thousands m^2/ha and for large – (4.5–20.0) thousands m^2/ha were regulated. Thus, a phased system of rationing insolation led (according to the Central Research Institute of Experimental Dwelling Design) to urban land saving.

We will illustrate what has been said on some examples and, at least in the most general terms, we

[6] Code of Rules SP 42.13330.2011 (SP 42.13330.2016) Urban planning. Planning and development of urban and rural settlements

[7] SP 476.1325800.2020 Territories of urban and rural settlements. Rules for planning, development and improvement of residential neighborhoods.

[8] SP XXX.1325800.20XX Urban planning. Integrated development of territories. General provisions for building models of the urban environment.

Fig. 2. The impact of the building density of the territory on the architectural appearance of the living environment on example of eastern working village in Moscow, which was created in 1939 to service the water supply station commissioned at the Akulovsky reservoir: *a*) general view of the 'Stalinist' residential building on main street (architects N. Geraskin, A. Samoylov); *b*) details of design at the entrance to the house; *c*) inter-house territory (density of about 1.8 thousand m^2/ha) with 3–4-storey residential buildings; *d*) functional and planning organization of the inter-house territory (photos and drawings by L.A. Solodilova)

will try to assess visually how in the considered periods of time the growing indicator of building density affected the architectural appearance of mass residential buildings and adjacent territories, Fig. 2.

The characteristics of the new residential complex, commissioned in 2022 under the Renovation Program, clearly show that with comparable indicators of inter-house spaces, 0.5–0.6 hectares, the new place of residence, of course, has much lower technical and economic indicators of comfort due to the insufficient amount of greenery, water devices, quiet recreation areas, as well as parking spaces. At the same time, the building density is many times higher than the usual indicators of the previous building, which cannot but negatively affect the quality of the living environment, Fig. 3.

Extensive development of green spaces for the construction of large-format housing led to the construction of identical parallelepipeds, devoid of any plasticity, Fig. 4.

Thus, the norms of insolation, which are decreasing in duration, became the basis for an in-

Fig. 3. Impact of the building density of the territory on the architectural appearance of the living environment, Eastern settlement, Moscow: *a*) line building with inter-house territory of about 0.4 ha; (building density (2.8–3.2) thousands m^2/ha) with 4-storey residential buildings, year 1962; *b*) general view of the territory with an abundance of greenery and sufficient space for quiet and active recreation; the first launch pad for demolition under the renovation program; *c*) compensation development for renovation (with density about (17–20) thousands m^2/ha); *d*) functional and planning organization of the residential complex territory on Main Street (year 2022) on the site of the former green zone as part of the renovation program (photos and drawings by L.A. Solodilova)

Fig. 4. Modern Multifunctional complex 'Metropolis', South-eastern Autonomous Area, Moscow: building density 39.271thousands m^2/ha (year 2021) on the territory of 3.68 hectares, includes eleven 30-storey residential buildings united by a two-level underground parking lot with total area 144517.31 sq. m; the project also provides for the construction of a kindergarten for a short stay for 79 places (photo by L.A. Solodilova)

crease in the density of buildings and, as a result, a deterioration in its architectural appearance. Such a consolidation of development is incomparable with the modern economic hypothesis of a 'compact and dense small-format city' with retail forms of service within a pedestrian radius, which should finally compensate for hypertrophied shopping centres. At the same time, untouched nature should remain a priority, since man-made natural complexes are not so effective from the ecological point of view. It is necessary to seek new opportunities for the development of high-density low-rise construction in the cities with a high cost of land and capital construction projects. Effective use of land resources of low-rise areas is possible when achieving high density and compactness of development, which will also be accompanied by compact placement of engineering and technical and transport communications.

CONCLUSION AND DISCUSSION

For all the attractiveness of low-rise construction, such houses are not being built in large and largest cities, so the demand for multi-storey buildings is still high. The time has come, instead of the standards imposed on the buyer, to form and offer an alternative from much more comfortable and economically efficient low and medium-rise housing up to 5 floors inclusive.

This study puts forward a hypothetical assumption about the possibility and need to switch to low-format high-density buildings [20] with the obligatory preservation of insolation standards, which will help to ensure high aesthetic and sanitary-hygienic quality of buildings. In connection with the above, a set of early architectural and spatial measures is required, including among other things the development of a mechanism for increasing the building density to 15–20.0 thousands sq. m per hectare while maintaining the comfort of living due to:

– Design of residential units with individual front gardens and courtyards without the possibility of organizing the territories of public centres;

– Introduction of differentiated insolation [15–20] and technological [21] requirements that affect the increase or decrease in density and number of storeys of buildings [15, 20], in the conditions of accounting for reflected solar radiation [22] as well;

– Loop-nest construction methods of development, providing the blocking of spatial elements on three sides.

These main measures are able to multiply the density of small-format buildings, and at the same time improve the comfort indicators of complex housing construction, which should provide not only a sufficient output of space and a corresponding reduction in the cost of sq. meters, but also a high comfort of the urban environment.

REFERENCES

1. Sinoo, M.M. Light Conditions in Nursing Homes: Visual Comfort and Visual Functioning of Residents // Eindhoven University of Technology, 2016.

2. Darula, S., Christoffersen, J., Malikova, M. Sunlight and insolation of building interiors // Energy Procedia, 2015, Vol. 78, pp. 1245–1250.

3. Vasilieva, A.V., Kosenkova, Ju. L., Shubenkov, M.V. From the history of Light and Engineering: issues of natural lighting in the Soviet residential architecture of the 1920s-1930s // Light & Engineering, 2021, Vol. 29, # 4, pp. 79–89.

4. Pushilina, Yu.N., Chebotarev, P.N. Norms of insolation and its impact on the appearance of residential buildings // International Scientific Journal Simvol nauki, 2015, # 6, pp. 355–356.

5. Popovskiy, Yu.B. History of sanitary and epidemiological rationing of insolation of residential premises in the USSR and the Russian Federation // National Association of Scientists, 2015,

6–3 (11), pp. 27–30.

6. Belikova, V.K. Bactericidal value of the sun radiation penetrating the room // Scientific journal. Hygiene and sanitation, 1957, # 11, pp. 8–11.

7. Vasilyeva, A.V. The history of the formation of sanitary rationing in domestic housing construction in the first third of the twentieth century // Construction: science and education, 2022, Vol. 12, # 3; http://nso-journal.ru.

8. Obolenskiy, N.V. Architecture and the Sun / M.: Stroyizdat, 1988, 14 p.

9. Korniyenko, V. Assessment of insolation of residential buildings in the area of influence of the designed building // Vestnik VolgGASU, Series: Construction and Architecture, 2012, # 27 (46), pp. 156–163.

10. Orlova, L.N. Problems and prospects for optimizing the light environment of cities // Urban Planning and Architecture, Samara State Technical University, Samara, 2017, Vol. 7, # 4, pp. 122–126.

11. Christa van Santen. Light Zone City. Light planning in the Urban Context / Brikhäuser – Publishers for Architecture, 2006, 127 p.

12. Brandi, U., Christoph Geissmar-Brandi, Ch. Light for Cities. Lighting Design for Urban Spaces / A Handbook, Brikhäuser – Publishers for Architecture, 2007, 168 p.

13. Turner, P.L., van Someren, E.J.W., Mainster, M.A. The role of environmental light in sleep and health: Effects of ocular aging and cataract surgery // Sleep Medicine Reviews, 2010, # 14 (4), pp. 269–80.

14. Kupriyanov, V.N., Khalikova, Ph. R. Proposals for rationing and calculation of residential insolation // Housing construction, 2013, # 6, pp. 50–53.

15. Shmarov, I., Zemtsov, V., Korkina, E. Insolation – practice of rationing and calculation [Insolyatsiya – praktika normirovaniya i rascheta] // Journal Housing Construction, 2016, # 7, pp. 48–53.

16. Popovskiy, Yu. B., Shchepetkov, N.I. Insolation and COVID 19: protection against the aggressor [Insolyatsiya i COVID 19: zashchita ot agressora] // Svetotechnika, # 3, 2020, pp. 23–26.

17. Solodilova, L.A. The quality of the architectural environment in residential areas of renovation [Kachestvo arkhitekturnoy sredy v zhilykh rayonakh renovatsii] // Science and business: development paths, 2022, # 1(127), pp. 155–157.

18. Solodilova, L.A. Impact of mass housing forms of ownership on the architectural appearance of the buildings // TGASU, Tambov, Science Prospects, 2021, # 1(136), pp. 38–40.

19. Kiryushechkina, L.I., Solodilova, L.A. Textbook: Economics of Architectural Solutions. Economic foundations for an architect / M: Prospekt, 2018, 135 p.

20. Chereshnev, I.V. Socio-economic and environmental aspects of the development of architecture of low-rise high-density buildings [Sotsial'no-ekonomicheskiye i ekologicheskiye aspekty razvitiya arkhitektury maloetazhnoy plotnoy zastroyki] // Housing Construction, 2007, # 10, pp. 6–9.

21. Dvoretsky A.T., Spiridonov A.V., Shubin I.L. Low-energy buildings: Windows. Facades. Sun protection. Energy efficiency // Monograph, 2022, Moscow: Direct-Media, 233 p.

22. Dvoretsky, A.T., Zavaliy, A.A., Spiridonov, A.V., and Shubin, I.L. Estimation of insolation of the mirror hall of a unique building // Light & Engineering, 2022, Vol. 30, # 4, pp. 42–48.

Lyubov A. Solodilova,
Ph. D., Associate Professor in Department of Architecture IGA, MGSU, Professor at Department of Architectural Practice in MArchI. She graduated in 1978 from the Faculty of Architecture of the Rostov Civil Engineering Institute. Area of her scientific interests is cost-effective types of housing. She is the Member of the Union of Moscow Architects

Light & Engineering
Vol. 33, No. 4, pp. 73–79, 2025

https://doi.org/10.33383/2025-005
Svetotekhnika # 3, 2025, pp. 41–45

QUASI-DIFFUSE APPROXIMATION FOR CALCULATION OF LIGHT FIELDS IN 3D TURBID MEDIA

Vladimir P. Budak and Pavel A. Smirnov

National Research University Moscow Power Energy Institute
(NRU MPEI), Light and Engineering Department
E-mail: budakvp@gmail.com

ABSTRACT

Currently, modelling light fields in a slab of a turbid medium is a fully solved task within the framework of the so-called discrete transfer theory. The slab model is of great practical importance, but there is a wide range of problems that cannot be reduced to it and have fundamentally three-dimensional (3D) geometry: twilight sky radiance, reflection from transparent objects, light fields in 3D-printed materials, and biological or medical tissues. To date, there is no general solution to the boundary value problems of the radiative transfer equation (RTE) in 3D geometry, and it is unlikely to exist given their diversity and multiparametric nature. Greater progress in solving 3D problems can be achieved by combining approximations with numerical methods.

In this paper, the solution is represented as the sum of an anisotropic part, approximated using a small-angle modification of the spherical harmonics method (SHM), and a smooth regular part, determined from the diffusion approximation, referred to as the quasi-diffusion approximation. The accuracy and applicability domain of this approximation are estimated by comparing the spatial-angular radiance distribution with the numerical solution of the RTE for a slab. It is shown that the difference does not exceed a few percent for most viewing angles. Further development of the method for 3D media is possible using advanced numerical tools for solving partial differential equations. The solution can be refined via the synthetic iteration method.

Keywords: 3D medium, radiative transfer, anisotropic scattering, diffusion approximation, small angle approximation

1. INTRODUCTION

Currently, the calculation of light fields in plane-parallel layers of a turbid medium has been fully addressed within the discrete theory of radiative transfer [1]. This framework provides a matrix solution to the RTE and efficient computational algorithms. For optical remote sensing (ORS) of the Earth's surface from space, the Independent Pixel Approximation (IPA) [2] accounts for the Earth's sphericity by treating the atmospheric layer as plane-parallel for each pixel while adjusting the solar incidence angle. This approximation yields acceptable errors for solar zenith angles up to 88°, but reliable radiance distribution under twilight conditions [3] remains challenging.

The problem of calculating the radiance distribution across the twilight sky is critical for modelling natural lighting during evening hours. These problems inherently require a three-dimensional (3D) approach and cannot be reduced to planar geometry, necessitating solutions to boundary value problems of the radiative transfer equation (RTE) for 3D media.

A significant number of practical applications involve 3D RTE boundary value problems. While a flat-layer model suffices for calculating surface radiance coefficients in many cases [4], reflections from translucent objects demand accounting for their 3D

shape. This is particularly relevant in 3D printing, where high-resolution imaging relies on UV-cured materials, requiring precise light-field determination within the material to reproduce high-frequency texture details [5]. Similar challenges arise in biomedical applications, where light is used for diagnostics and tissue interaction [6–9].

To date, there are no general methods for solving boundary value problems of RTE, and they are unlikely to be possible due to the large number of types of such problems and their multiparametric nature. The solution of such problems is significantly complicated by presence of highly anisotropic scattering in them, since suspended particles in these media are often much larger than the wavelength. An alternative is to solve the problem using Monte-Carlo methods. However, under conditions of strong anisotropy, achieving high accuracy in solutions remains very difficult. The task of transferring into three-dimensional environments turns out to be very time-consuming or resource-intensive, and therefore too inconvenient to use.

References [10,11] propose hybrid numerical-analytical solutions to RTE boundary value problems, following engineering computation approaches. These studies decompose the solution into anisotropic and regular (smooth) components. While the anisotropic part is treated analytically, the regular component is solved using diffusion approximation [12]. However, in [10], the anisotropic component only accounts for direct Bouguer-attenuated radiation, leaving the regular part with significant anisotropy that compromises solution accuracy. In contrast, [11] employs small-angle diffusion approximation [13] for the regular component, better preserving its anisotropic properties. Nevertheless, the mathematical complexity of this approximation [13] necessitated additional simplifications.

In this work, we propose determining the anisotropic component of the solution using a small-angle modification of the spherical harmonics method (MSH) [14]. As the most general formulation among small-angle approximations, MSH provides an analytical solution expressed as a spherical function series, offering exceptional versatility for RTE transformations.

Key features of MSH include azimuthal symmetry and insensitivity to radiation entrance angle (inherent to small-angle formulations) and surface geometry independence, enabling application to arbitrary 3D media.

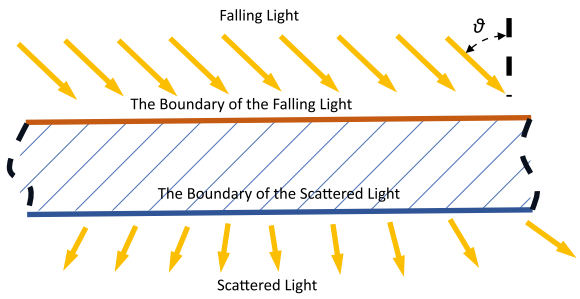

Fig. 1. Scheme of scattering of radiation from a FM source by an object of a flat-layered medium

To evaluate the method's accuracy and limitations, we examine solutions for a plane-parallel turbid medium, illuminated by a collimated monodirectional source, Fig. 1. While preliminary concepts were introduced in [15], the present study:

- Provides a concise formulation of the quasi-diffusion method;
- Presents comparison results combining synthetic iteration with MDOM-program solutions;
- Derives complete solutions to the equations in [15];
- Conducts direct comparisons with full boundary value problem solutions [16].

2. METHOD FOR SOLVING BOUNDARY VALUE PROBLEMS

The boundary value problem for the RTE in a flat layer of a turbid medium illuminated by a FM source at an angle ϑ_0 has the form:

$$\begin{cases} (\hat{\mathbf{l}},\nabla)L(\mathbf{r},\hat{\mathbf{l}}) = -\varepsilon L(\mathbf{r},\hat{\mathbf{l}}) + \dfrac{\Lambda\varepsilon}{4\pi}\oint L(\mathbf{r},\hat{\mathbf{l}}')x(\hat{\mathbf{l}}',\hat{\mathbf{l}})d\hat{\mathbf{l}}', \\ L(\mathbf{r},\hat{\mathbf{l}})\Big|_{\mathbf{r}\in\Sigma_{IP},(\hat{\mathbf{l}},\hat{\mathbf{R}})<0} = \delta(\hat{\mathbf{l}}-\hat{\mathbf{l}}_0),\ L(\mathbf{r},\hat{\mathbf{l}})\Big|_{\mathbf{r}\in\Sigma_{SP},(\hat{\mathbf{l}},\hat{\mathbf{R}})>0} = 0, \end{cases} \quad (1)$$

where $L(\mathbf{r},\hat{\mathbf{l}})$ is the luminance of the light field at the point r in the direction $\hat{\mathbf{l}}$, ε is the attenuation coefficient, Λ is the single scattering albedo, $x(\hat{\mathbf{l}},\hat{\mathbf{l}}')$ is the scattering indicatrix of light by an elementary volume of the medium, $\hat{\mathbf{l}}_0 = \left\{\sqrt{1-\mu_0^2}, 0, \mu_0\right\}$ is the direction of incidence of solar radiation; $\mu_0 = (\hat{\mathbf{z}},\hat{\mathbf{l}}_0) \equiv \cos\vartheta_0$, Σ_{IP} is the upper boundary of the layer at the level $z = 0$, Σ_{SP} is the lower boundary of the layer $z = z_0$. We assume that the medium is homogeneous $\varepsilon(\mathbf{r}) = const = \varepsilon$. From here on, the symbol " ^ " will denote unit vectors. It is also assumed that the radiation completely leaves the ob-

ject at the boundary and does not return to it, or that the boundary is completely absorbing.

Next, to consider the peculiarities in the angular distribution of luminance, we will select the anisotropic part:

$$L(\tau,\hat{\mathbf{l}}) = L_a(\tau,\hat{\mathbf{l}}) + L_r(\tau,\hat{\mathbf{l}}), \tag{2}$$

where $L_a(\tau,\hat{\mathbf{l}})$ is the anisotropic part of the solution; $L_r(\tau,\hat{\mathbf{l}})$ is the regular part of the solution, $\tau = \int_0^l \varepsilon(\mathbf{r}+\xi\hat{\mathbf{l}})d\xi$ is the optical thickness of the path along the direction $\hat{\mathbf{l}}$ of length l.

Taking into account (2), the boundary value problem (1) is transformed into the new form:

$$\begin{cases} (\hat{\mathbf{l}},\nabla)L_r(\mathbf{r},\hat{\mathbf{l}}) = -\varepsilon L_r(\mathbf{r},\hat{\mathbf{l}}) + \\ + \dfrac{\Lambda\varepsilon}{4\pi}\oint L_r(\mathbf{r},\hat{\mathbf{l}}')x(\hat{\mathbf{l}}',\hat{\mathbf{l}})d\hat{\mathbf{l}}' + q(\mathbf{r},\hat{\mathbf{l}}) \\ L_r(\mathbf{r},\hat{\mathbf{l}})\big|_{\mathbf{r}\in\Sigma_{IP},(\hat{\mathbf{l}},\hat{\mathbf{R}})<0} = 0, \quad L_r(\mathbf{r},\hat{\mathbf{l}})\big|_{\mathbf{r}\in\Sigma_{SP},(\hat{\mathbf{l}},\hat{\mathbf{R}})>0} = \\ = -L_a(\mathbf{r},\hat{\mathbf{l}}), \end{cases} \tag{3}$$

where $q(\mathbf{r},\hat{\mathbf{l}})$ is the source function associated with the residual of the solution of the RTE for the anisotropic part, which in the form of the SHM is represented as an expansion in Legendre polynomials:

$$q(\mathbf{r},\hat{\mathbf{l}}) = (1-\mu)\sum_{k=0}^{\infty}\sum_{m=-k}^{k}\frac{2k+1}{4\pi}\frac{(k-m)!}{(k+m)!}\times$$
$$\times\varepsilon\left(e^{-\varepsilon l(\mathbf{r})} - (1-\Lambda x_k)e^{-\varepsilon l(\mathbf{r})(1-\Lambda x_k)}\right)P_k^m(\mu)e^{im\varphi}, \tag{4}$$

where $P_k^m(\mu)$ are the associated Legendre polynomials, $\mu = (\hat{\mathbf{l}},\hat{\mathbf{z}})$, $l(\mathbf{r})$ is the distance from the upper boundary to the point $\mathbf{r}$ in the direction of incidence of $\hat{\mathbf{l}}_0$ the FM source radiation, x_k are the coefficients of the expansion of the scattering indicatrix in Legendre polynomials.

The solution for the regular part can be formulated based on the first two spherical harmonics, which represent the spatial irradiance and the light vector [15]:

$$\begin{cases} \varepsilon(1-\Lambda)E_{r0}(\mathbf{r}) + \nabla\mathbf{E}_r(\mathbf{r}) = q_0(\mathbf{r}), \\ \dfrac{1}{3}\nabla E_{r0}(\mathbf{r})\hat{\mathbf{l}} + \varepsilon(1-\Lambda\bar{\mu})\mathbf{E}_r(\mathbf{r})\hat{\mathbf{l}} = \mathbf{q}_1(\mathbf{r},\hat{\mathbf{l}})\hat{\mathbf{l}}, \end{cases} \tag{5}$$

where $E_0(\mathbf{r})$ is the spatial irradiance; $\mathbf{E}(\mathbf{r})$ is the light vector, $q_0(\mathbf{r})$ and $\mathbf{q}_1(\mathbf{r},\hat{\mathbf{l}})$ are the harmonics of the expansion $q(\mathbf{r},\hat{\mathbf{l}})$ in spherical functions, which is based on (4) will be presented in the form:

$$q(\mathbf{r},\hat{\mathbf{l}}) = \frac{1}{4\pi}q_0(\mathbf{r},\hat{\mathbf{l}}) + \frac{3}{4\pi}\hat{\mathbf{l}}\cdot\mathbf{q}_1(\mathbf{r},\hat{\mathbf{l}}). \tag{6}$$

Expressing $\nabla\mathbf{E}_r(\mathbf{r})$ from the first equation and substituting into the divergence of the second, we obtain:

$$\frac{1}{3}\Delta E_{r0}(\mathbf{r}) - \varepsilon^2(1-\Lambda\bar{\mu})(1-\Lambda)E_{r0}(\mathbf{r}) = \\ = \nabla\mathbf{q}_1(\mathbf{r},\hat{\mathbf{l}}) - \varepsilon(1-\Lambda\bar{\mu})q_0(\mathbf{r}). \tag{7}$$

For a flat-layered medium, it is advantageous to move from differentiation with respect $\mathbf{r}$ to differentiation of the function $f(\mathbf{r})$ with respect to the optical thickness of the medium τ based on the following relationship:

$$\nabla f(\mathbf{r}) = \varepsilon\nabla f(\tau), \tag{8}$$

as a result, taking into account minor transformations, the expression (7) will become:

$$\Delta E_{r0}(\tau) - 3(1-\Lambda\bar{\mu})(1-\Lambda)E_{r0}(\tau) = \\ = 3\frac{\nabla\mathbf{q}_1(\tau,\hat{\mathbf{l}}) - (1-\Lambda\bar{\mu})q_0(\tau)}{\varepsilon}, \tag{9}$$

which is equivalent to the second-order partial differential equation:

$$\frac{d^2E_{r0}(\tau)}{d\tau^2} - 3(1-\Lambda\bar{\mu})(1-\Lambda)E_{r0}(\tau) = \psi(\tau), \tag{10}$$

where $\psi(\tau)$ is the source function:

$$\psi(\tau) = \frac{3}{\varepsilon}\left(\nabla\mathbf{q}_1(\tau,\hat{\mathbf{l}}) - (1-\Lambda\bar{\mu})q_0(\tau)\right), \tag{11}$$

$\bar{\mu} = \frac{1}{4\pi}\oint x(\hat{\mathbf{l}},\hat{\mathbf{l}}')(\hat{\mathbf{l}},\hat{\mathbf{l}}')d\hat{\mathbf{l}}' \equiv x_1$ – average cosine of the scattering angle.

To simplify further calculations, we introduce the substitution:

$$V_{x1} = (1-\Lambda);\ V_{x2} = (1-\Lambda x_1);\ V_{x3} = \\ = (1-\Lambda x_2);\ a = \sqrt{3V_{x1}V_{x2}},$$

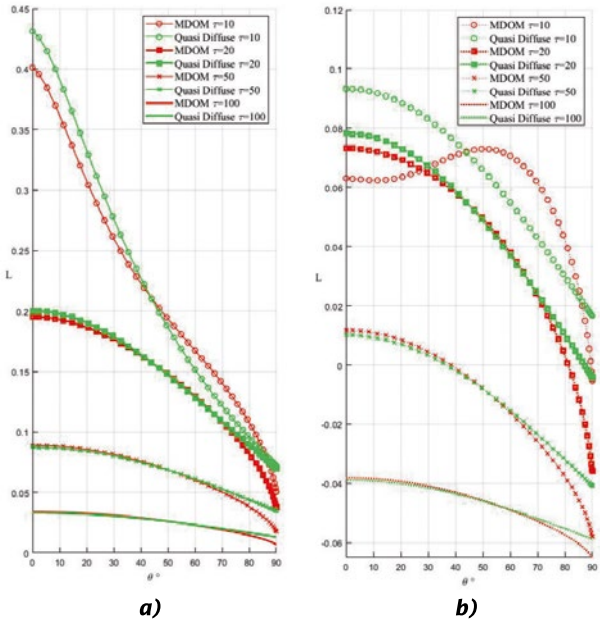

Fig. 2. Radiance distribution for the quasi-diffusion approximation (green) compared to MDOM (red) for optical thicknesses: τ = 10, τ = 20, τ = 50 and τ = 100: *a*) for the full solution; *b*) for the regular part

where x_1, x_2 are the coefficients of the expansion of the scattering indicatrix in Legendre polynomials, in the case of the Henyey-Greenstein indicatrix [17], respectively $x_1 = g = \overline{\mu}$, then the expression (10) will be rewritten as:

$$\frac{d^2 E_{r0}(\tau)}{d\tau^2} - a^2 E_{r0}(\tau) = \psi(\tau). \tag{12}$$

The equation (12) is the partial differential equation whose general solution is:

$$\begin{aligned} E_{r0}(\tau) &= C_1 \mathrm{e}^{-\tau a} + C_2 \mathrm{e}^{\tau a} + E_{ps}, \\ E_{ps} &= c_0 \mathrm{e}^{-\tau} + c_1 \mathrm{e}^{-V_{x1}\tau} + c_2 \mathrm{e}^{-V_{x2}\tau} + c_3 \mathrm{e}^{-V_{x3}\tau}, \end{aligned} \tag{13}$$

where $C_{1–2}$, $c_{0–3}$ are the integration constants.

Let's substitute (13) in (4) and taking into account (6) we get:

$$\begin{aligned} q_0(\tau, \hat{\mathbf{l}}) &= \varepsilon\left(-V_{x1} \mathrm{e}^{-V_{x1}\tau} + V_{x2} \mathrm{e}^{-V_{x2}\tau}\right), \\ \mathbf{q}_1(\tau, \hat{\mathbf{l}})\hat{\mathbf{l}} &= \frac{\varepsilon}{3}\left(V_{x1} \mathrm{e}^{-V_{x1}\tau} - 3V_{x2} \mathrm{e}^{-V_{x2}\tau} + 2V_{x3} \mathrm{e}^{-V_{x3}\tau}\right), \\ \nabla \mathbf{q}_1(\tau, \hat{\mathbf{l}}) &= \frac{\partial \mathbf{q}_1(\tau, \hat{\mathbf{l}})}{\partial \tau} = \\ &= \frac{\varepsilon}{3}\left(-{V_{x1}}^2 \mathrm{e}^{-V_{x1}\tau} + 3{V_{x2}}^2 \mathrm{e}^{-(1-\Lambda x_1)\tau} - 2{V_{x3}}^2 \mathrm{e}^{-V_{x3}\tau}\right). \end{aligned} \tag{14}$$

After substituting the obtained results into the equation (12), equating the coefficients with the same exponents, we find the constants $c_{0–3}$:

$$\begin{aligned} c_0 = 0;\ c_1 &= -\frac{{V_{x1}}^2 - a^2}{V_{x1}^2 - a^2} = -1; \\ c_2 = 0;\ c_3 &= -\frac{2{V_{x3}}^2}{V_{x3}^2 - a^2}. \end{aligned} \tag{15}$$

The expression for the projection of the light vector of the regular part onto the direction of radiation transfer is obtained from the system (5) with taking into account the gradient of the spatial irradiance (13):

$$\begin{aligned} &\mathbf{E}_r(\tau)\hat{\mathbf{l}} = \\ &= \frac{3\mathbf{q}_1(\tau, \hat{\mathbf{l}})\hat{\mathbf{l}} + C_1 a \mathrm{e}^{-\tau a} - C_2 a \mathrm{e}^{\tau a} - \nabla E_{ps}}{3V_{x2}}. \end{aligned} \tag{16}$$

To determine the coefficients $C_{1–2}$, we will use the boundary conditions in the form of Marshak [13]:

$$\begin{cases} \frac{1}{4}E_0(0) + \frac{1}{2}\mathbf{Å}(0)\cdot\hat{\mathbf{l}} = 0, \\ -\frac{1}{4}E_0(\tau) + \frac{1}{2}\mathbf{Å}(\tau)\cdot\hat{\mathbf{l}} = E_a(\tau). \end{cases} \tag{17}$$

where, taking into account the expression for spatial irradiance (13) and the light vector (16), let's find expressions for determining the coefficients C_1 and C_2:

$$\begin{cases} C_1 = C_2 \dfrac{(2a + 3V_{x2})\mathrm{e}^{\tau a}}{(2a - 3V_{x2})\mathrm{e}^{-\tau a}} + \\ + \dfrac{12V_{x2}E_a(\tau) + 3V_{x2}E_{ps} - 6\mathbf{q}_1(\tau)\hat{\mathbf{l}} + 2dE_{ps}}{(2a - 3V_{x2})\mathrm{e}^{-\tau a}}, \\ C_2 = -C_1 \dfrac{3V_{x2} + 2a}{3V_{x2} - 2a} + \\ + \dfrac{2dE_{ps}(0) - 3V_{x2}E_{ps}(0) - 6\mathbf{q}_1(0)\hat{\mathbf{l}}}{(3V_{x2} - 2a)}. \end{cases} \tag{18}$$

Thus, we have obtained expressions for all the coefficients of the expression of the luminance distribution of the regular part, and the anisotropic part is based on the SHM.

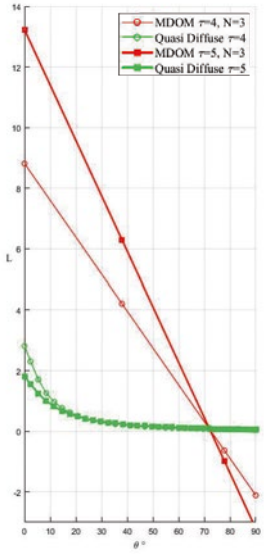

Fig. 3. Radiance distribution for the quasi-diffusion approximation (green) in comparison with MDOM at $N = 3$ (red) for optical thicknesses: $\tau = 4$ and $\tau = 5$

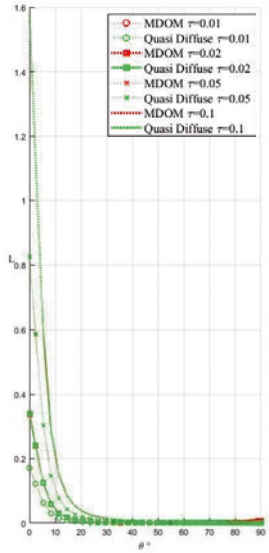

Fig. 4. Radiance distribution for the full solution of the quasi-diffusion approximation (green) in comparison with MDOM (red) for small optical thicknesses: $\tau = 0.01$, $\tau = 0.02$, $\tau = 0.05$, $\tau = 0.1$

3. RESULTS

The results of calculating the luminance distribution based on the quasi-diffusion approximation for calculating the regular part of the spatial luminance distribution for a flat layer are presented in Fig. 2 in comparison with the well-known program for calculating flat-layered media – MDOM [14, 16]. For comparison, the solutions were taken for radiation incident zenith angle of $\theta_0 = 0$ °, for flat layers with the Henyey-Greenstein scattering indicatrix with the parameter $g = 0.9$. The anisotropic part was solved in both cases based on the small-angle modification of the SHM with the number of harmonics $N_z = 401$. The following parameters were selected for MDOM: the number of discrete ordinates $N = 81$, the number of azimuthal harmonics $M = 0$ – only one zero harmonic on azimuth.

The relative deviation in irradiance on the underlying surface of the quasi-diffusion approximation from MDOM among the presented solutions is shown in Fig. 2. For the complete solution: the maximum relative deviation (for $\tau = 20$) was $\delta_{Fmax} = 1$ %, the minimum relative deviation (for τ=100) was $\delta_{Fmin} = 0.3$ %. For the regular part: the maximum relative deviation (for τ=20) was $\delta_{Rmax} = 3$ %, and the minimum relative deviation (for $\tau = 100$) was $\delta_{Rmin} = 0.2$ %.

An assessment of the average calculation time was also carried out using the algorithm based on the quasi-diffusion approximation and MDOM for the parameters selected above on a laptop with a 12-th Gen processor (Gen Intel (R) Core (TM) i7–1255 U 1.70 GHz, and 8 GB of RAM and a speed of 3200 MT/s). MDOM calculation time is 0.005 s. The average calculation time of the quasi-diffusion approximation is 0.00014 s.

For the MDOM solution, there are minimal possible values of discrete ordinates N =3, while the calculation speed of the quasi-diffusion approximation also exceeds MDOM. The average calculation time of MDOM is 0.0006 s, and the calculation time of the quasi-diffusion approximation remains the same. At the same time, the deviations in MDOM calculations increase significantly. For confirmation, we provide graphs in Fig. 3, which shows two acceptable options for presentation on one graph for $\tau = 4$ and $\tau = 5$.

Fig. 3 demonstrates a significant increase in the MDOM deviation at minimum N with increasing τ, which continues with increasing τ and for large τ, as shown in Fig. 2, the joint representation of quasi-diffusion and MDOM on the same graph is uninformative.

The behaviour of the quasi-diffusion approximation at small optical thicknesses is interesting, Fig. 4. In this case, the anisotropic part acquires a big influence in the solution and the graphs of the complete solution almost converge, the relative deviation of the quasi-diffusion approximation with MDOM lies in the range of (0.24–0.25) %.

CONCLUSION

For large optical thickness, the quasi-diffusion approximation converges to the exact solution while

maintaining significantly faster computation speeds compared to alternative methods for plane-parallel geometries. These advantages position the method as an efficient computational kernel for solving illumination problems involved:

1. Three-dimensional geometries with large optical depths (e.g., atmospheric twilight zone calculations);

2. Radiative transfer in composite materials containing arbitrary 3D inclusions with high optical thickness.

The approach also enables:

• Accurate estimation of material absorption properties;

• Determination of integral light field characteristics;

• Solution retrieval at arbitrary points within the medium (not just boundaries), substantially expanding its practical applicability.

Notably, our solution incorporates the anisotropic component through the Modified Spherical Harmonics (MSH) approach, enabling precise light field characterization in media with small optical thicknesses. While the conventional Spherical Harmonics Method fails to account for backscattering effects, this limitation is effectively compensated by the regular component derived from the diffusion approximation.

The solution's accuracy can be further enhanced through synthetic iteration [18], which:

• Utilizes the RTE integral form of our solution;

• Provides accurate energy field characterization;

• Substantially improves angular distribution accuracy.

The quasi-diffusion approximation's formulation as a Legendre polynomial series with exponentially dependent coefficients (on optical thickness τ) permits analytical expression of the synthetic iteration.

For implementing the regular component in 3D media models, we recommend employing specialized mathematical packages with finite element capabilities, particularly COMSOL Multiphysics [19,20]. Our future work will focus on:

• Implementing this complete solution framework;

• Incorporating synthetic iteration refinement;

• Conducting comprehensive comparisons with Monte Carlo-based solutions.

REFERENCES

1 Afanas'ev, V.P., Basov, A. Yu., Budak, V.P., Efremenko, D.S., Kokhanovsky, A.A. Analysis of the discrete theory of radiative transfer in the coupled "Ocean – Atmosphere" system: current status, problems, and development prospects // J. Mar. Sci. Eng., 2020, Vol. 8, p. 202; https://doi.org/10.3390/jmse8030202.

2 Cahalan, R.F., Ridgway, W., Wiscombe, W.J., Bell, T.L. The albedo of fractal stratocumulus clouds // J. Atmos. Sci., 1994, Vol. 51, p. 2434–2455.

3 Rozenberg, G.V. Twilight: A Study in Atmospheric Optics [Sumerki: Issledovaniya optiki atmosphery] / NY: Springer New York, 1963. 380 p.

4 Basov, A.Y., Boos, G.V., Budak, V.P., Grimailo, A.V., Efremenko, D.S. Slab radiance factor calculating methods // Proceedings of SPIE, 2021, Vol. 11916, 11 p.

5 Sumin, D. et al. Geometry-aware scattering compensation for 3D printing // ACM Trans. on Graphics (TOG), 2019, Vol. 38, # 4, Article 111.

6 Klose, A.D. Radiative transfer of luminescence light in biological tissue / In: Kokhanovsky, A.A. (eds) Light Scattering Reviews 4. Berlin, Heidelberg: Springer, 2009, pp. 293–345.

7 Qi, J., Xie, D., Jiang, J., Huang, H. 3D radiative transfer modelling of structurally complex forest canopies through a lightweight boundary-based description of leaf clusters // Rem. Sens. Env., 2022, Vol. 283, pp. 113–301.

8 Belov, M.L., Belov, A.M., Gorodnichev, V.A., Alkov, S.V. Multispectral Optical Reflectometry Method of Forest Resource Monitoring // Light & Engineering, 2022, Vol. 30, # 1, pp. 51–59.

9 Fedotov, Y.V., Ivanov, S.E., Belov, M.L., Belov, A.M., Gorodnichev, V.A., Chumachenko S.I., Shkarupilo, A.A. The Tree Species Classifying Possibilities Research in the Spectral Range (0.4–1.0) μm. // Light & Engineering, Vol. 32, # 4, 2024, pp. 43–50.

10 Goldin, V. Ya. Quasi-diffusion method for solving the kinetic equation [Kvazidiffuzionnuy method resheniya kinetic equation] // J. Comput. Mathematics and Mathematical Physics, 1964, Vol. 4, # 6, pp. 1078–1087.

11 Dolin, L.S. On the propagation of a narrow beam of light in a medium with highly anisotropic scattering [O rasprostranenii yzkogo lucha

sveta s vysokoy anizotropnost'yu rasseivayuschey sredu] // News of higher educational institutions, Radiophysics, 1966, Vol. 9, # 1, pp. 61–71.

12. Fick, A. Über Diffusion // Annalen der Physik, 1855, B.170, H.1, pp. 59–86; https://doi.org/10.1002/andp.18551700105.

13. Bothe, W. Die Streuabsorption der Elektronenstrahlen // Zeit.f. Physik, 1929, B.54, H.3, pp. 161–178.

14. Budak, V.P, Korkin, S.V. On the solution of a vectorial radiative transfer equation in an arbitrary three-dimensional turbid medium with anisotropic scattering // Journal of Quantitative Spectroscopy & Radiative Transfer, 2008, Vol. 109, pp. 220–234.

15. Budak, V.P., Zheltov, V.S., Lubenchenko, A.V., Freidlin, K.S., and Shagalov, O.V. A Fast and accurate synthetic iteration-based algorithm for numerical simulation of radiative transfer in a turbid medium [Bystryy i tochnyy sinteticheskiy iteratsionnyy algoritm dlya chislennogo modelirovaniya perenosa izlucheniya v mutnoy srede] //Atmospheric and Oceanic Optics, 2017, Vol. 30, # 1, pp. 70–78.

16. Budak, V.P., Klyuykov, D.A., Korkin, S.V. Convergence acceleration of radiative transfer equation solution at strongly anisotropic scattering / In: Kokhanovsky, A. (eds) Light Scattering Reviews 5, 2010, Berlin, Heidelberg: Springer, pp. 147–203.

17. Henyey, L., Greenstein, J. Diffuse radiation in Galaxy // Astrophys. J., 1941, Vol. 93, # 1, pp. 70–83.

18. Adams, M.L., Larsen, E.W. Fast iterative methods for discrete-ordinates particle transport calculations // Progr. Nuclear Energy, 2002, Vol. 40, # 1, pp. 3–159.

19. Krasnikov, G.E., Nagornov, O.V., Starostin, N.V. Modelling of physical processes using the COMSOL Multiphysics package [Modelirovaniye fizicheskikh protsessov s ispol'zovaniyem paketa COMSOL Multiphysics] / Moscow: NRNU MEPhI, 2012, 184 p.

20. Kovalenko, A.V., Uzdenova, A.M., Urtenov, M. Kh., Nikonenko, V.V. Mathematical modelling of physical and chemical processes in the COMSOL Multiphysics 5.2 environment: a tutorial [Matematicheskoye modelirovaniye fizicheskikh i khimicheskikh protsessov v srede COMSOL Multiphysics 5.2: uchebnoye posobiye] / St. Petersburg: Lan, 2022, 228 p.

Vladimir P. Budak,
Editor-in-chief of the Svetotekhnika / Light & Engineering Journals, Professor of the Light and Engineering subdepartment of the National Research University MPEI, Full Member of the Academy of Electrotechnical Sciences of Russia

Pavel A. Smirnov,
Ph. D., Associate Professor. He graduated from the Lighting Engineering Department of MPEI in 2001. At present, he is the Associate Professor of the Light and Engineering Department of RNU MPEI. His research interests are in light field theory, radiative transfer in the atmosphere, daylighting, visual perception

Light & Engineering
Vol. 33, No. 4, pp. 80–85, 2025

https://doi.org/10.33383/2024-092
Svetotekhnika # 3, 2025, pp. 81–84

SPATIAL SPECTRA FEATURES OF INHOMOGENEITIES FOR AN ATMOSPHERIC BACKGROUND FRAGMENT LIMITED BY THE FIELD OF VIEW IN AN OPTICAL-ELECTRONIC SYSTEM OF THE LWIR RANGE

Yuri I. Yakimenko, Tatyana S. Astakhova, Ekaterina A. Sapronenkova, Sergei P. Astakhov, Roman V. Polyakov, and Igor V. Yakimenko*

National Research University Moscow Power Engineering Institute (NRU MPEI), Smolensk branch, Russia
*E-mail: *jakigor@rambler.ru*

ABSTRACT

The results of experimental studies for spatial spectra of an atmospheric background inhomogeneities fragment in the long-wave infrared range (LWIR) are presented. The results of studies for the atmospheric background radiation inhomogeneities, depending on their angular size, made it possible to divide atmospheric backgrounds into two groups: the first group includes cloud classes, containing small-scale inhomogeneities of 1º – 2° in the vertical directions and of 1º – 3° in horizontal directions, such as altocumulus *(Ac),* cumulus *(Cu),* cirrocumulus *(Cc)* and cirrus *(Ci),* and altostratus *(As)*; the second group includes cloud classes containing large-scale inhomogeneities of > 6° in the horizontal directions and > 3° in the vertical directions such as stratus (*St*), stratocumulus (*Sc*), and clear sky.

Keywords: atmospheric background (AB), LWIR range, spatial spectrum, field of view

1. INTRODUCTION

In the works [1–5], devoted to the analysis of the results of studies for inhomogeneities spatial spectra of the cloudy atmosphere in the LWIR range, a method was used to obtain inhomogeneities spatial characteristics for cloud formations in the form of estimates of spatial correlation coefficients for arrays of frames obtained from video streams of various forms and cloudiness amount (points) in the vertical directions between rows and in the horizontal ones between columns, changing by a given discrete value, in accordance with the algorithm of scanning complex operation [6]. The main disadvantage of this method is the insufficient speed of the equipment used, due to the use of a single-element radiation receiver (for example, the time interval required to scan a sky fragment in a sector of 10°×60° was (on average) about 1 min), which made it impossible to obtain relatively accurate estimates for the characteristics of the spatial structures of the cloudy atmosphere radiation. This disadvantage was especially evident in the study of cumulus *(Cu)*, since the formation of this clouds class is characterized by rapid turbulent and thermodynamic processes.

The scientific problem of the work is to clarify the spatial spectra of atmospheric background inhomogeneities in the LWIR range based on a series of experimental studies.

2. METHODS

In the process of experimental study for spatial spectra of atmospheric background inhomogeneities in the LWIR range, a set of equipment was used, Fig. 1, including the following items:

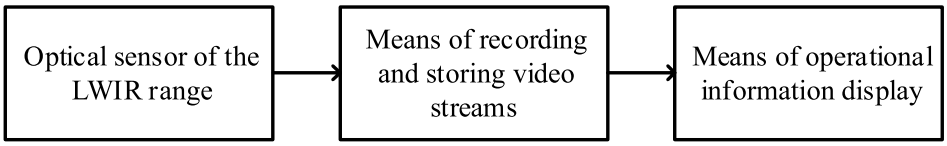

Fig. 1. Structural diagram of the equipment set for experimental study of the atmospheric background radiation spatial structure

1. As an optical sensor of the LWIR range thermal imager *Sii AT* was used, which has the following characteristics [13]:

– Working spectral range: (8–14) μm,

– Resolution: 640×480 pixels,

– Field of view (horizontal): 73.3°,

– Spatial resolution (iF_{ov} – instantaneous field of view): 1.999 mrad (≈ 7 ′),

– Noise equivalent temperature difference NETD: 0.5 K,

– Frame rate: 50 Hz;

2. As a means of recording and storing video streams a video recorder HIWATCH DS-H204GA was used:

– Supporting video compression formats *H.*265*+/ H.*265*/H.*264*+/ H.*264,

– Providing video recording for up to 6 TB;

3. LCD monitor as a means of operational information display was used.

During the summer months of 2023, 90 video streams were recorded, corresponding to meteorological situations with cloudiness of various classes and amounts (points).

Experimental studies of spatial spectra of atmospheric background inhomogeneities in the LWIR range were carried out in the following sequence:

– The type (class) and cloudiness amount (points) were determined;

– The spatial position of the thermal imager field of view was set (elevation angle ε, azimuth β of the thermal imager optical axis);

– The video stream was continuously recorded for a duration of 40 minutes to 1 hour, during which the random process of the atmospheric background radiation could be considered stationary;

– The video stream was divided into frames at equal intervals and, as a rule, the initial division of frames was carried out at intervals from 5 s to 1 min [12];

– The averaged spatial correlation coefficients were calculated in the vertical direction between rows $R(n)$ and in the horizontal direction between columns $R(m)$ for frame arrays $G(n, m)$, obtained from video streams for cloudiness of different classes and points, from correlation matrices in the vertical direction between rows $R_{n,(n+k)}$ and in the horizontal direction between columns $R_{m,(m+k)}$

$$R_{n,(n+k)} = \frac{1}{\sigma_n \sigma_{(n+k)}} \sum_{m=0}^{M} (u_{n,m} - \mu_n)(u_{(n+k),m} - \mu_{(n+k)}),$$

where $R_{n,(n+k)}$ is the coefficient of mutual correlation between the signal level proportional to the energy brightness (radiance) of the radiation for the AB inhomogeneities in the n-th and $(n+k)$-th lines of the segment; $u_{n,m}$, $u_{(n+k),m}$ is the signal level in n-th and $(n+k)$-th lines of the segment; μ_n, $\mu_{(n+k)}$ is the mathematical expectation of the signal level in n-th and $(n+k)$-th rows; σ_n, $\sigma_{(n+k)}$ is the standard deviations of the signal level in n-th and $(n+k)$-th rows; M is the number of elements in a column; k is the step for calculating correlation coefficients ($k = 0,1,2,3,...N$).

$$R_{m,(m+k)} = \frac{1}{\sigma_m \sigma_{(m+k)}} \sum_{n=0}^{N} (u_{n,m} - \mu_m)(u_{n,(m+k)} - \mu_{(m+k)}),$$

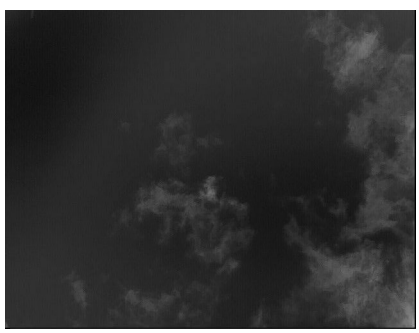

Fig. 2. Example for a frame of LWIR image for cumulus (*Cu*) clouds of 1–3 points

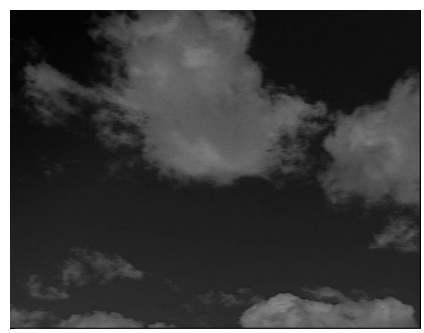

Fig. 3. Example for a frame of LWIR image for cumulus (*Cu*) clouds of 4–6 points

Fig. 4. Example for a frame of LWIR image for cumulus (*Cu*) clouds of 7–9 points

where $R_{m,(m+k)}$ is the coefficient of mutual correlation between the signal level proportional to the radiance of the inhomogeneities radiation AB in *m*-th and *(m+k)*-th frame columns; $u_{n,m}$, $u_{n,(m+k)}$ is the signal level in *m*-th and *(m+k)*-th columns; μ_m, $\mu_{(m+k)}$ is the mathematical expectation of the signal level in *m*-th and *(m+k)*-th columns; $\sigma_m, \sigma_{(m+k)}$ is the standard deviations of the signal level in *m*-th and *(m+k)*-th columns; *N* is the number of elements in a row; *k* is the step for calculating correlation coefficients $(k = 0,1,2,3,...N)$;

– Diagonal correlation matrices of the calculated spatial correlation coefficients for arrays of frames between rows and columns were constructed;

– The dependencies of the spatial correlation coefficients for the frame arrays were averaged in the vertical direction between the rows *R*(*n*) and in the horizontal direction between the columns *R*(*m*), taken discretely for the cloudiness of one class and point.

To analyse the dependencies of the spatial correlation coefficients for the frame arrays *G*(*n, m*) in

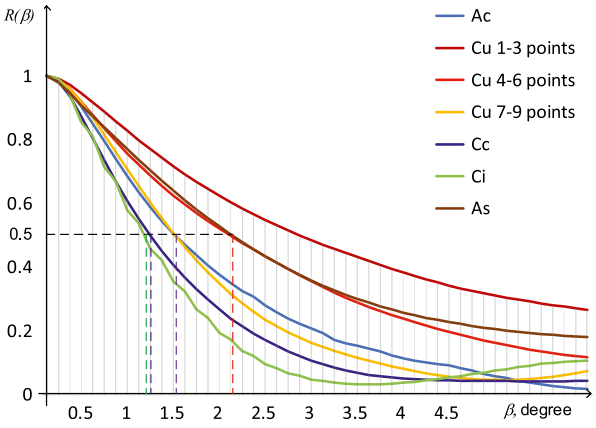

Fig. 6. Dependences for spatial correlation coefficients in the horizontal direction between rows on the elevation angle for cloud classes containing small-scale inhomogeneities of the atmospheric background

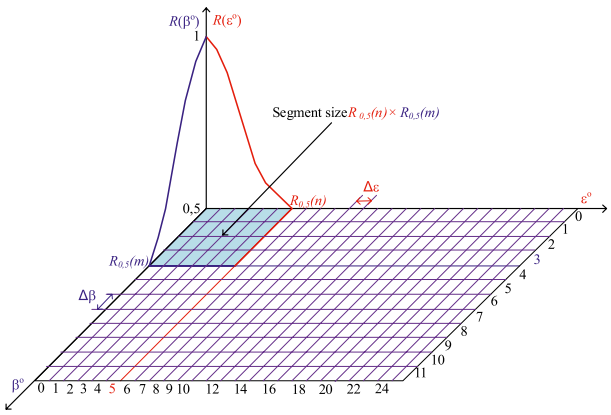

Fig. 5. Graphical explanation for the method of estimating the angular dimensions for atmospheric background inhomogeneities

the vertical directions between the rows *R*(*n*) and in the horizontal directions between the columns *R(m)*, meteorological situations were selected, in which the cloudiness of a certain class and point retained its parameters unchanged for a time interval of at least 40 min.

Meteorological situations in which the change in the characteristics of the atmospheric background (class or (and) cloudiness point) occurred faster than 30–40 minutes, or characterized by the presence of clouds of several classes at once (for example, clouds of the upper and lower layers), were ignored.

Examples of LWIR image frame selections for cumulus (*Cu*) clouds (with quantitative characteristics: 1–3, 4–6, 7–9 points), altocumulus clouds (*Ac*) and cloudless (clear) sky are shown in Figs. 2–4, respectively.

3. RESULTS

Experimental studies for spatial spectra of atmospheric background inhomogeneities consist of estimating spatial correlation coefficients for arrays of frames *G*(*n, m*), obtained from video streams frames of various forms and cloudiness points in the vertical directions between rows *R*(*n*) and in the horizontal directions between columns *R*(*m*).

It was established that the characteristic difference of the cloudiness inhomogeneities spatial spectra for different classes and points are the angular dimensions of their inhomogeneities, which were determined by the value of the spatial correlation coefficients in the vertical directions between the rows *R*(*n*) and in the horizontal directions between the columns *R*(*m*), exceeding the value of 0.5.

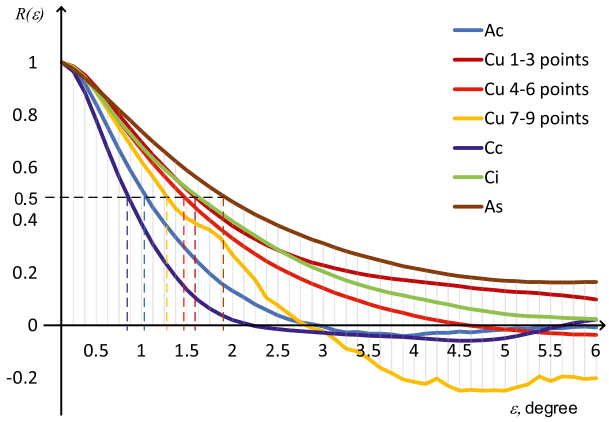

Fig. 7. Dependences for spatial correlation coefficients in the vertical direction between columns on azimuth for cloud classes containing small-scale inhomogeneities of the atmospheric background

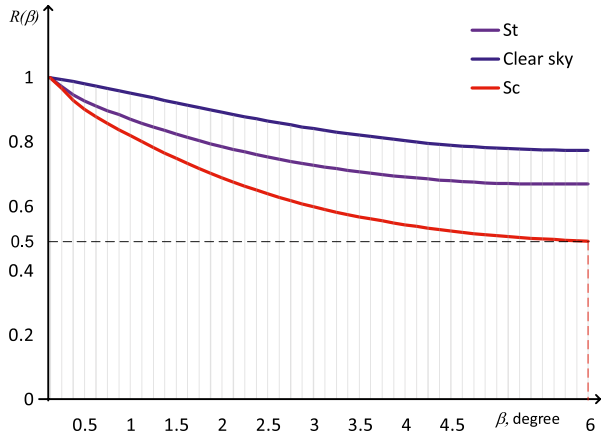

Fig. 8. Dependences for spatial correlation coefficients in the horizontal direction between rows on the elevation angle for cloud classes containing large-scale inhomogeneities of the atmospheric background

Consequently, based on the values of $R_{0.5}(n)$ and $R_{0.5}(m)$, respectively, the spatial correlation coefficients by rows and columns, and the corresponding steps of the angular shift by rows $\Delta\varepsilon$ and columns $\Delta\beta$, it is possible to estimate the angular dimensions of the atmospheric background inhomogeneities by elevation angle (ε) and azimuth (β), Fig. 5, [7–11].

As a result of the obtained results analysis, it was established that, depending on the angular dimensions of the inhomogeneities, atmospheric backgrounds can be divided into two groups:

– The first group includes cloud classes containing small-scale irregularities of 1º–2° in the vertical directions and 1º–3° in the horizontal directions: altocumulus (*Ac*), cumulus (*Cu*), cirrocumulus (*Cc*), cirrus (*Ci*), and altostratus (*As*), Figs. 6, 7;

– The second group includes cloud classes containing large-scale irregularities of > 6° in the horizontal directions and > 3° in the vertical directions: stratiform (*St*), stratocumulus (*Sc*) and clear sky, Figs. 8, 9, [1–5].

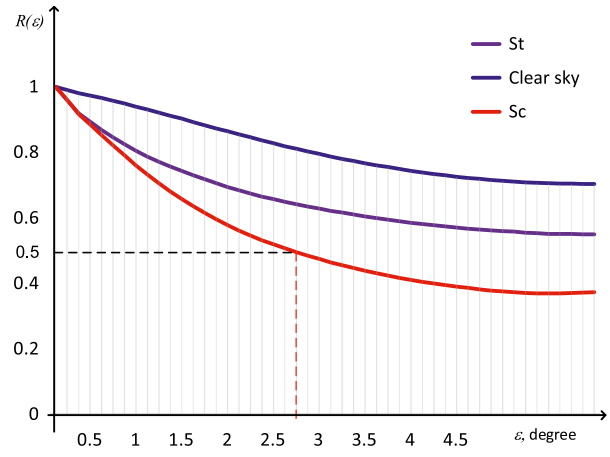

Fig. 9. Dependences of spatial correlation coefficients in the vertical direction between columns on azimuth for cloud classes containing large-scale inhomogeneities of the atmospheric background

CONCLUSION

Based on the obtained statistical material for the spatial spectra of atmospheric background inhomogeneities, it was established that the characteristic difference between clouds of different classes and points is the angular dimensions of their inhomogeneities, which were determined by the value of the spatial correlation coefficients in the vertical directions between rows *R(n)* and in the horizontal directions between columns *R(m)*, exceeding the value of 0.5.

As a result of the analysis for the obtained data, it was established that, depending on the angular dimensions of the inhomogeneities, atmospheric backgrounds can be divided into two groups:

– The first group includes cloud classes containing small-scale irregularities of 1º – 2° in the vertical directions and 1º – 3° in the horizontal directions: altocumulus (*Ac*), cumulus (*Cu*), cirrocumulus (*Cc*), cirrus (*Ci*), and altostratus (*As*);

– The second group includes cloud classes that contain large-scale irregularities of > 6° in the horizontal directions and > 3° in the vertical directions: stratiform (*St*), stratocumulus (*Sc*), and clear sky.

REFERENCES

1. Allenov, A.M., Soloviev, V.A. Objective parameterization for the states of the cloudy atmosphere by the structure of its own radiation in the range of 8–13 μm [Ob"ektivnaya parametrizaciya sostoyanij oblachnoj atmosfery po strukture ee sobstvennogo izlucheniya v diapazone 8–13 mkm] // Optical Journal, 1999, Vol. 66, # 12, pp. 99–100.

2. Allenov, A.M., Soloviev, V.A. Correlation (spatial) connections between brightness fluctuations created by cloud irregularities in the range of 8–13 μm [Korrelyacionnye (prostranstvennye) svyazi mezhdu fluktuaciyami yarkosti, sozdavaemymi oblachnymi neodnorodnostyami v diapazone 8–13 mkm] // Proceedings of the IEM, Moscow: Gidrometeoizdat, 1995, # 25 (160), pp. 3–14.

3. Allenov, M.I. Structure of optical radiation of natural objects. [Struktura opticheskogo izlucheniya prirodnyh ob"ektov] / Moscow: Gidrometeoizdat, 1988, 164 p.

4. Allenov, A.M., Ivanova, N.P. Temporal variability of the spatial structure of sky radiation in the range of 8–13 μm under cumulus clouds [Vremennaya izmenchivost' prostranstvennoj struktury izlucheniya neba v diapazone 8–13 mkm pri kuchevoj oblachnosti] // Optical Journal, 2001, Vol. 68, # 3. pp. 43–44.

5. Yakimenko, I. V., Smolin, V. A., Mishchenko, A.M. Results of studies of the spatial structure of atmospheric radiation in the spectral range of 1.5–2 μm [Rezul'taty issledovanij prostranstvennoj struktury izlucheniya atmosfery v spektral'nom diapazone 1.5–2 mkm] // Svetotekhnika, 2018, # 1, pp. 40–44.

6. Allenov, A.M., Bukhantsov, N.I., Gerasimov, V.V., Tretyakov, N.D. Scanning complex for measuring the spatial structure of atmospheric radiation in the range of 3–13 μm [Skaniruyushchij kompleks dlya izmereniya prostranstvennoj struktury izlucheniya atmosfery v oblasti 3–13 mkm] // Proceedings of the IEM, Moscow: Gidrometeoizdat, 1990, # 11 (132), pp. 54–61.

7. Alpatov, B.A., Blokhin, A.N., Muravyov, V.S. Image processing algorithm for automatic tracking systems of air objects [Algoritm obrabotki izobrazhenij dlya sistem avtomaticheskogo soprovozhdeniya vozdushnyh ob"ektov] // Digital signal processing, 2010, # 4**.**

8. Yakimenko, I.V. Methods, models and means of detecting air targets against the atmospheric background using wide-angle optical electronic systems: Monograph [Metody, modeli i sredstva obnaruzheniya vozdushnykh tseley na atmo-sfernom fone shirokougol'nymi optiko-elektronnymi sistemami: Monografiya] / St. Petersburg: Lan Publ., 2023, 168 p.

9. Smolin, V.A., Yakimenko, I.V., Rasskaza, D.S. Optical-information method for detecting unmanned aerial vehicles using a robotic optical-electronic system / [Optiko-informacionnyj metod obnaruzheniya bespilotnyh vozdushnyh sudov robotizirovannoj optiko-elektronnoj sistemoj] // GraphiCon 2022, 32nd International Conference on Computer Graphics and Machine Vision, September 19–22, 2022, Ryazan State Radio Engineering University named after V.F. Utkin, Ryazan, Russia, pp. 548–558.

10. Yakimenko, I.V., Yakimenko, Yu.I., Bobkov, V.I., Smolin, V.A. Optical Information Support for Artifact Detection robotic system on a complex background/ // Proceedings of International Symposium "Atmospheric Radiation and Dynamics" (ISARD-2023), Saint-Petersburg State University, 2023. pp. 80–82.

11. Yakimenko, Yu.I., Bobkov V.I., Yakimenko I.V. Method for detecting artifacts on a complex background using an optical-electronic system [Metod obnaruzheniya artefaktov na slozhnom fone optiko-elektronnoj sistemoj] // Photonics, 2023, # 4, pp. 272–283.

12. Yakimenko, Yu.I., Astakhov, S.P., Yakimenko, I.V., Stolyarevskaya, R.I. Results of the study of spatio-temporal structures of cloud radiation in the LWIR range [Rezul'taty issledovaniya prostranstvenno-vremennyh struktur izlucheniya oblachnosti v LWIR diapazone] // Svetotekhnika, 2024, # 2, pp. 68–72.

13. https://www.unibelus.by/upload/files/ac7814c8–0cea-11ea-813e-00155d045202.pdf

Yuri I. Yakimenko,
postgraduate student of the Department of Electronics and Microprocessor Technology at the NRU MPEI, Smolensk branch. He graduated from the NRU MPEI Smolensk Branch in 2015. His scientific interests: digital image processing, computer vision, optical range technical vision systems

Tatyana S. Astakhova
is a student of the NRU MPEI, Smolensk branch. Her scientific interests: electronics and microprocessor technology, optical range technical vision systems

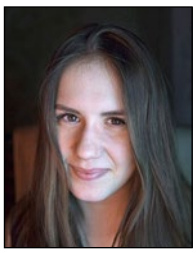

Ekaterina A. Sapronenkova,
an assistant of the Electronics and Microprocessor Engineering Department at the NRU MPEI in Smolensk. She graduated from the NRU MPEI Smolensk Branch in 2020. Her scientific interests are digital image processing, computer vision, optical range technical vision systems

Sergey P. Astakhov,
Ph. D. in Technical Sciences, Associate Professor. He graduated from Smolensk Higher Anti-Aircraft Missile Engineering School in 1989. At present, he is the Associate Professor at the Department of Electronics and Microprocessor Technology of the NRU MPEI Smolensk branch. His scientific interests: electronics and microprocessor technology, optical range technical vision systems

Roman V. Polyakov,
a postgraduate student of the Department of Electronics and Microprocessor Technology at the NRU MPEI, Smolensk branch. In 2018, he graduated from the Smolensk Military Academy of Air Defence. His research interests: digital image processing, machine vision, artificial intelligence, neural networks

Igor V. Yakimenko,
Doctor of Technical Sciences, Professor. He graduated from Smolensk Higher Anti-Aircraft Missile Engineering School in 1985; in 2006 graduated from the Smolensk Military Academy of Field Anti-Aircraft Defence. At present, he is the Head of the Department of Electronics and Microprocessor Technology at the NRU MPEI in Smolensk branch. His field of scientific interests is connecting with digital image processing, computer vision, and optical vision systems

Light & Engineering
Vol. 33, No. 4, pp. 86–92, 2025

https://doi.org/10.33383/2025-009
Svetotekhnika # 3, 2025, pp. 64–69

EXPLORING THE CONVERTERS IN ENHANCING EFFICIENCY AND SOFT STARTING IN SOLAR PV ARRAY BASED WATER PUMPING SYSTEMS

Mohammed Hasan Ali

Department of Electrical Power and Machines Engineering, University of Diyala, Iraq
E-mail: moh80mmed@gmail.com

ABSTRACT

One valuable resource is sunlight in the Middle East, especially in Iraq, because of the country's wealth and vast areas. Due to the scarcity of water, many people have turned to digging wells to grow various crops. To operate these wells, the need for solar energy systems has emerged. A model and simulation were designed in MATLAB for a solar energy system with a brushless DC motor. To attain optimal effectiveness of the PV array and facilitate the brushed DC motor's soft start., this paper discusses the use in solar photovoltaic array-based pumps, an intermediate DC-DC converter is placed between an inverter with a voltage supply (VSI) and the solar PV array. To maximize the PV array's power point, its incremental conductivity maximum tracking of power point modifies the motor speed reference. With the aid of MATLAB/Simulink software, the simulation results of the suggested system under various operating situations are confirmed.

Keywords: BLDC Motor, voltage source inverter, PV array, MATLAB/Simulink software

1. INTRODUCTION

The UN's three primary objectives are to double the share of renewable energy in the energy mix, increase global energy efficiency by twofold, and provide universal access to contemporary energy sources. One easy way to accomplish these three goals is through hybrid energy systems [1].

More than 95 % of those without access to modern electricity dwell in sub-Saharan Africa, with 84 % of them residing in rural regions, according to the international electricity Agency's 2022 report. However, because of the area's remoteness and poor national economic contribution, on-grid electricity generation is either impractical or too expensive [2]. Therefore, since the resource is plentiful and accessible locally, alternative energy sources like biomass, wind, or solar renewable energy could aid in meeting the energy requirement [3]. Renewable and non-renewable energy systems are frequently paired with or without energy storage technologies in emerging nations to enhance the quality and dependability of the power supply [4]. Although the intermittent and unpredictable nature of renewable energy supplies is a defining characteristic, the hybrid mix of these resources can assist overcome these characteristics, hence boosting their efficiency and appeal [5].

The feasibility of hybrid off-grid energy systems utilized in rural and semi-urban areas worldwide has been covered in research articles [6]. It is also discovered that these publications can be used to power necessary electrical loads in remote islands or grid-isolated settlements. To balance the annual equivalent investment cost with fuel cost when using diesel generators [7], proposed a scenario-based stochastic optimization model to estimate the capacity of residential photovoltaic (PV) batteries while accounting for solar radiation and hourly energy consumption patterns. The model in the paper determines the capacities of PV batteries needed to meet the energy requirement [8].

The BLDC motor's and the solar PV array's ratings are chosen so that the suggested system can

function well in any atmospheric situation. The MATLAB/Simulink environment is used to analyse the simulated results of the different performances [9]. The suggested system's appropriateness for solar PV-based water pumping is confirmed by the results of simulations. When used in SPV-based applications, a zeta converter has the following advantages over traditional buck, boost, buck – boost, and Cuk converters. PV technology is utilized in solar water pumping to convert sunlight into electricity, which is then used to pump water. A DC or AC motor connected to PV panels converts electrical energy into mechanical energy. It is then converted into hydraulic energy [10]. 3 factors – pressure, flow, and pump power – assess the water-pumping capacity of a solar pumping system. For design purposes, pressure is the amount of work a pump does to transfer a specific volume of water up to the tank for storage. The disparity in elevation between the storage tank and the water supply determines how much work a pump must perform. The energy required by the water pump must be provided by a PV array [11].

These converter advantages are advantageous for the suggested system for pumping water fed by SPV arrays. To accommodate various PV field configurations, the PV inverters used in small PV plants in the current system need to have a wide input voltage range [12]. Adopting inverters with an architecture with two stages ensures this capability. The 1st stage, typically a DC/DC converter is useful for adjust the PV array voltage to satisfy the needs of the DC/AC second stage, which is used to inject the generated power into the grid or supply an AC load. Because the 1st stage may be used to detect the PV array's highest power output and the 2nd stage is utilized to provide low total harmonic distortion (THD) AC current, this architecture is also useful in terms of controllability. The additional control scheme, which is necessary to regulate the speed of the BLDC motor, is more expensive and complex. Furthermore, high-frequency PWM pulses are typically used to run a voltage-source inverter (VSI), which raises switching loss and lowers efficiency [13].

Fig. 1 depicts the layout of the suggested SPV array-fed BLDC motor-driven water pumping system with a converter. A pump for water, a BLDC motor, a converter, a VSI, and an array make up the suggested system. The converter is run by the pulse generator [14].

2. THE PV WATER PUMPING DEVICE THAT IS BEING SUGGESTED

This paper proposes a stand-alone form of MATLAB/Simulink water pumping system. To meet the needs of a remote, isolated, low-maintenance, and inexpensive water pumping application, will be employed with a tank for storing water rather than storage of batteries. As seen in Fig. 2, the system's primary components are a PV array that uses sunlight as a source to generate electricity and a centrifugal pump load that is powered by a permanent magnet DC motor [15]. There will be a maximum power point tracker that incorporated into the system to attain high system performance efficiency and to increase energy that the load draws from the PV array during the day [16].

3. GOALS FOR THE WORK

This work's main goal is to examine how well a standalone water pumping system performs. To reduce maintenance, this will be powered solely by a PV source using an electrical power converter that converts DC to DC [17]. It won't be connected to any batteries for energy storage or smoothing. PV array, rotational pump, DC motor, and DC-DC power converter make up the system. The PV array's

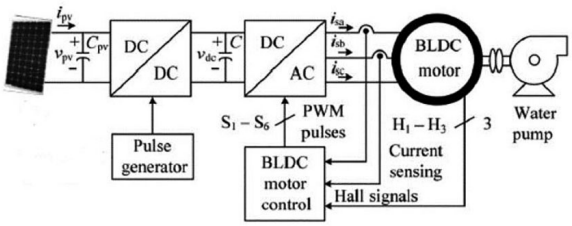

Fig. 1. Setup of the system

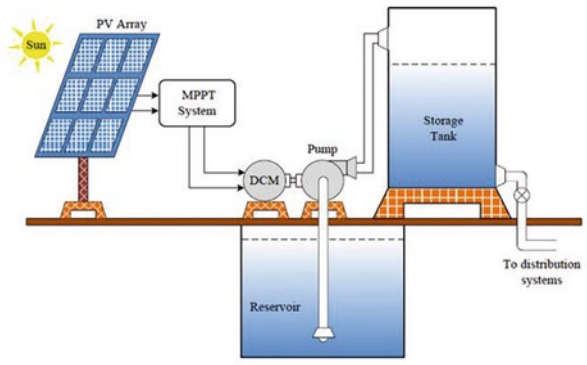

Fig. 2. Shape of a water storage system

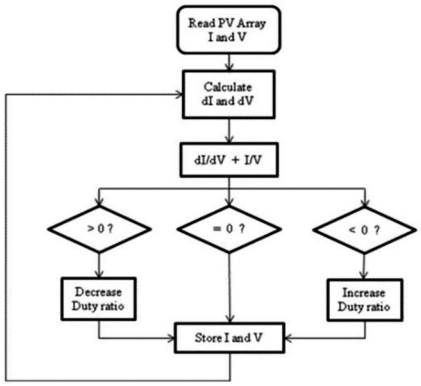

Fig. 3. Flowchart of the MPPT

output characteristics will be impacted by shifting atmospheric conditions, and the necessity of a method for tracking maximum power points will be considered [18].

The effectiveness of various MPPT strategies and kinds of DC-DC converters will be examined to boost system efficiency. The primary goal will be to find out how to use more effective MPPT techniques to increase the MPPT in a standalone PV pumping water system.

4. MONITORING MAXIMUM POWER POINT (MPPT)

This technique takes advantage of the presumption that the output conductance change ratio equals the output conductance negative [19].

$$P = V \cdot I, \tag{1}$$

where P is the power of PV array, V is its voltage, and I is its current. Then as the result of applying the chain rule on the derivative of products is

$$\partial P / \partial V = \left[\partial (VI)\right] / \partial V, \tag{2}$$

since ∂P/∂V=0 at MPP. Regarding array current I and array voltage V, the equation could be expressed as follows:

$$\partial I / \partial V = - I / V. \tag{3}$$

Until the condition $(\partial I / \partial V) + (I / V) = 0$ is met, the DC to DC is controlled by the MPPT boost, the PWM control signal of the converter. With this approach, the module's peak power is located greater than 98 % of its incremental conductance. The following flow chart, which is displayed in Fig. 3, makes the method simple to understand [20].

The changes in speed are not quick enough to offset the rapid PV voltage drop that happens once the power absorption beyond the maximum possible at the MPP if acceleration feedforward compensation is not used. At the intersection of the relationship of current energy vs. voltage and the VSI voltage saturation limit curve, on the left of the MPP, the working point rapidly shifts to the only stable equilibrium. Until the motor power demand (which is correlated with the motor speed) is reduced below the power availability at the equilibrium point, the system stays there. The working point then swiftly shifts to a stable operating position at the same power level, to the right of the MPP. The MPPT never reaches a stable MPP operating condition since it then begins to increase the speed once more, repeating the cycle endlessly [21].

5. DC MOTOR AND PUMP

Through an BLDC motor electronics commutation, a VSI is used to control the motor. An electronic BLDC motor using a decoder logic, commutation change the currents passing through its windings in a specific order [22]. The DC input current is symmetrically positioned at the middle of each phase voltage for 120°. According to the different possible combinations of three, six switching pulses are produced. An integrated encoder generates three Hall-effect signals based on the rotor position. At 60° intervals, a precise set of Hall-effect signals is generated for every rotor position range. Table 1

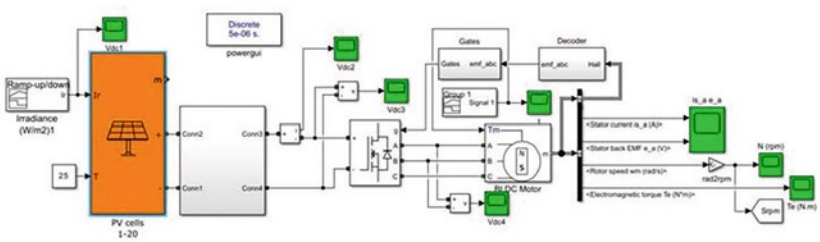

Fig. 4. PV water pumping system Simulink model with MPPT controller

Table 1. Signals and Switching of BLDC

Θ, °	Hall Signals			Switching States					
	H_a	H_b	H_c	S_1	S_2	S_3	S_4	S_5	S_6
N/A	0	0	0	0	0	0	0	0	0
0–60	0	0	1	1	0	0	0	0	1
60–120	0	1	0	0	1	1	0	0	0
120–180	0	1	1	0	0	1	0	0	1
180–240	1	0	0	0	0	0	1	1	0
240–300	1	0	1	1	0	0	1	0	0
300–360	1	1	0	0	1	0	0	1	0
N/A	1	1	1	0	0	0	0	0	0

Table 2. Specification of PV Model

Parameter	Value
Maximum power, W	305.226
Voltage at maximum power, V_{mp}, V	54.7
Current at maximum power, I_{mp}, A	5.58
Open circuit voltage, V_{oc}, V	64.2
Short-circuit current, I_{sc}, A	5.96
Total number of series-connected cells, N_s, pcs.	5
Total number of parallel cells, N_p, pcs.	66
Temperature coefficient of open circuit voltage, K_v, mV/°C	–272.7
Temperature coefficient of short-circuit current, K_i, mA/°C	61.745
Diode saturation current, I_0, A	6.3076×10^{-12}
Parallel resistance, R_p, Ω	393.2054
Serial resistance, R_s, Ω	0.37428

lists the six switching states that were produced using the rotor position estimation [23]. It is noticeable that just two switches conduct simultaneously, which causes the VSI to operate in a 120° conduction mode and, thus, have lower conduction losses [24]. In addition, the VSI's basic frequency switching is provided via electronic commutation, which eliminates the losses connected to high-frequency PWM switching. For the suggested system, a BLDC motor with an integrated encoder made by a motor power firm was chosen [25].

6. SOLAR PV ARRAY

To ensure that the system's performance is unaffected by the loss related to the motor and converters in order, a 1.5 kW peak power output of a PV array – a little more than what the motor needs is used. The usual solar insolation level of 1000 W/m^2 is used to estimate the solar PV array's characteristics. The VSI's DC link voltage and the BLDC motor's DC voltage rating are taken into consideration while choosing the voltage of the solar PV array at MPP. The parameters of the PV system are presented in Table 2.

7. SIMULATED RESULTS

The solar system for pumping water is modelled using the MATLAB/Simulink program. As seen in Fig. 4, the system's entire simulation model is made

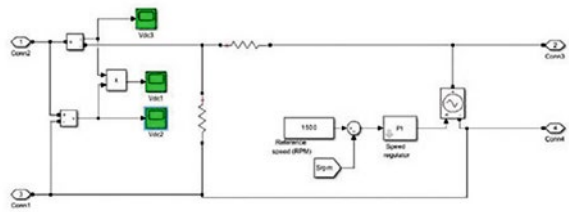

Fig. 5. Simulink model of BLDC motor

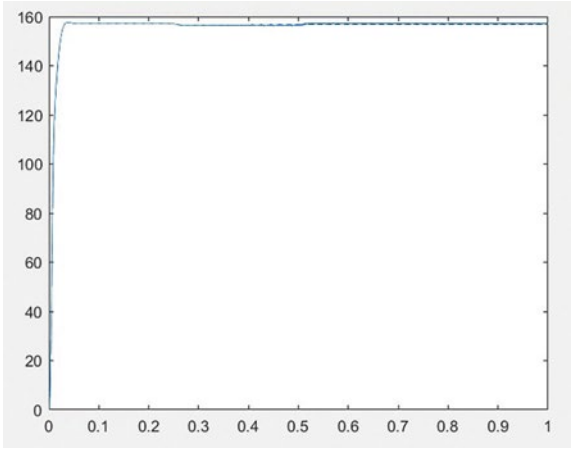

Fig. 6. Rotor speed

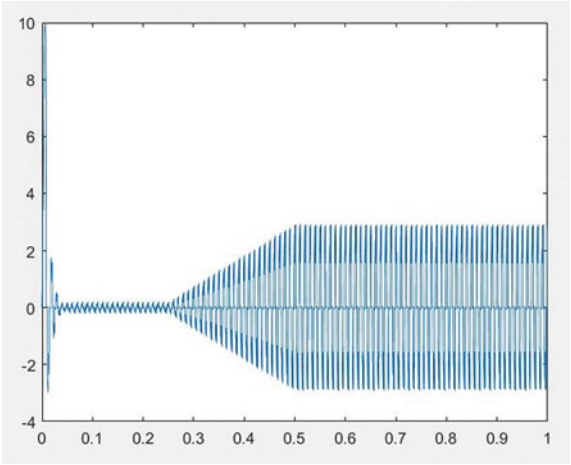

Fig. 7. Stator current

up of a few masked blocks joined together. The PV model was connected to a BLDCM that was driving a centrifugal pump load via a controlled buck chopper to perform the simulation. It also comes with an MPPT control device.

7.1. BLDM Motor Model

As seen in Fig. 5, the BLDM simulation model is constructed in the MATLAB environment using the SimPowerSystems and Simulink libraries.

The different motor-pump indices for BLDC, including speed, N, electro-magnetic torque, e_a, stator current, i_{sa}, and the back EMF created, T_e, and load torque, TL, change proportionately to the level of sun insolation. The simulated findings reveal two significant truths. The BLDC motor has a gentle beginning because, first, the stator current is managed at start-up so that it requires time to attain its value in the steady state. Second, the suggested system operates steadily regardless of the weather, since the electromagnetic torque produced by the BLDC motor, T_e, which is equivalent to the torque needed to operate the pump, TL, in spite of all changes in the amount of solar radiation. The obtained graphs of dependencies are shown in Figs. 6–11.

8. CONCLUSIONS

This paper presents a standalone solar water pumping system that provides clean, sustainable energy for the water supply in remote locations. This paper's primary goal was to increase the overall system efficiency by applying effective MPPT methods to deliver the greatest power to the load, particularly in the face of rapidly fluctuating meteorological conditions.

The suggested system's appropriateness for solar PV-based water pumping has been validated by its intended performance, even at 20 % of the typical solar irradiance.

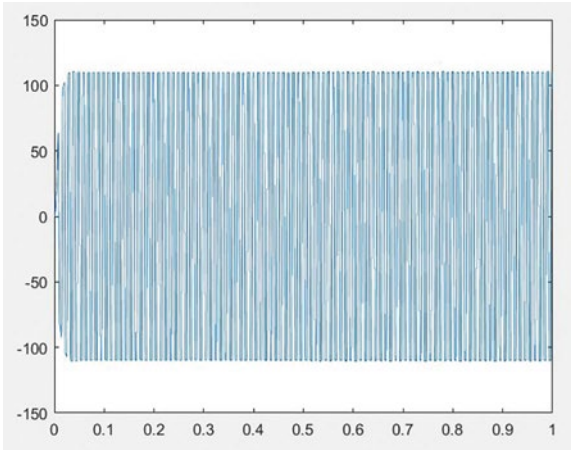

Fig. 8. Stator back EMF

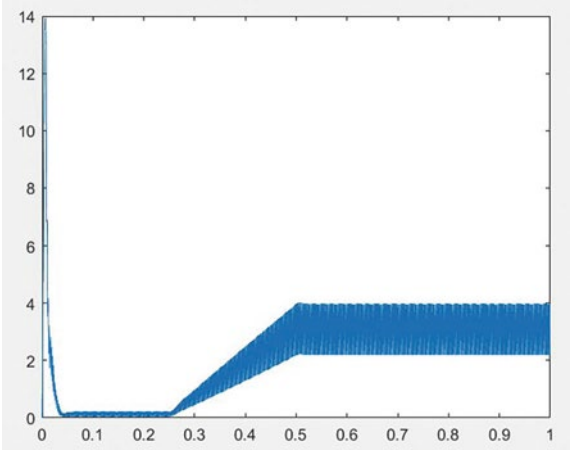

Fig. 9. Torque

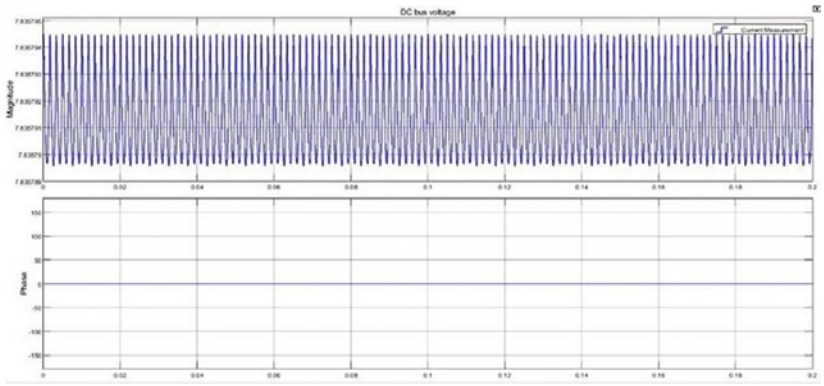

Fig. 10. DC bus voltage

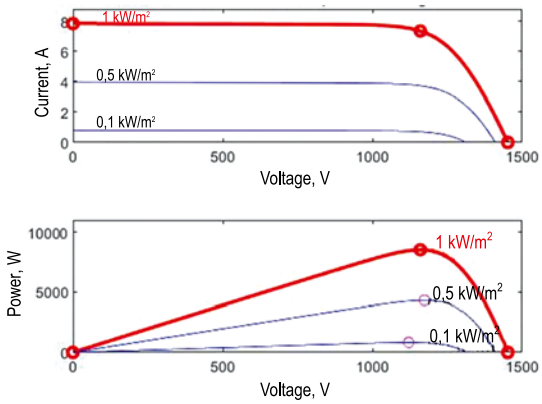

Fig. 11. PV current and power with voltage

REFERENCES

1. Uno, M., Kukita, A. Single-switch voltage equalizer using multitasked buck – boost converters for partially-shaded photovoltaic modules // IEEE Trans. Power Electron., 2015, Vol. 30, # 6, pp. 3091–3105.

2. Kumar, R., Singh, B. BLDC motor driven solar PV array fed water pumping system employing zeta converter // Proc. 6th IEEE India Int. Conf. Power Electron. (IICPE), Dec. 8–10, 2014, pp. 1–6.

3. Elgendy, M.A., Zahawi, B., Atkinson, D.J. Assessment of the incremental conductance maximum power point tracking algorithm // IEEE Trans. Sustain. Energy, 2013, Vol. 4, # 1, pp. 108–117.

4. Rajan, K., Singh, B. BLDC motor-driven solar PV array-fed water pumping system employing zeta converter // IEEE Transactions on Industry Applications, 2016, # 52.3, pp. 2315–2322.

5. Fathi, A. Maximum power point tracking techniques for photovoltaic water pumping system // Diss. University of Bath, 2015.

6. Olumuyiwa Taiwo, A., Nwulu, N.I., Gbadamosi, S.L. Optimal design and sizing of a hybrid energy system for water pumping applications // IET Renewable Power Generation, 2024, # 18.4, pp. 706–721.

7. Menka, D., Sharma, S., Saxena, R. Solar PV stand-alone water pumping system employing PMSM drive // 2014 IEEE Students' Conference on Electrical, Electronics and Computer Science. IEEE, 2014.

8. Mapurunga Caracas, J.V., De Carvalho Farias, G., Moreira Teixeira, L.F., De Souza Ribeiro, L.A. Implementation of a high-efficiency, high-lifetime, and low-cost converter for an autonomous photovoltaic water pumping system // IEEE Trans. Ind. Appl., 2014, Vol. 50, # 1, pp. 631–641.

9. Africa, S.S. Mid-Year Population Estimates. In: Statistical Release P0302, South Africa 2022. chromeextension:// efaidnbmnnnibpcajpcglclefindmkaj/https://www.statssa. gov.za/publications/P0302/P03022021.pdf.

10. Zakwan, M., Muzzammil, M., Alam, J. Application of spreadsheet to estimate infiltration parameters // Perspect. Sci., 2016 # 8, pp. 702–704.

11. Arulmurugan, R., Suthanthiravanitha, N. Model and design of a fuzzy-based Hopfield NN tracking controller for standalone PV applications // Elect. Power Syst. Res., 2015, Vol. 120, pp. 184–193.

12. Belgacem, A. Fuzzy logic direct torque control of induction motor for photovoltaic water pumping system // International Journal of Power Electronics and Drive Systems (IJPEDS), 2022, # 13.3, pp. 1822–1832.

13. Gurgi, Z.K., Ali, I.A., Hassan, E.D. Simulation analysis of DC motor based solar water pumping system for agriculture applications in rural areas // Int. J. Power Electron. Drive Syst, 2023, # 14, pp. 2409–2417.

14. Haripriya, T., Parimi, A.M. BLDC motor based solar water pumping system with grid interface // 2019 3rd International Conference on Recent Developments in Control, Automation & Power Engineering (RDCAPE). IEEE, 2019.

15. Sontake, V.C., Kalamkar, V.R. Solar photovoltaic water pumping system-A comprehensive review // Renewable and Sustainable Energy Reviews, 2016, # 59, pp. 1038–1067.

16. Chandel, S.S., Nagaraju Naik, M., Chandel, R. Review of solar photovoltaic water pumping system technology for irrigation and community drinking water supplies // Renewable and Sustainable Energy Reviews, 2015, # 49, pp. 1084–1099.

17. Aliyu, M. A review of solar-powered water pumping systems // Renewable and Sustainable Energy Reviews, 2018, # 87, pp. 61–76.

18. Li, Gl. Research and current status of the solar photovoltaic water pumping system – A review // Renewable and Sustainable Energy Reviews, 2017, # 79, pp. 440–458.

19. Shinde, V.B., Wandre, S.S. Solar photovoltaic water pumping system for irrigation: A review // African journal of agricultural research, 2015, # 10.22, pp. 2267–2273.

20. Verma, S. Solar PV powered water pumping system – A review // Materials Today: Proceedings, 2021, # 46, pp. 5601–5606.

21. Muralidhar, K., Natarajan, R. A review of various components of solar water-pumping system: Configuration, characteristics, and performance // International Transactions on Electrical Energy Systems, 2021, # 31.9, e13002 p.

22. Benghanem, M. Performances of solar water pumping system using helical pump for a deep well: A case study for Madinah, Saudi Arabia // Energy Conversion and Management, 2013, # 65, pp. 50–56.

23. Amna Samir, I. The contribution of adsorbent materials (silica gel and sawdust) in removing water vapor; Iraq as a study case, 2023.

24. Uddin, Md.H. Evaluation of the mechanical properties of PLA material used for 3D printing solar e-hub component // Diyala Journal of Engineering Sciences, 2024, pp. 163–172.

25. Abbas, M.K. Computation of hydrodynamic characteristics of water flow in electrical submersible pump // Diyala Journal of Engineering Sciences, 2012, pp. 37–51.

Mohammed Hasan Ali,
M. Sc. He received his B. Sc. from University Diyala/Iraq in 2006, M. Sc. from University of Belgorod, Russia, 2013. He is currently lecturer at the Department of Electrical Power Engineering, College of Engineering, University of Diyala Iraq. He has 19 years' experience in practice of Electrical Engineering. He is teaching several basic subjects of the Electrical Engineering, University of Diyala Iraq. He has 18 published papers. His current research interests are power system modelling, power quality, renewable energy, and power electronics

Light & Engineering
Vol. 33, No. 4, pp. 93–102, 2025

https://doi.org/10.33383/2025-013
Svetotekhnika # 3, 2025, pp. 11–17

A COMPARATIVE STUDY OF THE PHOTOBIOLOGICAL EFFECT OF HPS LAMPS AND DIMMABLE LED IRRADIATORS USED TO GROW TOMATO VEGETABLES UNDER ELECTRICAL LIGHTING

Alexander A. Tikhomirov [1,2,3], Vladimir V. Velichko [1,2], and Evgeniya A. Slyusareva [3]

[1]Institute of Biophysics SB RAS, Federal Research Centre "Krasnoyarsk Science Centre SB RAS", Krasnoyarsk, Russia
[2]M.F. Reshetnev Siberian State University of Science and Technology, Krasnoyarsk
[3]Siberian Federal University, Krasnoyarsk
*E-mail: *alex-tikhomirov@yandex.ru*

ABSTRACT

The paper reports an experimental photobiological study estimating the effectiveness of different spectral modes of photosynthetically active radiation (PAR) for cultivating tomato vegetables using LED irradiators as electrical grow lighting. Variety of Tomato cv. Katya F1 was used in the study.

The purpose of the study was to compare the photobiological efficiency of radiation from dimmable LED irradiators with an adjustable spectrum and high-pressure sodium lamps (DNaT-600).

PAR irradiance at the upper leaf level was maintained constant in the treatment (using LED) and control (using DNaT-600) and was (425 ± 15) μmol/(m^2·s). Energy consumption was measured using electronic electricity meters separately for the control and treatment part of experiment. The characteristics of plant growth and development were recorded throughout the experiment. The tomatoes were analysed for nitrate, sugar, and vitamin C contents.

The study showed that during the growing period of 80 days, a twofold saving in energy consumption was achieved in the treatments with LEDs compared to the control. At the same time, the yield of vegetables per illuminated area in the control was 63.9 kg, which exceeded the average values of this parameter in the treatments by 1.4 times. Taking into account the consumed electricity, the cost of the tomatoes produced in the treatment was lower by 38 % and amounted to 42.2 kW·h and in the control to 58.1 kW·h per one kg of tomatoes. The assumption is substantiated that the reasons for differences in tomato yields may be associated, first of all, with different qualitative and quantitative characteristics of infrared radiation in LED irradiators and sodium lamps. Ways to improve LED irradiators to increase the photobiological efficiency of their radiation are outlined.

Keywords: variable irradiation spectrum, energy efficiency of irradiation modes, dimmable LEDs, DNaT-600 irradiators, tomato productivity, quality of tomato produce

1. INTRODUCTION

Recent decades have seen a rapid growth in the development of northern territories. One of the challenges associated with this is providing the population with fresh plant food. This task is often complicated by major problems, both logistic ones, which are caused by difficult weather conditions, and the storage-related problems: the plant products delivered in advance are stored over long periods, which results in dramatic quality impairment, often af-

fecting their outward appearance and organoleptic properties.

These difficulties could be resolved by growing plant products at the places of residence of the people living in the north, using electrical lighting. For this, highly efficient sources of electrical light are needed. As light sources were created and improved, lighting engineering in Russia traditionally paid great attention to supporting research on assessing the spectral and energy efficiency of radiation for plant growth under electrical lighting. Such studies began to develop especially actively in the 1970s, with the production of various types of sufficiently powerful metal-halide lamps (MHL), which provided a technological basis for the formation of experimental physiologically sound approaches to selecting modes of plant cultivation that would be effective in terms of spectrum and irradiance under electrical illumination conditions [1, 2]. The modern lighting engineering offers various light sources for the greenhouse industry. The most widely used of them now are high-pressure sodium (HPS) lamps and various types of LEDs, which are used as the basis for designing LED irradiators with various spectral and energy characteristics.

In the greenhouse industry, the small-scale introduction of HPS lamps occurred in the 1980–90s, and they gradually replaced their predecessors, MHL, due to higher energy efficiency and longer operating time. However, the continuously improving LED lamps, which are superior to sodium lamps in these and other parameters, have been extensively used for growing plants under electrical lighting in recent decades. LED lamps have proven to be more promising for plant growth under electrical illumination because of a number of undeniable advantages such as their exceptionally long service life (more than 5 times longer than that of HPS lamps), lower thermal radiation temperature, which prevents plant burns, small size, and the possibility of regulating the spectrum and intensity of radiation [3]. The state and prospects for further development of technological lighting using LED technology are described in sufficient detail in Russian publications [4]. Owing to their special characteristics, LED devices can be used to change the spectral power dynamically, to influence various production and morphophysiological parameters of plants. In addition, LEDs can be easily controlled by intelligent lighting programs for plant photosynthesis by changing the ratio of radiation of different wavelengths [5].

Large-scale introduction of modern HPS grow lights into greenhouse industry in Russia began in the 2000s, stimulating a rapid increase in the scale of growing plants under electrical lighting. The main reasons for this are as follows: a relatively low cost due to long-established large-scale serial production, primarily for street lighting, as well as for greenhouses [6, 7]. HPS lights, unlike LEDs, are “hot” light sources, which emit a sufficient amount of heat for winter greenhouses that have insufficient thermal insulation [8–10]. These qualities of HPS lamps are their temporary advantage over LEDs: over time, they will be overcome by the increasing serial production of LEDs and, thus, the natural fall in their cost, as well as by the development of more modern greenhouse designs with better thermal insulation. Of special significance among the parameters of the compared light sources are their energy consumption and photobiological efficiency. The energy efficiency of light sources strongly depends on their radiant efficiency. Such efficiency for sodium lamps reaches (34–36) %, while for LEDs this value can reach 70 % [11]. In addition, the possibility of changing the spectrum and irradiance of LEDs programmatically during the growing season can create conditions for additional energy savings. Thus, it can be assumed that in the long term, the cost of plant products grown using LED irradiation may be significantly lower than that of the products grown under HPS radiation. Therefore, it would be interesting to estimate the energy consumption of HPS and LED irradiators at given irradiation levels in order to determine the energy costs per unit of edible produce.

To understand the reasons for the differences in the photobiological efficiencies of the radiation of the study light sources, which underlie the differences in the resulting yields, it seems important to conduct a comparative assessment of the efficiencies of the HPS and modern LED irradiators with adjustable spectral and energy characteristics. The general conclusion is that the energy efficiency coefficient, together with the photobiological efficiency of the light sources under study, underlies the formation of the cost price of the plant products. Such studies should be started using strictly controlled major environmental parameters (temperature, humidity, mineral nutrition, etc.). Under such conditions, the only varied factor should be the light regime char-

acteristic of a given radiation source. Such studies should be carried out strictly under electrical light in order to exclude the distorting role of daylight illumination on the spectral efficiency of the light source [12]. The study should be performed with the crop, which growth and development will show the fullest potential of LED light sources in terms of the dynamics of changes in spectral and energy characteristics, taking into account individual stages of plant growth and development.

The present study is devoted to a comparative assessment of the results of photobiological research on growing tomatoes under electrical grow lights using currently common irradiators with HPS (control) and modern LED irradiators, in which the LEDs are capable of changing the power and spectral composition of the radiation according to a program specified by the user. Comparison of such irradiators in photobiological experiments makes it possible, on the one hand, to estimate their energy consumption per unit of produce, and on the other hand, to identify differences in the rate and direction of plant yield formation due to the possibility of prompt regulation of the spectral composition of the radiation from LED irradiators.

2. METHODS

A comparative analysis of the photobiological efficiency of radiation from high-pressure sodium lamps DNaT-600, widely used at present in the greenhouse industry, and experimental LED irradiators with the adjustable spectrum and intensity of luminous flux was carried out. Each of the experimental LED irradiators (manufactured by OOO EK Enerkom, Moscow) included four types of diodes with the following characteristics: white light with a correlated colour temperature (CCT) of 6500 K; blue light with a maximum emission at the wavelength 450 nm, red light with a maximum emission at the wavelength 660 nm; far red irradiator with a maximum emission at the 730 nm wavelength. The maximum power consumption of the LED irradiators was about 630 W. The choice of LEDs and their power was based on the spectral and energy characteristics of LED irradiators that had previously shown fairly good efficiency in growing tomatoes of this variety under electrical grow lights [13]. The irradiator power source was equipped with a wireless control unit, which allowed changing the power of each power source channel. Data were transmitted to the control unit via Bluetooth (2.4 GHz) from a tablet (mobile device). Thus, the design of the experimental LED irradiator ensured remote control of the intensity of each channel for setting the required spectral composition and irradiance level of the luminous flux.

At the vegetative growth phase of tomatoes, the radiation spectrum, presented in Table 1 Spectrum 2, was used for all plants (36 plants) in the treatment. After the start of mass flowering, 38 days, Table 2, half of the plants in the planted area (18 plants) were irradiated with a radiation spectrum with a sharply decreased proportion of blue rays and an increased proportion of red rays, Table 1, Spectrum 3, and the remaining 18 plants were left under the radiation of Spectrum 2. At the last growth stage, characterized by the beginning of mass ripening of vegetables (76 days), 3 plants from Spectrum 3 were transferred to radiation in the range of (600–700) nm, Table 1, Spectrum 4, and the remaining 15 plants were left under Spectrum 3.

Thus, on the 80th day of vegetation, four spectral modes were used in the treatment:

– A stationary spectral mode using Spectrum 2;

– A variable spectral mode using Spectrum 2 and then Spectrum 3;

– A variable spectral mode using consecutively Spectra 2, 3, and 4.

In the first two spectral variants, the plants were harvested at the age of 80 days, and in the last spectral variant, the plants were left for post-harvest supplementary lighting without changing the irradiance and other environmental parameters for 4 days. Data on the biochemical composition of fruits for all spectral variants are presented in Table 3. The spectral energy distribution of the light sources was measured using an AvaSpec-ULS2048-USB2 spectrometer (Avantes, Netherlands). The irradiators were mounted on height-adjustable suspensions to create a uniform light field.

The DNaT-600 lamps were used as a control light source with constant spectral and energy characteristics, Table 1, Spectrum 1. These lamps were located at a fixed height from the trays and provided a uniform light field.

The irradiance in the PAR region at the level of the upper leaves for both types of irradiators was (425 ± 15) μmol/(m^2·sec) and was monitored by a Li-250A irradiance meter with a Q-35016 quantum sensor (Li-COR, U.S.). During the growing peri-

od of plants, the irradiance level was corrected every 3–4 days.

The energy consumption was recorded directly by taking readings from the meters, one of which recorded the energy consumed by the LED irradiators and the other – by the DNaT-600 lamps. In the first case, a fixed irradiance value at the level of the upper leaves (425 ± 15) μmol/(m^2·s) during plant growth was achieved by dimming the LEDs and affected directly the readings of the electricity meter. For DNaT-600 lamps, the reduction in luminous flux that was required to compensate for the reduction in the distance between the irradiator and the level of the upper leaves, which occurred during plant growth, was achieved by using a neutral filter – a mesh layer between the irradiator and the plant. Five such layers were installed during the experiment, and each layer had a transmission coefficient of 0.89±0.02. Correction factors were used to correct the value of the final energy consumption on DNaT-600 lamps. Thus, a correct comparison was made between the energy consumptions by the two types of irradiators. When calculating energy consumption, the productivity of fresh tomatoes per unit area (kg/m^2) where fruits were formed at the given irradiance equal to 425 μmol/m^2 was taken into account. Energy costs when using Spectrum 4 for 4 days were not taken into account, since this spectral variant was used only to assess the effect of red rays on changes in the biochemical parameters of tomato fruits, while productivity did not actually change due to additional lighting, Table 2. Therefore, the total irradiated area was combined to calculate the average energy costs in the treatment. In the control (DNaT-600) and the totality of treatments, the irradiated areas were 9 m^2 each. By taking into account the irradiated areas in the control and treatments, we managed to correlate correctly the energy costs recorded by the metering devices with the output of tomato products.

The experiments were carried out in a sealed, temperature-controlled growth chamber at the Institute of Biophysics, FRC KSC SB RAS. Tomato plants (*Solanum lycopersicum* L.) of the Katya F1 variety were selected for the study, because this variety is an early-ripening, determinate crop. Before planting, tomato seeds were germinated in Petri dishes. They were sowed in identical plastic pots (0.9 L each), 1 plant per pot. The rooting substrate was moistened peat, pH 5.5–6.5, 600 g per pot [13]. Tomato plants formed single-stemmed communities with four flower inflorescences with a total height of up to 80 cm. Sowing density was 4 plants per m^2. In each the control variant with DNaT-600 and the treatment with LED irradiators, 36 plants were used.

The air temperature during plant irradiation was 25 ± 1 °C during the photoperiod and 17 ± 1 °C at night. The photoperiod lasted 16 hours. Humidity was maintained at (50–60) %. The nutrient solution was Knop's solution supplemented with iron citrate and a complex of microelements, which was replaced weekly. The plants were watered during the day by flooding the root layer. Until the plants reached 20 days of age, watering was carried out every 3 hours to avoid drying out of the roots, and then every 6 hours. The growing period of the plants was 80 days from the moment of germination. During the growth of the plants, side shoots and old leaves were periodically removed to form single-stem tomato plants.

During the cultivation process, tomato plants were evaluated based on the dynamics of growth processes, the duration of the vegetative phase, the onset of mass flowering and fruiting, the temperature of the leaf apparatus and fruits, and the characteristics of the formation of the fruit yield. When harvesting ripe tomatoes, the nitrate content was determined using the GOST 34570–2019 methods [14]; the sugar content was determined using the permanganate method according to GOST 8756.13–87 [15]; and vitamin C was determined using a capillary electrophoresis system on a Kapel-105M device using the M 04–86–2016 method [16]. The errors in the biochemical analyses included in Table 3 are given taking into account the accuracy of the devices used in the analyses, ±5 %.

Statistical analysis of the results was performed by conventional methods using the standard Microsoft Excel software package. The significance of differences in means was determined using Student's *t*-test for a significance level of $p<0.05$.

3. RESULTS AND DISCUSSION

Analysis of the tomato plant growth processes is shown graphically in Fig. 1.

The graphs suggest that the intensity of growth processes in tomato plants grown under DNaT-600 irradiance was higher. Under LED irradiators, the transition to radiation with a lower proportion of blue rays led to an acceleration of the rate of in-

Table 1. Spectral Parameters of Light Sources Used to Grow Tomato Fruits (cv. Katya F1)

Spectrum number	Spectrum	Proportions of the blue (*b*), green (*g*), red (*r*), and far red (*fr*) regions in PAR*, %	The outward appearance of tomato plants in the mass fruiting period (at the age of 80 days) when cultivated in the rays of a given spectral variant
1	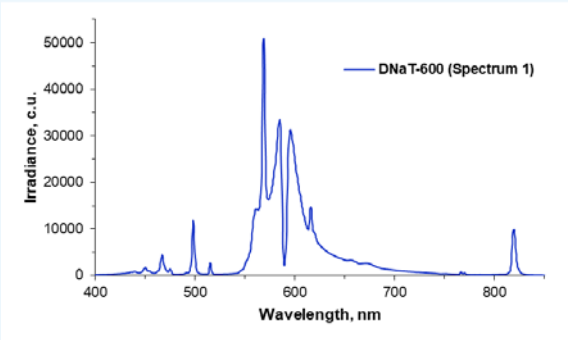	*b* – 5, *g* – 58, *r* – 34, *fr* – 3	
2	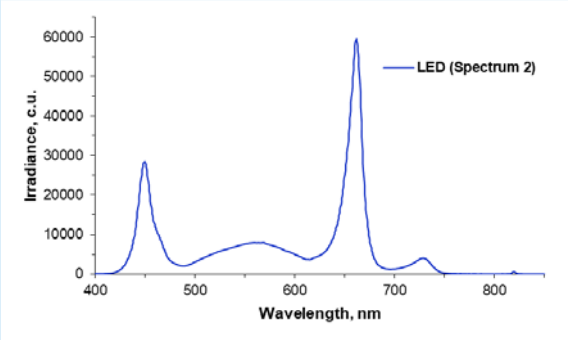	*b* – 24, *g* – 22, *r* – 50, *fr* – 4	
3	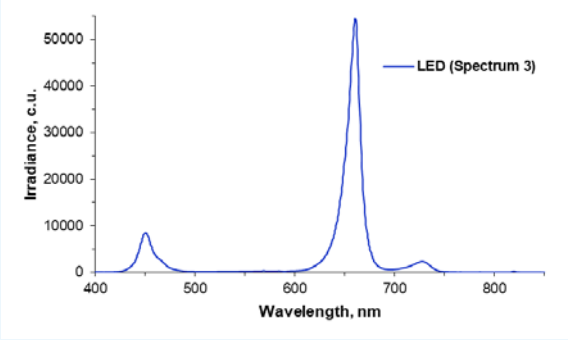	*b* – 13, *g* – 1, *r* – 82, *fr* – 4	
4	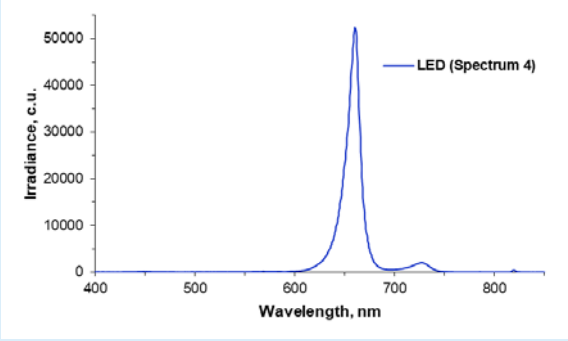	*b* – 0, *g* – 0, *r* – 95, *fr* – 5	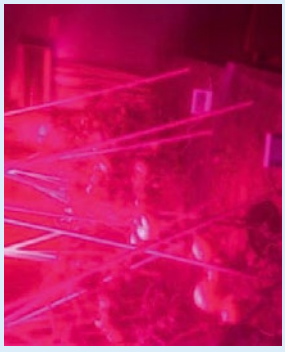

*Calculated as the proportions of the sub-integral areas of intensity in the wavelength ranges: *b*: (400–500) nm, *g*: (500–600) nm, *r*: (600–700) nm, *fr*: (700–750) nm.

Table 2. Major Growth, Development, and Yield Parameters of Tomato Plants Grown under DNaT-600 Lamps and Experimental LED Irradiators

No.	Irradiation spectra in different light treatments according to Table 1	Beginning of flowering, days	Mass flowering, days	Beginning of fruiting, days	Beginning of mass ripening, days	Tomato fruit yield, kg/m²	
						Total fresh weight	Proportion of red fruits, %
1.	LED (Spectrum 2)	32–34	38–40	38–40	76–78	5.1 ± 0.9	82.3 ± 5.6
2.	LED (variable* spectrum 2 3)	32–34	38–40	38–40	76–78	5.5 ± 0.8	83.2 ± 6.0
3.	LED (variable* spectrum 2 3 4	32–34	38–40	38–40	76–78	5.1±0.7	86± 5.8
4.	DNaT-600 (Spectrum 1)	20–22	35–37	35–37	76–78	7.1 ± 0.5	88.2 ± 3.4

*Reasons for and conditions of changing the irradiation spectrum are described in Methods

crease in the linear dimensions of plants, which decreased the difference in this parameter with the control, where DNaT-600 lamps were used. In general, the length of the stems became similar in all treatments by day 60 of the growing season, as plants had stopped growing by that time. Somewhat earlier, by day 50 of the growing season, the height of the plants became similar under the weight of ripening fruits.

Due to the presence of a dimming function in LED irradiators, it became possible to change dynamically the spectral composition of the radiation and estimate the effect of changing the radiation spectrum on the size and quality of the yield [13].

Analysis of Table 2 shows that before the flowering period, the growth and development of plants under DNaT-600 lamps occurred at a faster rate than under LED irradiators. However, by the beginning of mass fruiting, plants in the treatments and the control were developing at rather similar rates, and during the period of mass fruiting, those differences disappeared entirely. However, the reserve for the advancement of growth and organ-forming processes (in particular, flowering and fruiting) for tomatoes under DNaT-600 lamps, which was preserved mainly in the first half of the growing period, created conditions for earlier and faster formation of fruits, which led to the formation of larger sizes than in the treatment. As a result, the ultimate yield in the control was higher than under the LED irradiators.

Table 3 demonstrates that a consistent increase in the proportion of red rays in the PAR flux of LED irradiators contributed to an increase in the sugar content in tomato fruits, while the vitamin C content remained virtually unchanged, and the nitrate content remained within the MAC in all treatments.

According to the literature data, which will be discussed below, DNaT-600 lamps showed higher photobiological efficiency than LED irradiators, which had different emission spectra in the visible region. Some data obtained by growing tomatoes under radiation of different spectral PAR composition suggest that the irradiation mode with a sufficiently high proportion of green rays is very effec-

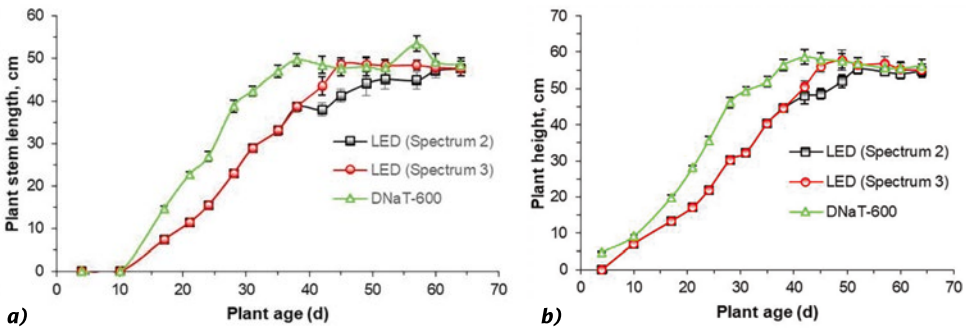

Fig. 1. Dynamics of the increase in stem length (*a*) and plant height (*b*) in tomato cv. Katya F1 cultivated under radiation from DNaT-600 lamps and experimental LED irradiators

Table 3. Biochemical Characteristics of Tomato Fruits under DNaT-600 Lamps and Experimental LED Irradiators with Relative Measurement Error ±5 %

Spectrum of the light source according to Table 1	Biochemical composition			
	Nitrates, mg/kg / MAC	Total sugar, %	Reducing sugars, %	Vitamin C, %
DNaT-600 (Spectrum 1)	80 / 300	6.961	3.902	0.0433
LED (Spectrum 2)	110 / 300	4.962	3.048	0.0483
LED (Spectrum 3)	88 / 300	7.236	3.800	0.0487
LED (Spectrum 4)	100 / 300	7.664	3.822	0.0437

tive for tomatoes [17]. The study [18] noted high efficiency of the yellow-orange spectral region in PAR for tomato biomass accumulation. Unfortunately, those experiments were not completed until the final yield was produced, and only hypotheses can be made about the effects of different regions of the spectrum on the productivity of the economically useful products. Summarizing these facts, it can be assumed that for the LED irradiator, the most promising option will be the distribution of the spectrum in the visible region with a small proportion of blue rays and increased proportions of yellow-green and orange-red rays. The visible spectrum of radiation from the DNaT-600 lamp rather roughly resembled such an energy distribution, while the spectrum of radiation from the LED irradiator used in the experiments clearly contained an insufficient proportion of yellow-green rays.

The main reason for the low yield in the treatment is most likely associated with fundamental differences in the emission spectra of the near infrared radiation of LED irradiators compared to DNaT-600 lamps. Table 1 shows, in particular, that in the 820 nm region there is a distinct peak in the spectrum of the DNaT-600 lamp.

There are no clear ideas yet about the physiological significance of radiation at wavelengths longer than 750 nm for the formation of plant yields. However, the overwhelming (more than an order of magnitude) dominance of the 820 nm peak for the DNaT-600 lamp compared with the LED irradiators suggests its possible influence on the differences in tomato yields between the treatments and control. These assumptions are in good agreement with the data reported in [19]. Comparison of the photobiological efficiency of LED irradiators with different PAR spectra and HPS lights showed that the fruit yield parameters under HPS lamps were higher than the corresponding parameters under the LED irradiators. However, adding near infrared radiation to the visible PAR radiation of LED irradiators resulted in an increase in the tomato yield, which exceeded the yield produced under HPS lamps. The authors of that study also noted that the addition of near infrared radiation in this region of the spectrum to the LED irradiator considerably accelerated the flowering process and, hence, reduced the time before the onset of the fruiting process. Unfortunately, the results of the cited work are significantly devalued by the effect of whitefly on the studied plants, which could considerably distort the results obtained; yet, the probability of a positive effect of additional infrared radiation in the radiation of the LED irradiator on increasing the tomato yield remains. Differences in infrared radiation from different light sources, like ones in the current study, can also affect the temperature of leaves, fruits, and shoot tips, flowering time, and plant development [20]. In our study, the temperature of tomato fruits was measured under sodium lamps and LED irradiators. The measurements showed that the average temperature under the DNaT-600 lamps was 26.7 °C, which was about 2 °C higher than under the LED irradiators. According to the above data and our results, this may also be one of the reasons for the difference in the tomato yields in the tested light options.

Although a number of researchers report that the photobiological efficiency of sodium lamps is higher than that of modern LED irradiators, the results

Table 4. Energy Consumption for Producing Tomatoes Using DNaT-600 Lamps and Experimental LED Irradiators

Light source	Energy consumption, kW·h	Fruit yield per area under light, kg	Cost per fruit from the working area, kW·h/kg
DNaT-600	3710.9	63.9	58.1
LED	1905.6	45.2	42.2

of scientific research show that if all factors associated with the operation of these light sources in greenhouses are taken into account, LED irradiators turn out to be more economical, and therefore, the cost of plant products grown under LED irradiators is, at least, commensurate. As noted above, energy savings when using LED irradiators compared to sodium lamps can reach 70 % or more according to various data. For the conditions of our experiments, these estimates are given in Table 4.

The total energy consumption of the LED lamps during the experiment was 1905.6 kW·h. For DNaT-600 lamps, this value according to the meter was 5948.7 kW·h. The correction of the latter value for the useful flow, taking into account the installation of neutral light filters, was 3710.9 kW·h, Table 4. The present study showed that over the plant growing period, almost twofold energy savings were achieved by using the LED irradiators compared to the control. At the same time, the yield of tomato fruits in terms of the illuminated area was 63.9 kg, which, according to Table 4, exceeded similar values in the treatments by an average of 1.4 times. Taking into account the consumed electricity, the cost of the produced fruits in the experiment was 42.2 kW·h and in the control – 58.1 kW·h per one kg of tomatoes.

The calculated cost of production for the consumed electric energy turned out to be lower for LED irradiators by approximately 38 %. In the literature, such estimates include a range of other associated costs, such as heating greenhouses, and the difference in the cost of production can be reduced to 10 % [7]. However, it makes sense to repeat that the cost of LEDs themselves continues to decrease as their production by the lighting industry is steadily growing. The service life of modern LEDs is also increasing, their spectral and energy characteristics are improving, and other LED parameters are being upgraded, which results in the reduction of the cost of plant products when LEDs are used in greenhouse industry. Therefore, the data in Table 4 can be considered as preliminary, which can be refined taking into account specific conditions associated with the costs of obtaining plant products.

Finally, the present study shows promising ways to improve the efficiency of using LEDs as electrical grow lights and the possibilities of increasing their photobiological efficiency compared with sodium lamps. Thus, it is necessary to consider the possibility of increasing the efficiency of LEDs by improving the radiation in the infrared region of the spectrum as a priority, as was discussed above. Another factor that can enhance the photobiological efficiency of modern dimming LEDs is the possibility of wider manipulation of the radiation spectrum in the entire PAR region. In particular, the last remark concerns the green region of the spectrum, as green (along with yellow-orange) rays, as noted by a number of researchers [9, 18], can be useful, in particular, for tomatoes at certain growing stages. At present, it is extremely important to solve the issue of the optimal intensity and spectrum of radiation required by the most popular crops to optimize the quality and yield of their products. LEDs are the most promising light sources for fulfilling this objective [4, 21]. Based on the above, the development of research in these areas should be considered promising for continuing to improve the photobiological efficiency of LED irradiators as an alternative to HPS and other possible light sources.

CONCLUSIONS

1. Average tomato yields per irradiated areas were higher under the radiation from DNaT-600 lamps by approximately 41 % than under LED irradiators. At the same time, in terms of energy consumption, the efficiency of LED irradiators was higher by approximately 38 %.

2. The reason for the higher efficiency of the DNaT-600 lamps compared to LED irradiators for tomato productivity is most likely associated with additional radiation in the infrared region of the spectrum with a maximum at the wavelength 820 nm. Additional amplification of the radiation

of LED irradiators in the green-yellow region of the spectrum may also enhance its photobiological efficiency for tomatoes.

3. Further research on improving the efficiency of dimmable LED irradiators for tomatoes based on the obtained results should be aimed at improving their radiation in the infrared region of the spectrum and, as an additional factor, creating a full spectrum by increasing the proportion of green rays. This will provide opportunities for designing a light device with the spectrum and radiation that can be regulated in wide ranges according to physiologically justified requirements.

ACKNOWLEDGEMENTS

The study was financially supported within the framework of the State Assignment

FWES-2024–0039 of the Ministry of Education and Science and the Strategic Academic Leadership Program "Priority-2030" for the Siberian Federal University.

The authors of the work express their gratitude to the management and employees of EK Enerkom LLC (Moscow) for supplying an experimental batch of dimmable LED irradiators and technical support in preparing the lighting part of the study, as well as to Selyansky Alexander Iosifovich (NPF Fitopiramida LLC) and Alekseev Yuri Borisovich (seed company Agrofirma Semko) for consulting in organizing the work and assistance in providing high quality seed material.

REFERENCES

1. Tikhomirov, A.A., Lisovsky, G.M., Sidko, F. Ya. Spectral composition of light and plant productivity [Spektral'nyy sostav sveta i produktivnost' rasteniy] / Novosibirsk: Nauka. Siberian Branch, 1991, 168 p.

2. Prikupets, L.B., Tikhomirov, A.A. Optimization of the radiation spectrum for growing vegetables under electrical grow lights [Optimizatsiya spektra izlucheniya dlya vyrashchivaniya ovoshchey pod elektricheskimi lampami] // Svetotekhnika, 1992, # 3, pp. 5–7.

3. Bantis, F., Smirnakou, S., Ouzounis, T., Koukounaras, A., Ntagkas, N., Radoglou, K. Current status and recent achievements in the field of horticulture with the use of light-emitting diodes (LEDs) // Sci. Hortic. 2018, Vol. 235, pp. 437–451, https://doi.org/10.1016/j.scienta.2018.02.058.

4. Prikupets, L.B. Technological lighting in the agro-industrial complex of Russia [Tekhnologicheskoye osveshcheniye v agropromyshlennom komplekse Rossii] // Svetotekhnika, 2017, # 6, pp. 6–14.

5. Prikupets, L.B., Boos, G.V. Irradiation installations in agriculture: Manual for university students [Obluchatel'nyye ustanovki v sel'skom khozyaystve: Uchebnoye posobiye dlya studentov vuzov] / Moscow: Editorial Office of the Journal Light & Engineering / Svetotekhnika, 2023, 136 p.

6. Morrow, R.C. LED Lighting in Horticulture // Hortscience, 2008, Vol. 43, pp. 1947–1950, https://doi.org/10.21273/HORTSCI.43.7.1947.

7. Katzin, D., Marcelis, L.F.M., Mourik van S. Energy savings in greenhouses by transition from high-pressure sodium to LED lighting // Applied Energy, 2021, Vol. 281, # 116019, https://doi.org/10.1016/j.apenergy.2020.116019.

8. Ahamed, M.S., Guo, H., Tanino, K. Energy saving techniques for reducing the heating cost of conventional greenhouses // Biosystems Engineering, 2019, Vol. 178, pp. 9–33, https://doi.org/10.1016/j.biosystemseng.2018.10.017.

9. Nelson, J.A., Bugbee, B. Analysis of environmental effects on leaf temperature under sunlight, high pressure sodium and light emitting diodes // PloS One, 2015, # 10(10): e0138930, https://doi.org/10.1371/journal.pone.0138930.

10. Katzin, D., Mourik van S., Kempkes, F., Henten van E.J. GreenLight – an open source model for greenhouses with supplemental lighting: Evaluation of heat requirements under LED and HPS lamps // Biosystems Engineering, 2020, Vol. 194, pp. 61–81, https://doi.org/10.1016/j.biosystemseng.2020.03.010.

11. Kuijpers, W.J.P., Katzin, D., Mourik van S., Antunes, D.J., Hemming, S., Molengraft van de M.J.G. Lighting systems and strategies compared in an optimally controlled greenhouse // Biosystems Engineering, 2021, Vol. 202, pp. 195–216, https://doi.org/10.1016/j.biosystemseng.2020.12.006.

12. Tikhomirov, A.A., Ushakova, S.A., Shikhov, V.N., Shklavtsova, E.S. Conceptual approaches to selecting radiation spectrum of lamps for plant cultivation under artificial conditions [Kontseptual'nyye podkhody k vyboru spektra izlucheniya lamp dlya vyrashchivaniya rasteniy v iskusstvennykh usloviyakh] // Moscow: Editorial Office of the Journal Light & Engineering/Svetotekhnika, Special Issue, 2019, pp. 19–23.

13. Tikhomirov, A.A., Molokeev, M.S., Velichko, V.V. Use of irradiators with phosphor LEDs with an adjustable radiation spectrum for growing tomatoes for seedlings and products under electrical light [Primeneniye obluchateley s fosfornymi svetodiodami s reguliruyemym spektrom izlucheniya dlya vyrashchivaniya tomatov na rassadu i produktsiyu pri elektricheskom osveshchenii] // Light & Engineering/Svetotekhnika, 2024, # 3, pp. 4–9.

14. Standard GOST 34570–2019 "Fruits, vegetables and their processed products. Potentiometric method for

determining nitrates" / Moscow: Standartinform, 2019 (in Russian).

15. Standard GOST 8756.13–87 "Processed fruit and vegetable products. Methods for determining sugars" / Moscow: Standartinform, 2010 (in Russian).

16. Druzhechkova, E.N., Velichko, N.A., Khanipova, V.A., Druzhechkov, N.K. Chemical composition of juice and pomace of fruits of common rowan (Sorbus aucuparia L.) [Khimicheskiy sostav soka i vyzhimok plodov ryabiny obyknovennoy] // Bulletin of KrasSAU [Vestnik KrasGAU], 2024, # 5, pp. 216–222; DOI: 10.36718/1819-4036-2024-5-216-222.

17. Kusuma, P., Swan, B., Bugbee, B. Does green really mean go? Increasing the fraction of green photons promotes growth of tomato but not lettuce or cucumber // Plants, 2021, Vol. 10, # 637; https://doi.org/10.3390/plants10040637.

18. Mansoori, M., Wu, B.S., Addo, P.W., MacPherson, S., Lefsrud, M. Growth responses of tomato plants to different wavelength ratios of amber, red, and blue light // Scientia Horticulturae, 2023, Vol. 322, # 112459; https://doi.org/10.1016/j.scienta.2023.112459.

19. Ali, A., Cavallaro, V., Santoro, P., Mori, J., Ferrante, A., Cocetta, G. Quality and physiological evaluation of tomato subjected to different supplemental lighting systems // Scientia Horticulturae, 2024, Vol. 323, # 112469; https://doi.org/10.1016/j.scienta.2023.112469.

20. Faust, J.E., Heins, R.D. Modelling leaf development of the African violet (Saintpaulia ionantha Wendl.) // Journal of the American Society for Horticultural Science, 1993, Vol. 118, # 6, pp. 747–751; DOI: 10.21273/JASHS.119.4.72.

21. Sena, S., Kumari, S., Kumar, V., Husen, A. Light emitting diode (LED) lights for the improvement of plant performance and production: a comprehensive review // Current Research in Biotechnology, 2024, Vol. 7, # 100184; https://doi.org/10.1016/j.crbiot.2024.100184.

Alexander A. Tikhomirov,
Dr. of Biological Sc., Professor. In 1970, he graduated from Krasnoyarsk State University with the major in physics and qualification of biophysicist and physicist. At present, he works at the Institute of Biophysics of the Siberian Branch of the Russian Academy of Sciences, Head of the Laboratory of Controlled Biosynthesis of Phototrophic Organisms, Head of the Closed Ecosystems Sub-department of the Reshetnyov Siberian State University of Science and Technology, scientific expert at SFU. His research interests: phytoactinometry, light physiology of plants, closed ecosystems

Vladimir V. Velichko,
Ph. D. in Biological Sc. In 2004, he graduated from Krasnoyarsk State University with the major in Plant Physiology and Biochemistry. In 2008, he was awarded the degree of the Candidate of Biological Sciences, specialty 03.00.12 – plant physiology and biochemistry. At present, he works at the Institute of Biophysics of the Siberian Branch of the Russian Academy of Sciences, Senior researcher of the Laboratory of Controlled Biosynthesis of Phototrophic Organisms. Since 2019, he is the Assistant Professor at the Closed Ecosystems Department of the M.F. Reshetnyov Siberian State University of Science and Technology. His research interests: photosynthesis and productivity of higher plants as phototrophic compartment of artificial ecosystems, effect of light conditions and mineral nutrition on growth and development of higher plants

Evgeniya A. Slyusareva,
Doctor of Physical and Mathematical Sciences, specialty 01.04.05 "Optics", Professor. In 1993, she graduated from Krasnoyarsk State University with a degree in Physics. She works at the Siberian Federal University as a Professor of the Basic Department of Photonics and Laser Technologies, Deputy Director for Research of the Institute of Engineering Physics and Radioelectronics. Her research interests: photonics of functional luminescent materials, optical spectroscopy

Light & Engineering
Vol. 33, No. 4, pp. 103–112, 2025

https://doi.org/10.33383/2025-11
Svetotekhnika # 3, 2025, pp. 20–26

ELECTROPHYSICAL REASONS FOR LIMITING THE OPERATING MODES OF QUANTUM WELL LIGHT EMITTING DIODES

Fedor I. Manyakhin[1*], Lyudmila O. Mokretsova[2], Arkady A. Skvortsov[1], and Dmitry O. Varlamov[1]

[1] *Moscow Polytechnic University, Moscow, Russian Federation*
[2] *National University of Science and Technology* (*MISIS*)*, Moscow, Russian Federation*
*E-mail: *zaomisis@yandex.ru*

The article is dedicated to Alexander E. Yunovich in honour of his 95th Anniversary

ABSTRACT

Based on long-term experimental studies and analysis of the specific features of the current-voltage characteristics of quantum well light emitting diodes (LEDs), based on wide-bandgap semiconductors, it has been found that modern quantum well LEDs have an inherent limitation on their operating current density, determined by existing design and technological parameters. This limitation is associated with the formation of a built-in electric field within the quantum well region, caused by the injection of excess charge from the incoming charge carriers. When such a built-in electric field forms in the quantum well region the efficiency decreases inversely with the potential difference between the outermost quantum wells, that is, inversely with the increasing current density.

Thus, a multiple quantum well structure can be modelled as a multi-plate parallel-plate capacitor, where the stored charge is proportional to the charge of the injected excess carriers or depends exponentially on the voltage that lowers the potential barrier of the space charge region. As a result, once a certain current density threshold is exceeded, the external voltage across the LED structure increases sharply.

The current density, at which the excess voltage U_i appears, is approximately the same for all quantum well LEDs with existing design and fabrication parameters. This threshold can be described by the expression $J_{KP}=(2kT\varepsilon\varepsilon_o)/(q^2\tau L)$, where τL is the product of the carrier lifetime in the quantum wells and the distance between the outermost wells. This value typically falls within the range of (1–10) A/cm^2.

Keywords: light emitting diodes, quantum wells, current-voltage characteristics, quantum efficiency, efficiency

1. INTRODUCTION

The advent of light emitting diodes (LEDs) with gallium nitride quantum wells (QWs) nearly thirty years ago [1, 2], characterized by high quantum efficiency, brought about revolutionary changes in the development and application of lighting technologies. Today, there is virtually no area of technology that does not employ these highly efficient LEDs.

Further improvement in their efficiency is driven by two main approaches: refinement of design and fabrication parameters, and optimization of electrical and thermal operating conditions.

In terms of design improvements, the performance has nearly reached its theoretical limits. For instance, Cree Corporation reported achieving a luminous efficacy of 276 lm/W [3] for white LEDs with the 4401 K colour temperature at the current of 350 mA under laboratory conditions. These results were obtained using SC3 technology and the latest advancements in crystal and phosphor architecture.

However, research continues to pursue higher internal and external quantum efficiencies at elevated current densities by reducing the concentration of non-radiative centres and suppressing Auger recombination, which significantly lowers quantum efficiency as the current increases.

The Russian Science Foundation has reported collaborative efforts by scientists from the Institute of Computational Mathematics and Mathematical Geophysics of the Siberian Branch of the Russian Academy of Sciences and colleagues from Germany to substantially enhance the efficiency of QW-based LEDs by improving the crystalline structure of the quantum well regions and reducing non-radiative recombination losses [4–6].

In addition, work is ongoing to reduce contact resistance, which, according to many researchers, contributes to decreased efficiency at current densities exceeding 10 A/cm^2. Notably, contact resistances as low as 1 Ohm have been achieved [7], yet the deviation of the current-voltage characteristic (CVC) from the exponential behaviour beyond this current density corresponds to an equivalent series resistance of (20–30) Ohms [8] for LEDs with a chip area of 1×10^{-3} cm^2 and approximately ten times lower for chips with an area of 1×10^{-2} cm^2. This resistance level has remained largely unchanged over the years despite continued technological advancements.

This raises the questions: what causes the electrical losses associated with the rise in forward voltage at current densities above 10 A/cm^2 and what approaches might mitigate these losses to enable higher current operation in LEDs?

The objective of this work is to identify the fundamental factors that limit the electrical operating regimes of quantum well LEDs.

2. MODELLING OF ELECTROPHYSICAL PROCESSES IN THE QUANTUM WELL REGION

The external quantum efficiency and overall efficiency are the most important quantitative characteristics of LEDs. The external quantum efficiency is defined as the ratio of the total number of photons emitted into the external environment (integrated over all frequencies and angles) to the number of charge carriers passing through the *p-n* junction per unit time:

$$\eta_{\mathrm{EQE}} = \frac{\Phi}{I/q} = \frac{\xi\cdot\Phi_0}{I/q}, \qquad (1)$$

where ξ is the light extraction coefficient that accounts for the reduction in the number of photons escaping into the external environment due to internal absorption and reflection, Φ_0 is the number of photons, generated in the LED active region via radiative recombination.

The overall efficiency is defined as the ratio of the total optical power emitted to the consumed electrical power:

$$\eta_{\mathrm{PE}} = \frac{P_{\mathrm{L}}}{P_{\mathrm{E}}} = \frac{\int h\nu\cdot\Phi(h\nu)d(h\nu)}{I(U_{\mathrm{b}}+U_{\mathrm{i}})}, \qquad (2)$$

where P_L is the optical power, P_E is the electrical power, U_b is the voltage that reduces the potential barrier of the *p-n* junction, and U_i is the voltage that arises in the diode structure in addition to that required to overcome the barrier potential. As will be shown below, U_i may not originate from resistive effects, but rather from an electric field created by excess charges in the quantum wells embedded in the space charge region (SCR). Therefore, it is denoted not as a product of current and resistance, but specifically as U_i.

The power radiated into the external environment is ξ times less. Accordingly, the ratio of external efficiency to external quantum efficiency is expressed as:

$$\eta_{\mathrm{VE}} = \frac{1}{q(U_{\mathrm{b}}+U_{\mathrm{i}})}\cdot\frac{\int h\nu\cdot\Phi(h\nu)d(h\nu)}{\int\Phi(h\nu)d(h\nu)} \approx \approx \frac{h\nu_{\mathrm{m}}}{q(U_{\mathrm{b}}+U_{\mathrm{i}})}. \qquad (3)$$

where $h\nu_m$ is the effective photon energy, averaged over the emission spectrum.

This relation implies that the efficiency of the LED begins to degrade with the onset and growth of U_i.

Moreover, analysis of current-voltage characteristics (CVC) in the current density region above 10 A/cm^2 shows that U_i under rated operating conditions may amount to 10 % or more of U_b.

Thus, it can be concluded that deviation of the CVC from the exponential current-voltage relationship significantly limits the efficiency of the electrical power supplied to the LED.

In the vast majority of studies on CVC behaviour, the emergence of U_i is attributed to the ex-

Table 1. Design and Technological Parameters of the LED Structure Model Based on *AlGaN/InGaN/GaN*

$\mu_1 \cdot 10^6$, cm	$\mu_2 \cdot 10^6$, cm	$\mu_3 \cdot 10^6$, cm	$\mu_4 \cdot 10^6$, cm	$\mu_5 \cdot 10^6$, cm	$H \cdot 10^7$, cm	N_a, cm^{-3}	N_d, cm^{-3}	S, cm^2
5.85	7.05	8.25	9.45	10.65	3.5	$2 \cdot 10^{19}$	$2 \cdot 10^{17}$	10^{-3}

ternal resistance of the contact pads and the quasi-neutral volume of the crystal [9, 10], with this resistance considered temperature-dependent. However, analysis of efforts to reduce the contact resistance of external terminals shows that a resistance value of approximately 1 Ohm has been achieved [11], which is virtually independent of current magnitude. Therefore, the ratio U_i/I should reach a constant value at low forward currents and remain nearly constant across the entire current range.

Nevertheless, for all quantum well LEDs based on *GaN* and *AlInGaP*, the U_i/I ratio at low currents, approaching zero, is also near zero. As the current density increases to several tens of A/cm², the ratio U_i/J initially grows from zero, reaches a maximum of (0.015–0.030) Ω·cm², and then gradually decreases [12]. This maximum depends on the crystal area, but not on the area of the contact pad. For a crystal area of 1×10^{-3} cm² this ratio reaches (15–30) Ω at its peak, whereas for a crystal with an area of 1×10^{-2} cm² the ratio U_i/I equals to 1.5–3 Ω what is comparable to the contact pad resistance.

These findings indicate that U_i does not result from a voltage drop across an external resistor due to current flow. Instead, it arises from the spatial separation of injected charge carriers and excess charges in the quantum well layers.

This mechanism can be illustrated using a model structure with five quantum wells. The energy band diagram of this structure at a forward bias voltage U_b (lowering the barrier potential) is shown in Fig. 1.

Table 1 presents the design and technological parameters of the model structure.

In this table, μ is the coordinate of the centre of the quantum well, with the index indicating its number. The wells are numbered from the metallurgical boundary of the *p-n* junction, i.e., practically from the heavily doped *n*-region. *H* represents the QW width, while N_a and N_d are the concentrations of acceptors and donors in the *p*- and *n*-regions, respectively. In our case, the quantum wells are located within the SCR of the *p*-region, since the SCR width at zero bias voltage for this structure is $W(0) = 3.4\times10^{-5}$. As shown in ref. [13], to ensure efficient recombination within the QWs, they must be placed in the first half of the SCR under zero bias conditions.

At relatively low current densities (up to 1 A/cm²) in a QW LED structure, the current is primarily generated due to the recombination of charge carriers within the quantum wells via the Sah – Noyce – Shockley (SNS) recombination mechanism [14] with a significant distinction: recombination occurs not through localized centres, but between the energy bands of the QW semiconductor. In reference [13], an expression was obtained for the current – voltage characteristic (CVC) valid in the regime before deviation from the exponential dependence, i.e., up to current densities of (0.1–1) A/cm²:

$$J = q\sigma V_T N_d H \cdot \exp\left(\frac{-\varphi_k + qU_b}{kT}\right) \times \times \sum_{g=1}^{N} E_W(U_b) + J_0 \exp\left(\frac{-\varphi_k + qU_b}{kT}\right), \quad (4)$$

where the first term describes the sum of recombination currents in the QWs, and the second term corresponds to the diffusion component of the total current. Here J_0 is the saturation current due to the diffusion mechanism, q is the elementary charge, σ is the carrier capture cross-section, V_T is the thermal velocity of carriers, kT is the thermal potential, U_b is the voltage that reduces the potential barrier for electrons and holes, and φ_k is the built-in potential of the *p-n* junction. The pre-exponential factor implicitly includes the recombination centre concentration, $N_t = 1$ cm^{-3}, corresponding to the first quantum well in the summation.

In the Eq. (4)

$$E_W(U_b) = = \left[\begin{array}{l} r \cdot \exp\left\{ \left(\frac{-\varphi_k + qU_b}{kT} \right) \left[\frac{2\mu_g}{W(U_b)} - \frac{\mu_g^2}{W(U_b)^2} \right] \right\} + \\ + \exp\left\{ \left(\frac{-\varphi_k + qU_b}{kT} \right) \left[1 - \frac{2\mu_g}{W(U_b)} + \frac{\mu_g^2}{W(U_b)^2} \right] \right\} \end{array} \right]^{-1}, \quad (5)$$

where $W(U_b)$ is the width of the SCR at the potential barrier voltage U_b.

The factors $\left[\frac{2\mu_g}{W(U_b)}-\frac{\mu_g^2}{W(U_b)^2}\right]$ and $\left[1-\frac{2\mu_g}{W(U_b)}+\frac{\mu_g^2}{W(U_b)^2}\right]$ define the proportionality between the edge potentials of electrons and holes in the QWs and the built-in potential minus U_b, assuming a parabolic potential distribution.

This model significantly differs from the classical SNS CVC model due to the inclusion of the coordinates (μ) and widths (H) of the QWs, as well as the interband recombination mechanism occurring within QWs placed inside the SCR.

This operation mode holds up to current densities of (0.1–1) A/cm^2. At higher current densities, the applied forward voltage exceeds U_b by a value denoted as U_i, the origin of which is discussed below.

During injection, QWs acquire a charge of excess carriers:

$$Q_g = qV_TSH\left\{\begin{array}{l} N_a exp\left\{\left(\frac{-\varphi_k+qU_b}{kT}\right)\left[\frac{2\mu_g}{W(U_b)}-\frac{\mu_g^2}{W(U_b)^2}\right]\right\}exp\left(\frac{\varphi_{pg}}{kT}\right)- \\ -N_d exp\left\{\left(\frac{-\varphi_k+qU_b}{kT}\right)\left[1-\frac{2\mu_g}{W(U_b)}+\frac{\mu_g^2}{W(U_b)^2}\right]\right\}exp\left(\frac{\varphi_{ng}}{kT}\right)\end{array}\right\}, \quad (6)$$

where τ is the carrier lifetime, S is the area of the p-n junction, φ_p and φ_n are the potential depths of the QW for holes and electrons, respectively, and the subscript g denotes the QW number.

The absolute values of the potentials of the QW edges are calculated using the equations

$$\varphi_{pg}=\left[1-\frac{2\mu_g}{W(U_b)}+\frac{\mu_g^2}{W(U_b)^2}\right]\left(\frac{\varphi_k-qU_b}{kT}\right),\ \varphi_{ng}=\left[\frac{2\mu_g}{W(U_b)}-\frac{\mu_g^2}{W(U_b)^2}\right]\left(\frac{\varphi_k-qU_b}{kT}\right). \quad (7)$$

In the Eq. (6), $q\sigma V_T N_d \tau \exp\left\{\left(\frac{-\varphi_k+qU_b}{kT}\right)\left[1-\frac{2\mu_g}{W(U_b)}+\frac{\mu_g^2}{W(U_b)^2}\right]\right\}$ is the thermal flux of the electron charge to the QW numbered g, and $q\sigma V_T N_a \tau \exp\left\{\left(\frac{-\varphi_k+qU_b}{kT}\right)\left[\frac{2\mu_g}{W(U_b)}-\frac{\mu_g^2}{W(U_b)^2}\right]\right\}$ is the thermal flux of the hole charge to the QW numbered g.

The factors $SH\cdot exp\left(\frac{\varphi_{pg}}{kT}\right)$ and $SH\cdot exp\left(\frac{\varphi_{ng}}{kT}\right)$ normalize the charges of electrons and holes in the QW with the volume SH and the energy depth φ_{ng} and φ_{pg}.

Thus, a structure with quantum wells can be modelled as a flat capacitor consisting of several plates carrying unequal charges both, in magnitude and sign, depending on the voltage drop across the potential barrier.

It is evident that the first QW is always negatively charged, while the last one is positively charged. With typical values of barrier width between QWs [21], the excess carrier concentrations in the inner QWs are an order of magnitude lower than in the outermost ones.

An internal electric field arises between the QWs, opposing the SCR field. As a result, an additional voltage U_i is induced, which has the same polarity as the applied bias voltage.

Taking this into account and with an acceptable approximation that does not affect the conclusions, the system of multiple charged QWs can be represented as a two-plate capacitor, in which the plates correspond to the outermost quantum wells.

The charge of the first quantum well, neglecting the insignificant excess hole concentration, is given by:

$$Q_1 = q\sigma V_T N_a \tau SH \exp\left\{\left[\frac{2\mu_1}{W(U_b)}-\frac{\mu_1^2}{W(U_b)^2}\right]\left(\frac{-\varphi_k+qU_b}{kT}\right)\right\}\exp\left(\frac{\varphi_{n1}}{kT}\right), \quad (8)$$

Similarly, the charge of the last quantum well (numbered *N*), ignoring the excess electron concentration, is:

$$Q_{\mathrm{N}} = q\sigma V_{\mathrm{T}} N_{\mathrm{d}} \tau SH \exp\left\{\left[\frac{2\mu_{\mathrm{N}}}{W(U_{\mathrm{b}})} - \frac{\mu_{\mathrm{N}}^2}{W(U_{\mathrm{b}})^2}\right]\left(\frac{-\varphi_{\mathrm{k}} + qU_{\mathrm{b}}}{kT}\right)\right\}\exp\left(\frac{\varphi_{\mathrm{pN}}}{kT}\right). \tag{9}$$

Accordingly, the excess electron and hole concentrations in the QWs are defined as:

$$\Delta n = \sigma V_{\mathrm{T}} N_{\mathrm{d}} \tau \exp\left\{\left[\frac{2\mu_{1}}{W(U_{\mathrm{b}})} - \frac{\mu_{1}^2}{W(U_{\mathrm{b}})^2}\right]\left(\frac{-\varphi_{\mathrm{k}} + qU_{\mathrm{b}}}{kT}\right)\right\}\exp\left(\frac{\varphi_{\mathrm{n1}}}{kT}\right), \tag{10}$$

$$\Delta p = \sigma V_{\mathrm{T}} N_{\mathrm{a}} \tau \exp\left\{\left[\frac{2\mu_{\mathrm{N}}}{W(U_{\mathrm{b}})} - \frac{\mu_{\mathrm{N}}^2}{W(U_{\mathrm{b}})^2}\right]\left(\frac{-\varphi_{\mathrm{k}} + qU_{\mathrm{b}}}{kT}\right)\right\}\exp\left(\frac{\varphi_{\mathrm{pN}}}{kT}\right). \tag{11}$$

The calculated values of the excess charge carrier concentrations in the outermost QWs, based on equations (10) and (11) and accounting for the injection of electrons and holes into the QWs at the barrier-lowering voltage U_b, are equal to $n = 1.4\times10^{13}$ cm^{-3} electrons in the first quantum well, holes $p = 2.5\times10^{9}$ cm^{-3} in the fifth quantum well at $U_b = 1.0$ V and $n = 1.8\times10^{17}$ cm^{-3} and holes $p = 8.1\times10^{18}$ cm^{-3}, respectively, at $U_b = 2.0$ V. As mentioned above, in internal quantum wells, the charge is more than an order of magnitude smaller, therefore, it can be ignored with some approximation.

The electric field strength between the first and last QWs is equal in magnitude to $E_{1} = \dfrac{Q_{1}}{2\varepsilon\varepsilon_0 S}$, and that between the last and the first QWs is $E_{\mathrm{N}} = \dfrac{Q_{\mathrm{N}}}{2\varepsilon\varepsilon_0 S}$.

The excess voltage U_i arising in the SCR between the first and last QWs, aligned in polarity with the external forward bias voltage U_b, is given by:

$$U_{\mathrm{i}} = (E_{1} + E_{N})(\mu_{\mathrm{N}} - \mu_{1}) =$$

$$= \frac{q\sigma V_T \tau \cdot SH \cdot (\mu_{\mathrm{N}} - \mu_{1})}{2\varepsilon\varepsilon_0 S}\left\{\begin{array}{l} N_{\mathrm{a}} \exp\left[\left[1 - \dfrac{2\mu_{\mathrm{N}}}{W(U)} + \dfrac{\mu_{\mathrm{N}}^2}{W(U)^2}\right]\left(\dfrac{-\varphi_{\mathrm{k}} + qU_{\mathrm{b}}}{kT}\right)\right]\exp\left(\dfrac{\varphi_{\mathrm{pN}}}{kT}\right) + \\ + N_{\mathrm{d}} \exp\left[\left[\dfrac{2\mu_{1}}{W(U)} - \dfrac{\mu_{1}^2}{W(U)^2}\right]\left(\dfrac{-\varphi_{\mathrm{k}} + qU_{\mathrm{b}}}{kT}\right)\right]\exp\left(\dfrac{\varphi_{\mathrm{n1}}}{kT}\right) \end{array}\right\}. \tag{12}$$

If the total external forward bias is denoted as U, it consists of the barrier-lowering voltage U_b and the additional internal voltage U_i generated between the QWs:

$$U = U_b + U_i. \tag{13}$$

Then, taking into account the expression for the forward current obtained in reference [13], the equation describing the current – voltage characteristic of the structure with quantum wells can be presented as a system:

$$J = J_{\mathrm{r}} + J_{\mathrm{d}} = q\sigma V_{\mathrm{T}} N_{\mathrm{d}} H \cdot \exp\left(\frac{-\varphi_{\mathrm{k}} + qU_{\mathrm{b}}}{kT}\right)\sum_{\mathrm{g}=1}^{\mathrm{N}} E_{\mathrm{W}}(U_{\mathrm{b}}) + J_0 \exp\left(\frac{-\varphi_{\mathrm{k}} + qU_{\mathrm{b}}}{kT}\right),$$

$$U = U_{\mathrm{b}} + U_{\mathrm{i}} = U_{\mathrm{b}} + \frac{q\sigma V_{\mathrm{T}} \tau SH(\mu_{\mathrm{N}} - \mu_{1})}{2\varepsilon\varepsilon_0 S}\left\{\begin{array}{l} N_{\mathrm{a}} \exp\left[\left[1 - \dfrac{2\mu_{\mathrm{N}}}{W(U)} + \dfrac{\mu_{\mathrm{N}}^2}{W(U)^2}\right]\left(\dfrac{-\varphi_{\mathrm{k}} + qU_{\mathrm{b}}}{kT}\right)\right]\exp\left(\dfrac{\varphi_{\mathrm{pN}}}{kT}\right) + \\ + N_{\mathrm{d}} \exp\left[\left[\dfrac{2\mu_{1}}{W(U)} - \dfrac{\mu_{1}^2}{W(U)^2}\right]\left(\dfrac{-\varphi_{\mathrm{k}} + qU_{\mathrm{b}}}{kT}\right)\right]\exp\left(\dfrac{\varphi_{\mathrm{n1}}}{kT}\right) \end{array}\right\}, \tag{14}$$

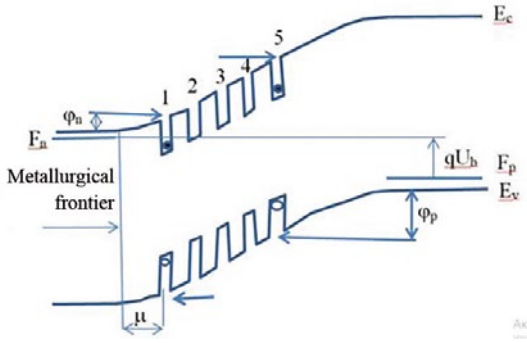

Fig. 1. Energy band diagram of a model structure with quantum wells under forward bias voltage U_b: the numbers denote the quantum well indices; black dots represent electrons; white dots represent holes; the quantum wells are located within the space charge region of the lightly doped part of the *p-n* junction

where J_r and J_d are the recombination and diffusion components of the total current, respectively.

The modelled current – voltage characteristic based on the parameter values from Table 1 is shown in Fig. 2. At forward biases corresponding to the exponential portion of the CVC (Fig. 2, mode 1), the current increases nearly exponentially, with a slope in semilogarithmic coordinates approximately twice smaller than that of an ideal diode. This behaviour continues until the excess charge concentration in the outermost QWs becomes comparable to the concentration of fixed ionized impurity centres in the SCR. At that point, the electric field due to the QW charge becomes comparable in magnitude to the field U_b compensated by the space charge, significantly altering the electrostatics of the quantum well region.

At a certain value of the electric field between quantum wells, the potential barrier separating them becomes equalized, allowing the injected charge carriers to diffuse freely within the quantum well region, Fig. 3, (*b*), corresponding to mode 2 in Fig. 2.

A further increase in current leads to a rise in the excess carrier concentration in the quantum wells and, consequently, to an increase in the total forward bias voltage due to the growing electric field between the wells, expressed as $U=U_b+E_{DR}L$. Experimental data indicate that in a sufficiently wide range of current variations, the excess voltage U_i increases almost proportionally to the forward current, i.e., proportionally to the concentration of excess free charge carriers in the quantum wells.

Thus, for the presented mode at $U_i = 1.2$, mode 3 in Fig. 2, the electric field strength between the first and fifth quantum wells E_{DR} is 3×10^5 V/cm. However, the E_{DR} vector is directed opposite to the potential barrier field and acts as an accelerating (drift) field for the injected charge carriers. The energy diagram for this mode is shown in Fig. 3, (*c*). Here, the charge carriers injected from the *n*- and *p*-regions are accelerated by the resulting drift field and heated. Calculations indicate that they can acquire an energy ΔE of 0.165 eV, which is sufficient to cause a noticeable probability of atomic displacement from lattice sites [8, 16]. This mode is referred to as the subthreshold atomic displacement mode [16], since the atomic displacement energy in *GaN*, $E_d = 12$ eV, is much greater than ΔE, and the displacement probability is given by $p = exp[-E_d/2(kT+2\Delta E/3)]$.

The onset of U_i and the deviation of the CVC from an exponential dependence can be taken to occur when $U_i > kT/q$. This value of U_i, according to Eq. (12), corresponds to the current density

$$J_{KP} = \frac{2kT\varepsilon\varepsilon_0}{q^2\tau L},, \text{ where } (L = \mu_N - \mu_1.). \qquad (15)$$

This equation shows that the current density, at which the CVC deviates from the exponential dependence, given typical design and technological parameters for LED structures [15], is nearly constant and on the order of a few amperes per square centimetres for LEDs operating in the visible spectrum. Only the product τL in the denominator varies slightly, since according to the ABC model $\tau = 1/(A+Bn+Cn^2)$, i.e., it is practically determined by the same excess carrier concentration, while $L \approx W(0)/2$ is determined by the doping lev-

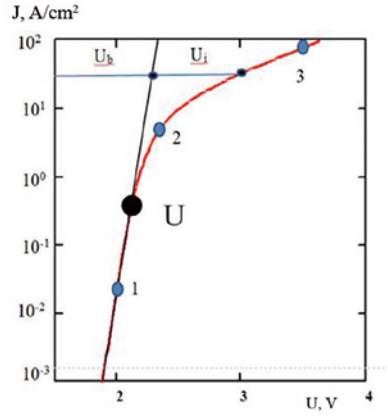

Fig. 2. Modelled current – voltage characteristic of the *AlGaN/InGaN/GaN* semiconductor structure with five quantum wells, taking into account excess injection charge in the quantum wells: 1) low current density mode; 2) mode of the beginning of deviation from the exponential dependence; 3) strong drift field mode between quantum wells

el in the quantum well region, typically (5×10^{16}–$1\times\times10^{17}$) cm^{-3} [13].

When an electric field arises between the quantum wells, the narrowing of the SCR in the QW structure significantly slows down as the external bias voltage U increases. Ultimately, in such structures, the SCR width is limited by the distance between the outermost quantum wells. However, experimental results show that this limit cannot be reached due to the high electric field strengths between QWs, which lead to electrical breakdown. In this mode, the increase in current mainly results from a slight reduction in the potentials φ_n and φ_p, Fig. 3, (*c*), while the significant increase in the bias voltage is due to the growth of U_i.

A characteristic feature of the U_i/I ratio is its increase from zero to a certain maximum, followed by a gradual decrease. To explain this, consider the current expressions in Eq. (14). Before the electric field arises, the current is described by the first term in Eq. (14), where the capture cross-section can be assumed constant and close to unity. Upon reaching mode 3, where the electric field between the QWs becomes accelerating for the injected carriers, they gain enough energy to traverse over the QW barriers. Consequently, the probability of carrier capture in the QWs decreases, equivalent to a reduction in the capture cross-section. As a result, the growth of U_i slows down, and the diffusion component of the current increases due to the drift of injected carriers into the quasi-neutral regions. This explains the decrease in the U_i/I ratio as the forward current increases.

If we denote U_{b0} as the voltage, at which a drift electric field arises between the quantum wells for the injected carriers, mode 2, in Fig. 3, (*b*), then the dependence of the capture cross-section on the voltage U_b can be modelled hypothetically as:

$$\sigma = \frac{1}{1+\exp\left(\frac{q(U_b - U_{bo})}{kT}\right)}, \qquad (16)$$

where U_{b0} is the voltage at which the drift field arises between the outermost QWs and depends on the QW depth.

From the above, it follows that, for typical parameters of LED structures with quantum wells, the formation of a drift field in the QW region and the emergence of voltage U_i occur within nearly the same current density range of (1–10 $A/cm^{2)}$,

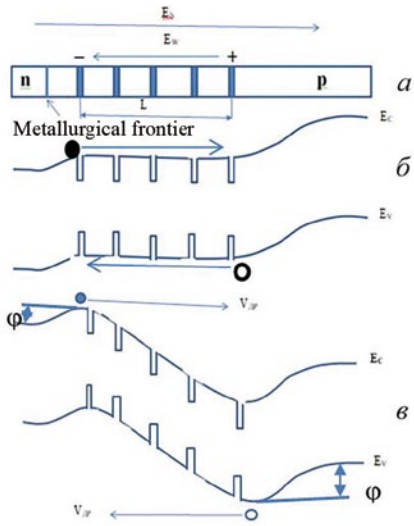

Fig. 3. Technological structure of the model with quantum wells: quantum wells are shown as shaded stripes – *a*; energy band diagram corresponding to mode 2 in Fig. 2 – *b*; energy band diagram corresponding to mode 3 in Fig. 2 – *c*

corresponding to a specific electric power JU of (2–35) W/cm^2 at external bias voltages of (2–3.5) V. At higher bias voltages, the proportion of voltage U_i increases sharply, leading to a rapid decrease in efficiency, i.e., an increase in electrical losses.

3. DEPENDENCE OF EFFICIENCY ON INJECTION MODE

Having established the nature of the voltage U_i, we analyse the dependence of the LED efficiency with quantum wells on the current density. For this purpose, the ABC recombination model [17] is employed.

Having established the nature of voltage U_i, we reveal the dependence of efficiency of a LED with quantum wells on the current density. For this purpose, we use the ABC model of recombination [17].

The current through the LED according to this model is calculated by the equation:

$$I = qS\sum H_g\left(A\sum n_g + B\sum n_g^2 + C\sum n_g^3\right), \qquad (17)$$

where q is the elementary charge, S and H are the area and width of the quantum wells, n is the excess concentration of charge carriers in the quantum well numbered g; A, B, C are the ABC model coefficients.

The flux of photons generated in quantum wells is calculated using the equation

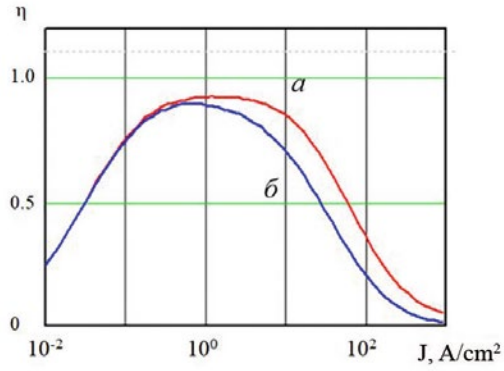

Fig. 4. Dependence of the external quantum yield – *a* and efficiency – *b* on the current density; the dependencies are normalized by their maximum value

$$\Phi_0 = S\sum H_g \cdot B\sum n_g^2, \qquad (18)$$

where $B \quad n_g^2$ is the radiative component of the recombination rate.

From Eqs. (17) and (18), the external quantum efficiency, depending on the injection level into the quantum wells, can be expressed as:

$$\eta_{EQE} = \frac{\xi B\sum n_g^2}{A\sum n_g + B\sum n_g^2 + C\sum n_g^3}. \qquad (19)$$

The LED efficiency, considering the ABC recombination model and equation (19), is described by:

$$\eta_{PE} = \frac{\xi\int h\nu\cdot\Phi(h\nu)d(h\nu)}{I(U_b+U_i)} = \frac{h\nu_э}{q(U_b+U_i)}\cdot\frac{\xi\Phi_0}{I/q} =$$
$$= K\frac{1}{1+U_i/U_b}\cdot\eta = K\beta\eta, \qquad (20)$$

where $K=h\nu_m/qU_b$ is a coefficient close to unity, and $\beta = \frac{1}{1+U_i/U_b}$ is the efficiency reduction coefficient.

Eq. (20) indicates that at the maximum achievable external quantum efficiency, the efficiency of electric power utilization in powering the LED depends on losses caused by the voltage U_i. As mentioned above, U_i is largely determined by the design and technological parameters, as well as the electrophysical properties of LED structures with quantum wells.

Figs. 4 and 5 present the dependences of the external quantum yield and efficiency of the model structure, as well as the efficiency reduction factor

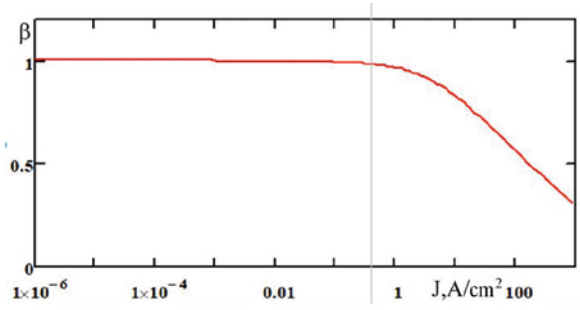

Fig. 5. Dependence of the efficiency reduction factor on the current density

on the current density through the LED for the values of the ABC model coefficients of A = 2×10^5 s^{-1}, B = 5×10^{10} $s^{-1}cm^3$, C = 8×10^{-29} $s^{-1}cm^6$, ξ = 0.5, K = 1.

The presented graphs show that significant electrical power losses of up to 30 % occur already at a current density of 35 A/cm², which corresponds to the specified operating mode with a specific power of 105 W/cm² at a forward voltage of 3.0 V. For a crystal with an area of 1×1 mm² this corresponds to a specified power of 1 W with electrical power losses, amounting to 0.3 W. At a current of 1 A, the losses can reach up to 50 %, i.e., 1.75 W. These losses are unavoidable and are dissipated as heat in the crystal, caused by electrophysical processes in structures with quantum wells.

Another detrimental effect of the drift electric field appearing in the mode where the current – voltage characteristic deviates from the exponential behaviour – is the formation of non-radiative centres in the form of point defects due to interactions between hot charge carriers and the atoms of the crystal lattice. This results in gradual degradation of the emission, i.e., an irreversible reduction in the external quantum efficiency [18].

CONCLUSION

The use of electrical operating modes with elevated current densities (J > (1–10) A/cm²) in quantum well LEDs is limited by objective factors related to electrophysical processes, specifically, the formation of a built-in drift electric field within the space-charge region (SCR) where the quantum wells are located. Starting at a current density of approximately 1 A/cm², the LED efficiency decreases proportionally to the coefficient $\beta = \frac{1}{1+U_i/U_b}$, where U_i is proportional to the current density and

corresponds to the potential difference between the outermost quantum wells. This potential difference arises due to excess charge from the injected carriers.

The deviation of the current – voltage characteristic from exponential behaviour leads to conditions that accelerate the degradation of luminous flux over time. This is a result of the formation of an internal electric field with an intensity on the order of 10^5 V/cm within the quantum well region. Such a strong field gives rise to hot electrons, which in turn displace atoms from their lattice sites, forming non-radiative recombination centres.

ACKNOWLEDGMENTS

The work was performed within the state assignment to universities of the Ministry of Science and Higher Education (project FZRR-2023–0009).

REFERENCES

1. Nakamura, S., Iwasa, M.S. Method of manufacturing *p*-type compound semiconductors / Patent N5,306,662. Apr.1994. Japan.

2. Amano, H., Akasaki, I. et.al. Method for producing a luminous element of III-group nitride / Patent N5,496,766. Mar. 1996. Japan.

3. https://signbusiness.ru/news/svetotechnika/svetootdacha-svetodiodov-preodolevaet-planku

4. Uwe Jahn, Vladimir M. Kaganer, Karl K. Sabelfeld, Anastasya E. Kireeva, Jonas Lähnemann, Carsten Pfüller, Timur Flissikowski, Caroline Chèze, Klaus Biermann, Raffaella Calarco, and Brandt, O. Carrier diffusion in *GaN* – a cathodoluminescence study. I: Temperature-dependent generation volume // arXiv:2002.08713v4 [cond-mat.mtrl-sci] 23 Nov 2021.

5. Oliver Brandt, Vladimir M. Kaganer Jonas Lähnemann, Timur Flissikowski, Carsten Pfüller, Karl K. Sabelfeld, Anastasya E. Kireeva, Caroline Chèze, Raffaella Calarco, Holger T. Grahn, and Uwe J. Carrier diffusion in GaN – a cathodoluminescence study. II: Ambipolar vs. exciton diffusion // arXiv:2009.13983v3 [cond-mat.mtrl-sci] 23 Nov 2021.

6. Jonas Lähnemann, Vladimir M. Kaganer, Karl K. Sabelfeld, Anastasya E. Kireeva, Uwe Jahn,1 Caroline Chèze, Raffaella Calarco, and Oliver Brandt1, Carrier diffusion in GaN – a cathodoluminescence study. III: Nature of nonradiative recombination at threading dislocations // arXiv:2009.14634v2 [cond-mat.mtrl-sci] 23 Nov 2021.

7. Zhelannov, A V, Ionov, A S, Seleznev, B I, Fedorov, D.G. Ohmic contacts to device structures based on gallium nitride [Omicheskiye kontakty k pribornym strukturam na osnove nitrida galliya] // Fizika Tekhn. Polurpovodn., 2020, 54(3), 246–250.

8. Manyakhin, F. I., Mokretsova, L.O. The Regularity of Quantum Efficiency Reduction in Quantum Well LEDs under Prolonged Current Flow from the Perspective of the ABC Model // Light & Engineering, 2021, # 5(2), 62–70.

9. Schubert, F. Light Emitting Diodes / Translated from English under the editorship of A.E. Yunovich, 2nd ed., FIZMATLIT, 2008, 496 p.

10. S. Chhajeda, Y. Xib, Th. Gessmanna, J.-Q. Xib, J.M. Shaha, J.K. Kima, and Schubert E.F. Junction temperature in light emitting diodes assessed by different methods // 2007 IEEE International Symposium on Industrial Electronics, DOI: 10.1117/12.593696 ID: 95125905.

11. Zhelannov, A.V., Ionov, A.S., Seleznev, B.I., Fedorov, D.G. Ohmic contacts to device structures based on gallium nitride [Omicheskiye kontakty k pribornym strukturam na osnove nitrida galliya] // Fizika Tekhn.Polurpovodn., 2020, 54(3), 246–250.

12. Manyakhin, F.I., Varlamov, D.O., Mokretsova, L.O., Skvortsov, A.A., Krylov, V.P. The mechanism of formation of the Volt-Ampere dependence of LEDs with quantum wells // JMRS, 2025 (the article is currently under peer-review).

13. Manyakhin, F.I., Varlamov, D.O., Mokretsova, L.O., Skvortsov, A.A., Krylov, V.P., Skvortsov, A.A., and Nikolaev, V.K. Physico-mathematical model of the volt – current characteristics of light-emitting diodes with quantum wells based on the Sah – Noyce – Shockley recombination mechanism // Journal of Semiconductors, 2024, V.32, https://doi: 10.1088/1674-4926/23120044.

14. Sah C.T., Noyse R.N., Shokley W. Carrier Generation and Recombination in P-N Junction Caracteristics // Proceedings of the Institute of Radio Engineers. 1957. Vol. 45. Iss.9. P. 1228–1243; https://ieeexplore.ieee.org/document/4056679.

15. Vigdorovich, E.N. Mechanism of formation of quantum-sized layers in *AlGaN/InGaN/GaN* heterostructures [Mekhanizm formirovaniya kvantovo-razmernykh sloyev v geterostrukturakh AlGaN/InGaN/GaN] // Izv. Vuzov. Elektronika, 2017, 22(4), 323–330.

16. Kovalev, A.N., Manyakhin, F.I., Kudryashov, V.E., Turkin, A.N., Yunovich, A.E. Changes in the luminescent and electrical properties of *InGaN/AlGaN/GaN*-based LEDs during long-term operation [Izmeneniye lyuminestsentnykh i elektricheskikh svoystv svetodiodov na osnove InGaN/AlGaN/GaN pri dlitel'noy ekspluatatsii] // Fizika Tekhn.Polurpovodn., 1999, 33(2), 224–232.

17. Karpov, S. Yu. ABC-model for interpretation of internal quantum efficiency and its drop in III-nitride LEDs: a review // Opt. Quantum Electron. 2015, Vol. 47, # 6, P. 1293–1303 / DOI 10.1007/s11082–014–0042–9.

18. Manyakhin, F.I., Varlamov, D.O., Kuksa, V.V., Mokretsova, L.O. Mechanism and Regularity for Luminous Flux Decreasing of Efficient Small Powered LEDs Based on *GaN/InGaN* Structures at High Current Density // Light & Engineering, Vol. 32, # 2, pp. 20–29, 2024; https://doi.org/10.33383/2023–027 (Svetotekhnika No 6, 2023, pp. 68–75).

Fedor I. Manyakhin,
Doctor of Physical and Mathematical Sciences, Professor. He graduated from the Moscow Institute of Electronics and Mathematics in 1973. Currently, he is a professor at Moscow Polytechnic University, he is the author and co-author of over 180 publications. He has been awarded a Certificate of Honour by the Ministry of Education and Science of the Russian Federation and was a laureate of the *Golden Names of Higher Education 2018* competition in the category *For Contribution to Science and Higher Education*. His research interests include semiconductor electronics and the physics of semiconductor devices

Lyudmila O. Mokretsova,
Ph. D. in Engineering, Associate Professor. She graduated from the Moscow Institute of Steel and Alloys (MISIS) in 1978 and is currently an Associate Professor in the Department of Computer-Aided Design and Engineering at the National University of Science and Technology MISIS. She was a laureate of the *Golden Names of Higher Education 2018* competition in the category *For the Implementation of Innovative Teaching Methods*. Her research interests include three-dimensional modelling in lighting design

Arkady A. Skvortsov,
Doctor of Physical and Mathematical Sciences. He is Head of Department at Moscow Polytechnic University and the author or co-author of more than 150 scientific articles and monographs on semiconductor materials science, as well as on the degradation of metallization systems and contact structures in micro- and nanoelectronics

Dmitry O. Varlamov,
engineer. He graduated from Moscow State Technical University “MAMI” in 2005 and is currently a Senior Lecturer in the Department of Electrical Equipment and Industrial Electronics at Moscow Polytechnic University. He is the author and co-author of more than 40 publications. His research interests include microcontroller systems and LED technologies

CONTENTS

VOLUME 33 **NUMBER 5** **2025**

LIGHT & ENGINEERING

PARTNERS OF LIGHT & ENGINEERING JOURNAL

Editorial Board with big gratitude would like to inform international lighting community about the Journal Partners Institute establishment. The list with our partners and their Logo see below. The description of partner's collaboration you can found at journal site *www.l-e-journal.com*

BL Group
International Lighting Engineering Corporation
BOOS LIGHTING GROUP

ВНИСИ

interlight
RUSSIA

intelligent building
RUSSIA